Neural degeneration and plasticity following damage to the post-chiasmal visual pathway

Thesis submitted for the degree
Doctor of Philosophy

Rebecca S. Millington

New College

Supervisors: Dr Holly Bridge & Prof Christopher Kennard

Vision Group
FMRIB Centre, Nuffield Department of Clinical Neurosciences

University of Oxford

Trinity Term 2013

Abstract

Neural degeneration and plasticity following damage to the post-chiasmal visual pathway

Thesis submitted for the degree
Doctor of Philosophy

Rebecca S. Millington

New College

Trinity Term 2013

Hemianopia is a disorder where a patient loses vision in one half of their visual field, following damage to the post-chiasmal visual pathway. If the hemianopia does not spontaneously resolve within the first few months, the prognosis for recovery is poor, with very few patients recovering vision in the affected area of the visual field. The reasons for this are unclear, although it is likely that both degeneration and plasticity in the visual system have an impact on patient outcome. The goal of this research is to investigate the changes that occur in hemianopia, and how these differ for lesions at different locations in the visual pathway and with differing underlying pathologies.

Patients with hemianopia arising from different causes were recruited, including 17 with a hemianopia acquired in adulthood, 9 with congenital hemianopia, and 6 patients with hemianopia due to posterior cortical atrophy (PCA). Structural, functional, and diffusion-weighted MRI data were acquired for each patient, in order to examine changes in the structural and function of the visual pathways. Analyses focused on either atrophy, or plasticity and residual function. Atrophy was assessed in acquired and congenital hemianopia by quantifying transneuronal degeneration in the optic tract, which was present in all patients with long-term lesions. Degeneration was also assessed more generally in PCA, who have substantial loss of white and grey matter in posterior brain regions. Investigation of plasticity and residual function focused on the motion processing area (MT), quantifying the level of functional activity in MT, and assessing whether subcortical pathways from the pulvinar to MT exist in hemianopia. A wide degree of variation existed between patients in the extent to which motion processing was preserved, which had no clear link to lesion location, however was related to the size of the lesion.

Acknowledgements

It would not have been possible to complete this thesis without the help of Holly Bridge and Chris Kennard, and my 'unofficial' supervisors Gordon Plant and John Barbur, all of whom gave me invaluable advice and guidance. Thank you all for giving me your time, and the benefit of your expertise.

To Holly - I don't know where to start! Thank you for all your help and patience, and for managing to put up with me for three years! It has been a pleasure to be part of your group, so thank you for taking me on.

To Chris - Thank you for introducing me to the clinicians in Oxford, and for all the advice you have given me on my project and my medicine applications - I doubt I would have been starting this term without you!

To Gordon - Your help on the TRD work and PCA patients has been invaluable, as have been your comments on my work - thank you so much, and I hope the PCA project continues to go well.

To John - thank you for taking the time to discuss and comment on my work with me, and for letting me use your lab. Your enthusiasm for vision is infectious, and I have very much enjoyed getting to know you.

A number of people helped me along the way, whether by helping with data collection, working out how to do analysis, or other general support. Thanks especially to Merle James-Galton, Panitha Jindahra, Patsy Terry, Caroline Dodridge, Wei Bi, Johannes Klein, Giovanna Zamboni, Guilherme Beltramini and Mark Jenkinson - your help has been much appreciated. Special thanks also to Steven Knight, for making scanning possible, and for keeping me going even when nothing seemed to be working!

During the first year of my DPhil I had the opportunity of spending a period at Unicamp, in Brazil. I'd like to thank Professor Cendes and his lab for making me so welcome, and in particular to Clarissa for her invaluable help with collecting my data, and for being a great friend.

Thanks to my friends and family for their support. The vision girls for the many lunchtimes and coffee breaks. Anderson for teaching me LaTeX and giving me unlimited access to your snack drawer. BSD for keeping me sane and giving me an excuse to start my mornings with the Lion King. Daniel for always being able to pick me up when I'm down, and for helping me get to the finish line. And my parents, gran, AD and Alex, for supporting me throughout everything.

Finally, thanks to all the patients who agreed to participate in my research, without whom this thesis would not have been possible.

Contents

Abstract **3**

Acknowledgements **5**

Abbreviations **11**

1 Introduction **13**
1.1 Structure of the visual system . . . 13
1.2 Hemianopia . . . 16
1.3 Different forms of hemianopia . . . 18
1.4 Residual vision . . . 21
1.5 Anatomy underlying residual visual function in the blind field . . . 22
1.6 Rehabilitation in hemianopia . . . 24
1.7 Degeneration may hinder attempts to rehabilitate hemianopia . . . 27
1.8 The use of imaging to investigate visual dysfunction . . . 28
1.9 Synopsis of thesis . . . 30
1.9.1 Overview of experimental chapters . . . 31
1.9.2 Summary . . . 35

2 General Methods **37**
2.1 Patients . . . 37
2.1.1 Patients with sudden onset acquired hemianopia . . . 38
2.1.2 Patients with congenital visual pathway damage . . . 39
2.1.3 Patients with posterior cortical atrophy . . . 40
2.2 Perimetry . . . 41
2.3 Image acquisition and pre-processing . . . 42
2.3.1 Structural imaging . . . 42
2.3.2 Functional MRI . . . 43
2.3.3 Diffusion-weighted imaging . . . 47

3 Quantifying the pattern of optic tract degeneration in human hemianopia **49**
3.1 Abstract . . . 49
3.2 Introduction . . . 50
3.2.1 Potential for recovery in hemianopia . . . 51

3.2.2 TRD in non-human primates . . . 51
3.2.3 TRD in the human visual system . . . 52
3.2.4 Aims of the present study . . . 54
3.3 Methods . . . 55
3.3.1 Subjects . . . 55
3.3.2 Data acquisition . . . 56
3.3.3 Analysis of degeneration using T1-weighted imaging . . . 57
3.3.4 Analysis of degeneration using diffusion-weighted imaging . . . 59
3.4 Results . . . 61
3.4.1 TRD is present in all patients with stable adult-onset hemianopia 61
3.4.2 Optic tract degeneration is a result of processes beyond the effects of the initial insult . . . 64
3.4.3 Congenital hemianopia leads to a significant decrease in white matter integrity . . . 66
3.4.4 Optic tract degeneration is proportional to amount of occipital damage in acquired, but not congenital, hemianopia . . . 66
3.4.5 Diffusion-weighted measures can provide measures of laterality . 70
3.5 Discussion . . . 74
3.5.1 Human TRD appears to follow a similar pattern to non-human primate . . . 74
3.5.2 TRD is extensive in cases where a hemianopia was acquired prenatally . . . 75
3.5.3 Lesion size and field deficit correlate significantly with LI in patients with acquired damage . . . 76
3.5.4 Diffusion-weighted imaging is less reliable than structural measures 78
3.5.5 Conclusion . . . 80

4 Motion processing in hemianopia 81
4.1 Abstract . . . 81
4.2 Introduction . . . 82
4.2.1 Motion perception in the blind hemifield . . . 83
4.2.2 Neuroimaging evidence for function in MT . . . 84
4.2.3 Aims of the present study . . . 86
4.3 Methods . . . 86
4.3.1 Subjects . . . 86
4.3.2 Functional imaging . . . 87
4.3.3 Motion discrimination tasks . . . 91
4.4 Results . . . 94
4.4.1 Hemianopia patients have reduced activity bilaterally when viewing centrally presented moving dots . . . 94
4.4.2 Hemianopia patients have reduced activity bilaterally when viewing hemifield motion stimuli . . . 97
4.4.3 Impact of lesion location on activity in area MT . . . 100
4.4.4 Impact of lesion size on activity in MT . . . 102

4.4.5 Activity in area MT does not differ between patients with acquired and congenital hemianopia . . . 103
4.4.6 Motion discrimination tasks . . . 104
4.5 Discussion . . . 109
4.5.1 Hemianopia patients have reduced activity in the visual cortex when viewing motion stimuli . . . 109
4.5.2 Activity in MT cannot easily be predicted according to the type of lesion present . . . 110
4.5.3 Problems with measuring the neural response to motion stimuli with fMRI . . . 111
4.5.4 Patients demonstrating strong residual motion processing did not have V1 damage . . . 113
4.5.5 Conclusion . . . 114

5 Non-striate vision: investigating connectivity between the pulvinar and motion area MT using diffusion imaging 117
5.1 Abstract . . . 117
5.2 Introduction . . . 118
5.2.1 Visual pathways exist which bypass V1 . . . 119
5.2.2 Cortical connections of the pulvinar . . . 121
5.2.3 Investigating connectivity using DTI . . . 123
5.2.4 Aim of the present study . . . 124
5.3 Methods . . . 125
5.3.1 Subjects . . . 125
5.3.2 Image acquisition . . . 125
5.3.3 Image preprocessing . . . 125
5.3.4 Creation of ROIs . . . 126
5.3.5 Probabilistic tractography . . . 129
5.3.6 Function in area MT . . . 130
5.4 Results . . . 131
5.4.1 Segmentation of the pulvinar in healthy controls . . . 131
5.4.2 Cortical connections of the pulvinar in hemianopia . . . 134
5.4.3 Overlap of connectivity in the visual areas . . . 140
5.4.4 Relationship between pulvinar connectivity and functional activation to motion stimuli . . . 142
5.5 Discussion . . . 144
5.5.1 The pulvinar can be segmented using DTI . . . 144
5.5.2 Connectivity between the pulvinar and area MT is not greater in congenital than acquired patients . . . 144
5.5.3 The relationship between connectivity and function in area MT is unclear . . . 146
5.5.4 Limitations of DTI . . . 147
5.5.5 Conclusions . . . 149

6 The neurological basis of hemianopia in posterior cortical atrophy 151
6.1 Abstract . . . 151
6.2 Introduction . . . 153
6.2.1 Common visual processing deficits in PCA . . . 153
6.2.2 Hemianopia in PCA . . . 155
6.2.3 Neuroimaging in PCA . . . 157
6.2.4 Aims of the present study . . . 160
6.3 Methods . . . 161
6.3.1 Subjects . . . 161
6.3.2 Neuropsychological assessment . . . 162
6.3.3 Perimetry . . . 163
6.3.4 Image acquisition . . . 164
6.3.5 Imaging analysis . . . 165
6.4 Results . . . 170
6.4.1 Relative atrophy of white and grey matter . . . 172
6.4.2 Grey matter degeneration . . . 177
6.4.3 White matter degeneration . . . 182
6.4.4 Cortical response to visual stimuli . . . 186
6.5 Discussion . . . 191
6.5.1 Posterior cortical atrophy shows a distinct pattern of grey and white matter degeneration . . . 191
6.5.2 Comparability of AD and PCA patients . . . 194
6.5.3 Visual field deficits in PCA may not reflect direct damage to the primary visual cortex . . . 197
6.5.4 Conclusions . . . 199

7 General Discussion 201
7.1 Overview of thesis . . . 201
7.2 Factors to consider when studying hemianopia patients . . . 204
7.3 Future directions . . . 206
7.4 Final conclusions . . . 210

A Additional patient details 213
A.1 Patients scanned in the UK . . . 213
A.2 Patients scanned in Brazil . . . 216

B Perimetry Results 219

Abbreviations

AD Alzheimer's Disease

BET Brain Extraction Tool

BOLD Blood Oxygen Level Dependent

CSF Cerebrospinal Fluid

DTI Diffusion Tensor Imaging

FA Fractional Anisotropy

FAST FMRIB's Automated Segmentation Tool

FDT FMRIB's Diffusion Toolbox

FEAT FMRIB Expert Analysis Tool

FLIRT FMRIB's Linear Image Registration Tool

FNIRT FMRIB's Non Linear Image Registration Tool

fMRI Function Magnetic Resonance Imaging

FSL FMRIB Software Library

GM Grey Matter

LGN Lateral Geniculate Nucleus

MD Mean Diffusivity

MNI Montreal Neurological Institute

MRI Magnetic Resonance Imaging

MT Middle Temporal area (also area V5/Motion area)

OCT Optical Coherence Tomography

PCA Posterior Cortical Atrophy

RGC Retinal Ganglion Cells

RNFL Retinal Nerve Fibre Layer

ROI Region of Interest

S1 Primary Somatosensory Cortex

TBSS Tract-Based Spatial Statistics

tDCS Transcranial Direct Current Stimulation

TE Echo Time

TR Repetition Time

TRD Trans-synaptic Retrograde Degeneration

V1 Primary Visual Cortex (also striate cortex)

VBM Voxel-Based Morphometry

VRT Visual field Restitution Therapy

WM White Matter

Chapter 1

Introduction

1.1 Structure of the visual system

The retina is the point at which visual information first enters the brain, as light hitting the retina is converted into neural signals via phototransduction. From the retina, the majority of fibres project to the occipital cortex via the optic nerve, lateral geniculate nucleus (LGN) and the optic radiation, as shown in Figure 1.1. This projection, termed the geniculo-striate pathway, accounts for 90% of the fibres from the optic nerves. As these signals travel through the visual system, the retinal location from which they originated is preserved, as the optic nerve fibres maintain a topographic map of the retina, which provides a map of the visual world. Having passed through the optic nerves, the axons of ganglion cells originating in the nasal retina cross at the optic chiasm before entering the optic tract. In this way, visual information from each hemifield is split, and processed by the contralateral hemisphere. The axons terminate in the LGN, with fibres from each eye reaching different layers of the LGN, a separation that persists into the primary visual cortex (V1). In V1, the retinotopic organisation

of visual information is still in place, with neighbouring cells in the cortex processing adjacent locations in the visual field. Hemianopia, a visual field loss affecting one half of the visual field up to the vertical midline, results from damage along this route. Beyond V1, cortical visual processing broadly follows two streams, the ventral and dorsal pathways, which process 'what' and 'how' information respectively. The ventral stream projects to areas including V4, which has a role in the processing of colour (Bartels and Zeki, 2000) and the inferotemporal lobe. The dorsal stream projections include the middle temporal area (MT), a region that is important for the perception of motion (Newsome and Paré, 1988), and end in the parietal lobe. These pathways are also referred to as 'vision for perception' and 'vision for action' (Goodale and Milner, 1992). Both of these pathways receive information from the early visual areas, striate cortex and area V2.

There are a number of additional pathways from the eye to the brain, although they are considerably smaller, and often overlooked. The biggest retinal projection outside of the LGN is to the superior colliculus, which in turn projects to the pulvinar, which projects directly to extrastriate cortex (Warner et al., 2012). This pathway has roles in the control of eye movements and visual attention. Another substantial pathway which bypasses V1 also exists, projecting from the retina to the koniocellular layers of the LGN and then directly to area MT (Sincich et al., 2004). As these routes reach the visual cortex without passing through the primary visual cortex, the collicular and koniocellular pathways are often suggesting as candidates for the pathway underlying non-conscious residual vision, a phenomenon known as 'blindsight' (Leh et al., 2006a;

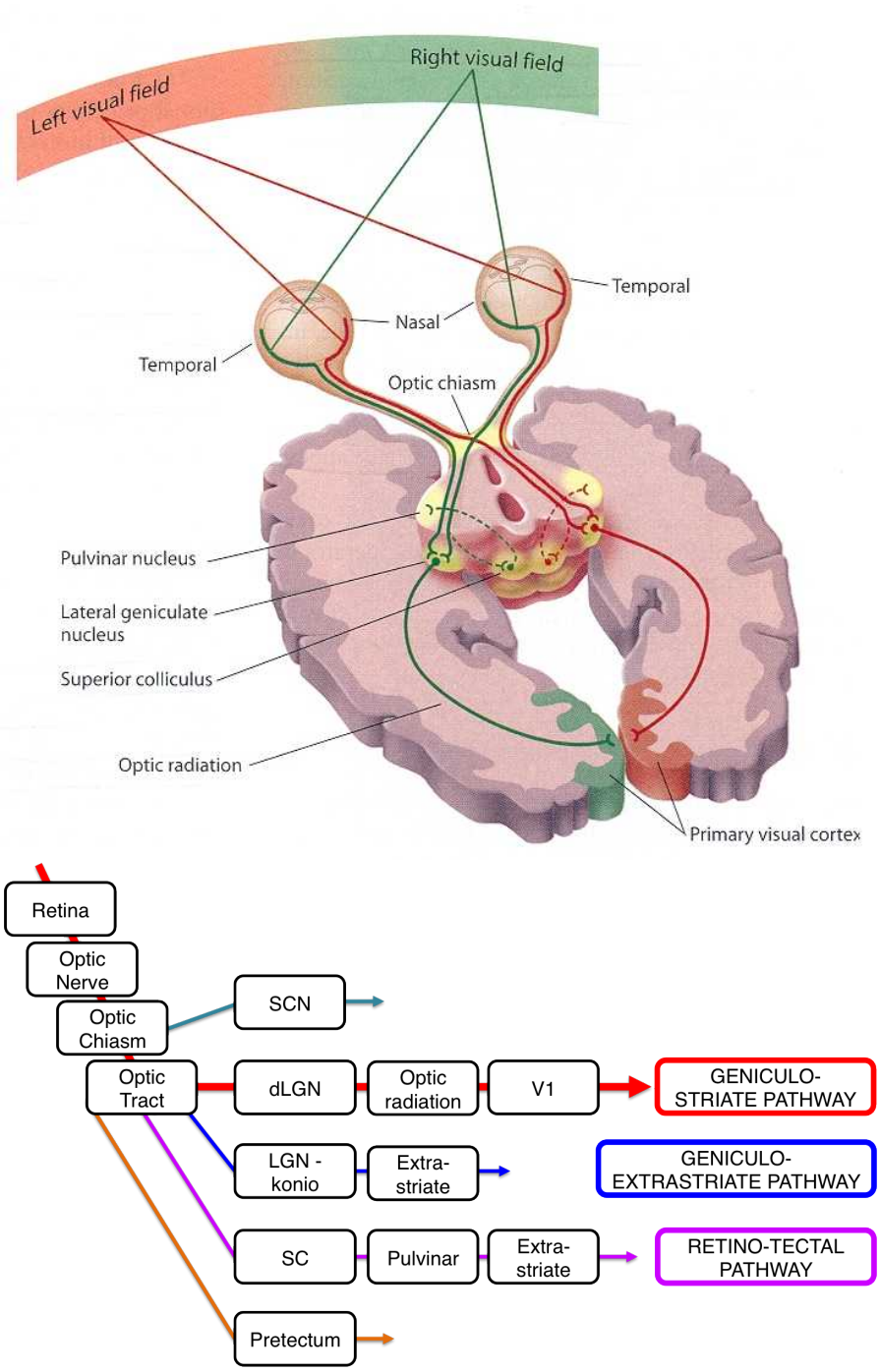

Figure 1.1: The main visual pathways. The top diagram depicts the primary visual pathway, showing the separate pathways that retinal information from the left and right visual fields follows into the contralateral hemispheres (Diagram reproduced from Hubel (1995)). Below, the key structures in this processing stream (the primary visual pathway, red arrow) are outlined, together with the structures in two known pathways that bypass V1 by passing through either the koniocellular layers of the LGN (blue) or the pulvinar (purple).

Cowey and Stoerig, 1991).

Other pathways also exist which relay various kinds of visual information. For example, direct retinal projections exist to the suprachiasmatic nuclei, which receive input from melanopsin expressing retinal ganglion cells, and help to entrain circadian rhythms. The pretectum, which modulates the pupil light reflex, also receives direct input from these photosensitive retinal cells without passing through the LGN.

1.2 Hemianopia

Hemianopia occurs when a patient suffers damage to the post-chiasmal visual pathway, most commonly the occipital lobe or optic radiation (Zhang et al., 2006c), resulting in a visual field deficit corresponding to the size and location of the damage. Hemianopia affects approximately 8% of stroke victims (Luu et al., 2010), and resolves in around 50% of cases, with spontaneous recovery rarely occurring more than two or three months post damage (Pambakian and Kennard, 1997; Zhang et al., 2006c).

Damage to different locations in the post-chiasmal visual pathway result in different visual field deficits, due to the ordering of the nerve fibres at different locations, as shown in Figure 1.2. Damage to the optic tract results in a full dense homonymous hemianopia, as this is the sole route for visual information leaving the optic chiasm once the fibres have decussated. Damage to the LGN will typically result in a superior quadrantanopia, presumably because LGN lesions are generally small and therefore complete destruction of the LGN is rare, usually affecting the regions that project through Meyer's loop of the optic radiation, which will also result in a superior quad-

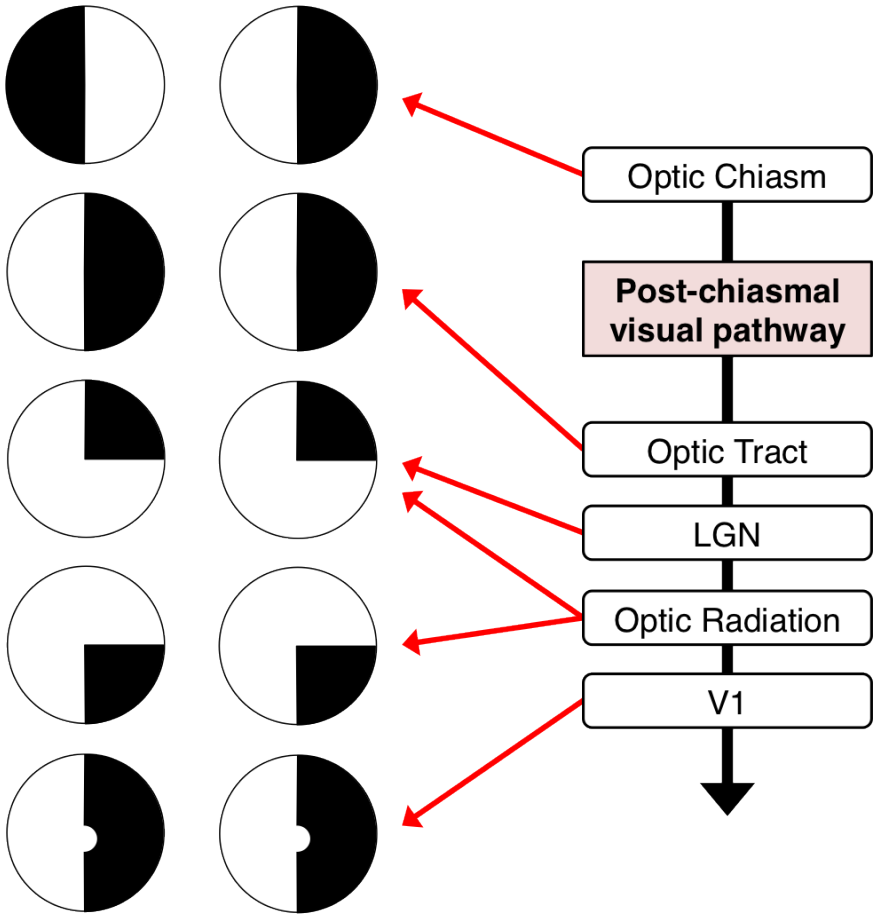

Figure 1.2: Visual fields deficits resulting from damage to different locations in the visual pathway. Lesions at any point after the optic chiasm in the primary visual pathway will result in a homonymous field deficit, which will vary in size and location according to the exact damage, as shown. While lesions to V1 often result in a hemianopia with macular sparing (as shown in the diagram), hemianopia can also be complete following V1 damage, with the same visual field loss as shown for optic tract damage. Lesions to the optic chiasm itself result in a bitemporal hemianopia. Left and right visual fields are shown, with the visual field deficit represented by black shading.

rantanopia when damaged. Damage to the shorter parietal portion of the optic radiation will result in an inferior quadrantanopia. Finally, damage to the striate cortex itself will result in a visual field deficit representative of the proportion of striate cortex that has been lost; a macular sparing hemianopia is typical of striate cortex damage where some portion of V1 is preserved, usually the occipital pole.

Homonymous field defects have been found to affect approximately 0.8% of persons over 49 years of age (Gilhotra et al., 2002), with between half (Gilhotra et al., 2002) and 70% (Zhang et al., 2006b) of these occurring in people who have had a stroke. Common difficulties experienced by hemianopia patients include increased likelihood of falls and collisions with objects due to a decreased field of vision and impaired distance perception (Luu et al., 2010). Perhaps the greatest negative impact on quality of life for some patients is the loss of the ability to drive, as any substantial visual field defect is considered grounds for revoking a driving licence. This is also frequently true in the case of patients with congenital (or peri-natal) field deficits that are discovered in adulthood, who may lose a driving license even though their vision has not changed. Another significant problem for hemianopia patients is a difficulty in reading, termed hemianopic alexia. The combination of mobility problems, loss of freedom to drive, and reading difficulties means that hemianopia can have a considerable impact on quality of life for patients. In spite of this, however, many patients are offered little in the way of rehabilitative assistance.

1.3 Different forms of hemianopia

Adult onset acquired hemianopia

Hemianopia is most commonly found following a sudden brain injury, for example following a stroke, trauma, or surgical intervention. Most homonymous hemianopias diagnosed occur following strokes, with ischemic strokes outnumbering haemorragic

strokes by more than 5 to 1 (Zhang et al., 2006a). These most often result in damage to the occipital cortex (54%), although lesions to other locations in the visual pathway do also occur. In contrast, hemianopias that do not have stroke as an initial cause typically result from locations other than the visual cortex, at various points in the retrochiasmal pathway.

Trauma is the second most prevalent cause of hemianopia. In an investigation of 880 patients with traumatic hemianopia, the majority following motor vehicle accidents, approximately 40% of patients were found to have a complete hemianopia (Bruce et al., 2006). In the majority of these patients, multiple lesion sites were observed. However, a reasonable number of patients studied suffered lesions restricted to either the optic tract, optic radiation, or occipital cortex. While the majority of hemianopias result from either stroke or trauma, a smaller but significant proportion occur due to other neurological causes, including brain tumours, epilepsy, and multiple sclerosis. In the case of epilepsy patients, several of whom were included in this study, a hemianopia could exist as a feature of the pathology giving rise to epilepsy, or could result from corrective surgery designed to stop or reduce the frequency of seizures (Blume et al., 1991).

Congenital hemianopia

Some patients are born with hemianopia, due to either congenital or perinatal brain damage. Such patients provide an interesting opportunity to investigate the potential for the visual system to reorganise in the face of damage, as the visual system is

considered to be at its most plastic early in life (Bourne, 2010); indeed studies of children with congenital or acquired lesions do appear to show a greater capacity for cortical reorganisation when the lesion occurs congenitally (Tinelli et al., 2012). Where the patient is otherwise healthy, the cause of the hemianopia is thought to usually be a developmental abnormality in the occipital cortex (Ragge et al., 1991). Such hemianopias frequently go undetected for many years, even until adulthood, as patients may be unaware of their unusually restricted visual field (Huber, 1992). In these cases, the hemianopia is often detected during routine testing at the opticians. The asymptomatic nature of the deficit in the majority of congenital patients is in stark contrast to the noticeable and debilitating deficit experienced by patients who acquire hemianopia later in life.

Posterior cortical atrophy

Posterior cortical atrophy (PCA) is a progressive neurodegenerative disease (Benson et al., 1988), commonly described as the visual variant of Alzheimer's disease. Patients show an early presentation of higher order visual processing deficits and only mild memory impairments, although memory deteriorates with progression of the disease. Neuroimaging typically shows marked atrophy of the parietal and occipital lobes, with the frontal lobes relatively spared. Up to 50% of PCA patients have a visual field deficit (Tang-Wai et al., 2004), the majority of which are asymmetric, resulting in a homonymous hemianopia or quadrantanopia. These types of visual field deficits have recently been characterised by Formaglio et al. (2009) and Pelak et al. (2011). However,

the neurological basis of the hemianopia is unknown.

1.4 Residual vision

While damage to the main post-chiasmal visual pathway usually results in a homonymous field deficit, the existence of other visual pathways suggests that some visual processing may still remain. Indeed, although visual field loss following damage to striate cortex is usually sufficiently extensive for patients to be reported clinically blind in one hemifield, a substantial literature exists reporting the existence of residual visual processing in the blind hemifield of some patients. The most famous of these so-called 'blindsight' (Sanders et al., 1974; Weiskrantz et al., 1974) patients is GY, whose ability to respond to consciously unseen visual stimuli has been well documented. The term blindsight refers to the ability of patients with damage to striate cortex to detect and discriminate visual stimuli in regions of the visual field where they are cortically blind, and which they claim not to be able to see (Cowey, 2010). The term has been extended to dissociate between fully unconscious 'unaware' processing (type 1 blindsight), and visual processing combined with some degree of 'aware' perception, a 'feeling of knowing' or some sensation that a visual event has occurred (type 2 blindsight) (Weiskrantz, 1998). Under these conditions, patients can localise stimuli and discriminate orientation of lines (Sanders et al., 1974; Weiskrantz et al., 1974), detect motion and discriminate direction of movement in simple stimuli (Azzopardi and Cowey, 2001). Patients have also been reported to discriminate between different wavelengths (Stoerig and Cowey, 1992), although this remains controversial, with other studies suggesting that

the ability to do so depends on other cues being present (Alexander and Cowey, 2010). While most studies into blindsight have focused on relatively low level processes, patients have also shown higher level processing, being able to distinguish different types of emotional facial expressions (de Gelder et al., 1999; Pegna et al., 2005). However it should be noted that many of the reported blindsight abilities remain controversial, with rigorous experimental protocols required to ensure that results are not the product of artefacts (Campion et al., 1983), and that effects are not mediated by components of the visual stimulus other than the ones being tested.

1.5 Anatomy underlying residual visual function in the blind field

The existence of blindsight raises interesting questions with regard to the potential neural pathways that may underlie this non-conscious processing. As outlined above, a number of pathways exist to the visual cortex that do not rely on the main geniculostriate pathway, and various studies have attempted to determine which of these pathways are being co-opted for residual processing in these patients. It has variously been argued that blindsight must depend on a pathway including the superior colliculus (Leh et al., 2010; Pegna et al., 2005), the pulvinar (Pegna et al., 2005) and the lateral geniculate nucleus (Schmid et al., 2010).

Sincich et al. (2004) confirmed the existence of a direct projection from the LGN to MT using retrograde tracers in macaque monkeys, finding that the majority of cells

projecting to MT lie in the koniocellular layers of the LGN. These cells carry the blue/yellow opponent signal to the visual cortex, thus if this pathway plays a role in subserving residual visual function, some colour selectivity favouring blue stimuli may be expected in blindsight. This appears however not to be the case, as when examining responses in the blind field to coloured moving stimuli, Alexander and Cowey (2013) found that even when the stimulus was blue, patients could not detect motion while the stimuli were isoluminant. There is however strong support for this route being important in the anatomy underlying blindsight. Schmid et al. (2010) found that blindsight could be eradicated following deactivation of the LGN in macaque monkeys with lesions to V1, with monkeys losing the ability to detect stimuli in the blind field. Additionally, fMRI showed that extrastriate responses to stimuli in the blind field disappeared after the LGN was deactivated, strongly suggesting that the responses were mediated by the retino-geniculo-extrastriate pathway.

Evidence also exists for involvement of the colliculo-pulvinar pathway in blindsight. A feature of the collicular route to vision is that it is blind to S-cone stimuli; this means that it has been possible for studies into residual vision to investigate a possible involvement of the superior colliculus in blindsight performance in human patients (Leh et al., 2006b, 2010). Thus far, evidence had supported the notion that at least some aspects of blindsight may be subserved by this collicular-pulvinar route to extrastriate cortex. For example, hemispherectomy patients have been shown not to exhibit 'attention blindsight' (where reaction times are enhanced following blind field stimulation) when stimuli that rely on S cone activation are presented in the blind field, in contrast

to a priming effect that is observed when otherwise identical achromatic stimuli are used (Leh et al., 2006b). In addition to this route, Warner et al. (2010) have demonstrated that a direct projection exists from the retina to the pulvinar, and from there on to area MT. It is not therefore necessary that pathways through the pulvinar to extrastriate cortex must include the superior colliculus.

1.6 Rehabilitation in hemianopia

Over the past few years, attempts have been made to develop therapies that may improve residual visual function in hemianopic patients, using behavioural training and interventions such as transcranial direct current stimulation (tDCS). The most widely used interventions fall into three main groups: optical therapies, eye movement training, and visual field restitution therapy (VRT), reviewed by Schofield and Leff (2009) and Ajina and Kennard (2012).

The least labour intensive approach to rehabilitating hemianopia involves the use of optical aids. Optical therapy typically involves using prisms to distort the visual field, giving patients a larger useful field of vision. This field expansion occurs as the prism shifts the visual scene by 15 to 20°, bringing the area at the edge of the scotoma into visual awareness. This can have a crucial impact on the ability of a patient to interact with the visual world, as foveated scenes will no longer be cut off at the midline. Indeed, studies investigating the effectiveness of optical therapy have reported an increase in the size of the visual field, and a noticeable improvement in function for patients, as they find it easier to avoid obstacles in their path (Bowers et al., 2008; Peli, 2000).

Perhaps the most heavily investigated compensatory technique in hemianopia has been training patients in the use of eye movements to bring the missing field of vision into play. Unlike unilateral spatial neglect, where patients cannot attend to the affected field of vision, hemianopia patients are aware of their blind area, and so can be trained to make saccades into the blind field. The majority of hemianopia patients have impaired visual search abilities, showing unusual search patterns characterised by repetitious scanpaths and fixations, both in the impaired hemifield, and, to a lesser extent, the unaffected hemifield (Zihl, 1995). Protocols have been developed to improve patients' ability to search the visual scene effectively. These generally involve patients performing target localisation, visual search, and, in the case of alexia rehabilitation, practice of specific eye movements useful for reading. These tasks encourage the use of larger eye movements and more systematic scanpaths, enlarging the searchable visual field. Eye movement training has had substantial levels of success in improving patients' ability to read in cases of hemianopic alexia (Schuett et al., 2008) and more generally in improving patients' ability to search the visual scene, including the hemianopic field (Zihl, 1995; Nelles et al., 2001).

These two methods both aim to increase the efficiency of any remaining visual processing. The third technique, VRT (Kasten et al., 1998), is significantly different in that it specifically aims to restore vision in the affected hemifield. VRT is an intensive treatment protocol, involving visual stimulation within the transition zone between the blind and unaffected area of the visual field while patients foveate a fixed point on a screen. An exceptionally labour intensive procedure, patients perform this

task daily for several months, and typically gain around 5° of vision. Recent work combining VRT with the application of tDCS has suggested that the clinical benefit of VRT can be increased with the application of electrical stimulation to the occipital cortex (Plow et al., 2011, 2012). Patients given tDCS stimulation showed more greatly reduced visual field deficits following VRT than patients given sham tDCS. Surprisingly however, it was the patients given sham tDCS who experienced a greater subjective experience of improvement, which raises the question of how useful the degree of visual field enlargement gained actually is in daily life. While a number of studies have found enlargements in the visual field following VRT and similar methods (Mueller et al., 2007; Schmielau and Wong, 2007), the technique remains controversial and has sparked much debate on the validity of these results (Horton, 2005b; Sabel, 2006). It has been argued that rather than effecting an enlargement in objective visual field size due to cortical reorganisation, the improvement in visual processing observed is instead a result of learned compensatory eye movements (Horton, 2005a; Reinhard et al., 2005).

Similar techniques to VRT have been employed to restore vision further inside the affected hemifield, with stimuli focused inside the blind field instead of on the borderline of the hemianopia. Sahraie et al. (2006) found increased visual sensitivity in the stimulated area following this form of rehabilitative training. The stimuli used in this protocol were specifically designed according to parameters known to enable blindsight in hemianopic patients, drawing on previous studies showing that the more patients are tested for sensitivity to blindsight stimuli, the better their visual performance becomes (Zihl, 1980). Such studies have raised interesting questions about blindsight as a route

to rehabilitation, however it is unclear to what extent this can translate to improving quality of life for patients, as they tend not to be overtly aware of these gains in sensitivity. Furthermore, as with VRT, commentators have suggested that any observed gains in performance may be related to increases in the usable visual field, due to the use of more effective eye movements post training (Pambakian and Kennard, 1997).

While various studies into the efficacy of rehabilitation in hemianopia have found positive results, others have found little noticeable improvement for patients, or none at all. There is also a high degree of variance in the extent to which different patients benefit from such interventions; while one may improve greatly, another may see no benefit, and it is difficult to predict which category any given patient will fall into.

1.7 Degeneration may hinder attempts to rehabilitate hemianopia

To different extents, the various rehabilitative approaches discussed require either that the neural pathways of the visual system do not significantly degenerate, or that some level of plasticity occurs, enabling the co-option of alternative pathways to vision. This is particularly true with respect to VRT and the use of blindsight pathways, which rely on access to functioning fibres in the damaged hemisphere.

It has been shown however, that following the loss of axonal target regions, trans-synaptic retrograde degeneration (TRD) occurs in the human visual system, such that cells earlier in the visual pathway atrophy over time. The existence of TRD has been

extensively investigated in non-human primates, since Van Buren (1963)'s demonstration of retinal ganglion cell loss following occipital ablation in a macaque monkey. The process appears to be rapid, with Weller and Kaas (1989) finding evidence of transneuronal degeneration as early as 3.5 weeks after ablation of striate cortex in infant monkeys. These examples bear a close parallel to hemianopia in humans, where the occipital cortex, specifically primary visual cortex, is frequently lesioned. Evidence from magnetic resonance imaging (Bridge et al., 2011) and optical coherence tomography (Jindahra et al., 2009) shows that the optic tracts and retinal ganglion cells do degenerate following damage to striate cortex. However, the degeneration that occurs following hemianopia has not been sufficiently well described to know how this may be impacting on attempts at rehabilitation. A better understanding of the time scale of this, as well as the impact of size and location of the lesion on degeneration, may help inform rehabilitative attempts, leading to better outcomes for patients.

1.8 The use of imaging to investigate visual dysfunction

Recent years have seen the development of a range of novel neuroimaging techniques, which allow non-invasive investigation of human brain structure and function with a level of detail that was not previously available. Whereas in the past, research investigating the fine detail of how brain regions interact and function has relied on invasive techniques in animals which can provide detailed information on neural circuitry, to-

gether with the relatively coarse information non-invasive techniques can provide in humans. However, with the advent of higher field magnetic resonance imaging (MRI) and increasingly sophisticated image acquisition and analysis protocols, the brain can now be imaged in enough detail to answer questions that were not previously accessible to patient studies.

The main MRI techniques currently being used to investigate the visual system include high-resolution structural imaging, diffusion-weighted imaging (or diffusion tensor imaging, DTI), and functional MRI (fMRI). As MRI advances, increasingly higher resolution structural images are becoming possible, to the point where researchers have been able to image small structures such as ocular dominance columns (Yacoub et al., 2007) using a 7 Tesla scanner. Although 3 T imaging is more standard in vision research, T1-weighted structural images can be used for a number of purposes, from cortical thickness analysis to segmentation of different cortical areas, to analysis of grey matter atrophy using voxel-based morphometry.

Diffusion tensor imaging is sensitive to water diffusion within the brain, and can therefore be used to identify white matter pathways in the brain, and quantify their integrity. The most commonly used approaches are to measure levels of fractional anisotropy (FA), which can indicate both the direction and strength of white matter tracts, and mean diffusivity (MD), high levels of which suggest white matter deterioration. An advantage of DTI is the ability to investigate connectivity between different brain regions, as demonstrated by Bridge et al. (2008) in an elegant investigation into the pathways which underlie residual vision exhibited by blindsight patient GY.

Functional MRI enables us to investigate how the brain responds to different types of stimuli, and therefore analyse how the function of patients with disordered vision differs from that of healthy controls. Functional reorganisation that has occurred in the visual system following either direct damage or loss of visual input may be revealed using fMRI, for example using retinotopic mapping to show reorganisation of striate cortex (Dilks et al., 2007), or by examining cortical activation to stimuli shown in the blind area of blindsight patients (Tinelli et al., 2012).

Neuroimaging enables analysis of the broad spectrum of structural and functional changes that occur in patients with disorders of the visual system, in a manner which is non-invasive, and generally undemanding of the patient. The ability to compare and combine results from these different techniques in patients with hemianopia may help to give a more complete picture of how the visual system reacts to damage than can be obtained using other methodologies. Increased knowledge may be used as a guide to better inform rehabilitative approaches and give patients an indication of their prognosis.

1.9 Synopsis of thesis

The overarching goal of this thesis is to characterise the structural and functional changes that occur in patients with different forms of hemianopia. Degeneration, functional activity, and visual pathway plasticity will be investigated, as will the effect of different type and location of lesion on these. A combination of structural and functional imaging, behavioural testing, and ophthalmological investigation will be used to

investigate these questions.

Four main research questions are asked, each forming a separate chapter. An overview of the experimental methods that are common to all subsequent chapters is given in Chapter 2, including scanning protocols and patient information. The first experimental chapter (Chapter 3) will examine the trans-synaptic retrograde degeneration that occurs in hemianopia. Chapter 4 investigates basic residual visual function in the blind field of patients, and uses functional MRI to measure responses to motion stimuli in the occipital cortex. Chapter 5 uses diffusion tensor imaging to investigate whether alternative visual pathways through the pulvinar are present in hemianopic subjects. Chapter 6 examines the neurological changes present in an unusual group of patients who have hemianopia as a result of posterior cortical atrophy, in an attempt to understand why these patients show visual field deficits. The implications of these investigations, together with suggestions for future work, are discussed in Chapter 7. The rationale and goals of each experimental chapter are briefly summarised below.

1.9.1 Overview of experimental chapters

Degeneration of the visual pathway (Chapter 3)

The first experimental chapter of this thesis examines atrophy of the early visual pathway using T1-weighted and diffusion imaging, specifically examining degeneration in the optic tract. While there is evidence that the visual system is able to adapt to some extent following damage, studies have also shown that considerable degeneration may occur. In cases where the striate cortex has been damaged, loss of retinal gan-

glion cells (RGCs) in foveal areas corresponding to the vision loss has been found in both monkeys and humans, despite no direct damage to pre-striate locations. This trans-synaptic retrograde degeneration (TRD) of RGCs, following the destruction of axonal target locations, has been demonstrated extensively in monkeys (Weller and Kaas, 1989; Cowey et al., 1999, 2011), with the greatest degeneration occurring 1-3 years post striate cortex ablation, although some degree of degeneration is present as soon as one month after the damage occurred. It has also been shown that degeneration of RGCs is greater in cases where the cortical lesion is more extensive (Cowey et al., 1999).

The existence of TRD in humans has been more controversial, however following a number of recent studies using optical coherence tomography and MRI, it has now been conclusively shown that the visual pathway does degenerate in patients with hemianopia (Bridge and Plant, 2012). However, small patient numbers in previous studies, together with a lack of range of lesions, has meant that the effect of lesion location, size and duration on TRD in human patients is unknown. As efforts at rehabilitation require that the visual system has not significantly degenerated, an understanding of the impact of these factors on degeneration will aid clinicians in planning rehabilitative strategies for individual patients.

Function in the damaged hemisphere (Chapter 4)

In the absence of early spontaneous recovery, evidence of reduction of the visual field deficit either naturally or though rehabilitation is rare, and controversial. Nonetheless,

even where there is no reduction in the size of the visual field deficit, there is evidence that visual function may not be completely lost within the blind field. A number of studies have demonstrated that some patients with damage to striate cortex retain the ability to localise stimuli in the blind field, and discriminate various features of the stimuli under certain conditions (Azzopardi and Cowey, 2001; Alexander and Cowey, 2010; Cowey, 2010), an ability known as blindsight. The capacity to discriminate moving stimuli is perhaps the least difficult form of blindsight to elicit in patients, and indeed converging evidence from transcranial magnetic stimulation (Silvanto et al., 2009), diffusion tensor imaging (Bridge et al., 2008), and functional MRI (Goebel et al., 2001) suggests that area MT can retain connectivity and some level of function in the absence of striate cortex, although these studies have for the most part focused on a single blindsight patient, GY.

To investigate the extent to which motion processing is preserved in a range of patients with hemianopia, functional activity in primary visual cortex and area MT in response to motion stimuli are examined using functional MRI. To explore whether patients are able to utilise any available motion processing, a subset of patients were tested for the ability to discriminate the direction of movement of luminance and colour defined stimuli in their blind field. In addition to being of interest in itself, as these questions have rarely been investigated in hemianopia patients with lesions outside of striate cortex, the results from this investigation are used in conjunction with structural analyses in the following chapter, in order to better interpret changes in the visual pathways in patients.

Alteration of the visual pathways (Chapter 5)

The existence of blindsight, and the capacity of the visual system to recover normal fields of vision following damage sustained very early in life (Werth, 2006) suggests that either cortical reorganisation must be possible in these patients, or that other visual pathways exist that bypass the lesioned area, usually V1. Evidence for plasticity in the visual system after damage has come from a number of imaging studies, where both functional and structural reorganisation have been documented (Nelles et al., 2007; Bridge et al., 2008; Brodtmann et al., 2009).

Diffusion tensor imaging provides a method of examining these visual pathways in patients, and here it is used to investigate a potential route by which retinal information may reach area MT via the pulvinar, thereby bypassing both the LGN and primary visual cortex. Results from this investigation are compared to the findings from functional analyses in the preceding chapter (Chapter 4), to ascertain whether any structural alterations found could underlie preserved visual function.

Changes in structure and function in posterior cortical atrophy (Chapter 6)

The final experimental chapter examines a different cohort of patients from the previous three chapters. The patients studied here have visual field deficits resulting from posterior cortical atrophy. While a number of studies have investigated the differences between PCA patients and both healthy controls and Alzheimer's patients, the pathological basis of the hemianopia patients is unknown. To address this question, a range of structural and functional imaging techniques are employed to characterise the

pattern of atrophy that underlies this loss of visual function.

1.9.2 Summary

Hemianopia is a highly heterogeneous disorder, with a large variation in outcomes for patients, both in terms of recovery, and capacity for residual visual function in the blind field. Changes in structure and function are investigated in patients with hemianopia that has occurred either congenitally, in adulthood, or as a result of a neurodegenerative disease, with a view to understanding the ways these forms of hemianopia differ, and how atrophy, plasticity, and preserved function are affected by variations in the type of lesion causing the hemianopia.

Chapter 2

General Methods

2.1 Patients

Patients were recruited with hemianopia caused by three broad aetiologies: congenital, sudden onset acquired, and posterior cortical atrophy (PCA). In addition to the patient groups, twelve healthy controls were scanned for the hemianopia group (age range 21-74, mean age 46, 6 females) together with 8 older healthy controls for the PCA study (age range 73-85, mean age 77, 4 females). All healthy controls had normal or corrected to normal vision. PCA patients are described in Chapter 6. Twenty-six subjects with substantial unilateral visual field deficits were recruited. Hemianopia patients are labelled according to lesion location (optic tract (T), LGN (L), optic radiation (R), striate cortex (S), full occipital cortex loss (O)), and whether their field deficit was congenital (c) or acquired (a). Patients were recruited in either the UK or Brazil. UK patients were recruited from either London or Oxford and imaged in Oxford, and

Brazilian subjects were recruited and imaged at the Hospital das Clínicas, Unicamp. The Oxford study was granted ethical approval from the Oxfordshire National Health Service Research Ethics Committee (08/80605/156), and the University of Campinas' ethics committee approved the Brazilian study, project 1158/2009. All subjects gave written informed consent prior to participation.

2.1.1 Patients with sudden onset acquired hemianopia

Seventeen subjects with substantial acquired unilateral visual field deficits were recruited. The patient group included 6 females, with an age range of 27-73 (mean age 46) at the time of being scanned. All seventeen acquired subjects sustained visual pathway damage in adulthood, with the exception of S3a whose lesion was acquired at age 8. The oldest age of acquisition was age 67. Details for these patients are given in Table 2.1, and more detailed information regarding each patient's lesion can be found in Appendix A. Two patients with temporal lobe resections were initially reported by the referring clinician as having damage to Meyer's loop, however on inspection of structural scans and in light of their dense hemianopia, they were classified as having direct damage to the optic tract (T3a and T4a).

Six patients who had recently acquired a hemianopia were scanned on more than one occasion (starred in Table 2.1). In these cases, the first scan took place within eighteen months of lesion acquisition, and the second scan took place at least one year later. Details for these patients in Table 2.1 refer to the latest scan acquired.

Table 2.1: Acquired patient details.

	Gender	Age	Lesion location		Cause	Duration	HVF	Scan
T1a*	M	40	Right	optic tract	Trauma	3	−31.7	UK
T2a	M	56	Left	optic tract	Trauma	3.5	−30.8	UK
T3a	F	55	Left	optic tract/radiation	Resection	1.5	−30.0	BR
T4a*	F	42	Right	optic tract/radiation	Resection	4	−32.6	BR
L1a*	F	44	Left	LGN	Stroke	3	−22.1	UK
R1a	M	48	Right	radiation	Stroke	3	−30.2	UK
R2a	M	54	Right	radiation	Stroke	5	−31.3	UK
R3a	F	50	Right	radiation (Meyer's loop)	Resection	2.5	−16.6	BR
S1a	M	73	Left	V1+	Resection	18	−23.2	UK
S2a	M	46	Left	V1+	Stroke	5	−29.3	UK
S3a	M	53	Left	V1+	Trauma	45	−31.5	UK
S4a*	M	67	Right	partial V1	Stroke	2	−15.6	UK
S5a*	M	31	Left	partial V1+	Resection	3	−17.2	BR
S6a*	F	57	Right	partial V1	Stroke	3	−16.0	UK
O1a	F	29	Right	full visual ctx	Resection	7	−32.2	BR
O2a	F	46	Left	full visual ctx	Resection	7	−30.8	BR
O3a	F	40	Right	full visual ctx	Resection	6	−30.9	BR

HVF Mean deviation scores are given, averaged over the affected hemifield in each eye
Duration Time elapsed since lesion acquisition in years

2.1.2 Patients with congenital visual pathway damage

Nine subjects with congenital visual field deficits were recruited (see Table 2.2). At the time of scanning, patient ages ranged from 27 to 58 (mean age 42). In this group, none of the patients were aware of having experienced any incident where their vision changed; they either reported that the VF loss had always been present, or that their visual field had never changed. In most cases, they did not consider the VF deficit to have any noticeable impact on daily life, and indeed were usually unaware that the deficit existed. Note that this lack of awareness was not in these patients an indication of neglect, rather that they were unaware of a visual field loss, as the visual field that they had was normal for them. Subjects described as congenital may in some cases

Table 2.2: Congenital patient details.

Patients	Gender	Age	Lesion location		HVF	Scan
L2c	F	30	Left	LGN/radiation	−20.8	UK
R4c	M	30	Left	radiation/V1	NA	UK
R5c	M	30	Right	radiation/ extrastriate ctx	−12.6	UK
S7c	F	27	Left	V1	−34.0	UK
S8c	M	37	Right	V1	NA	UK
S9c	F	58	Left	V1	−24.3	UK
S10c	M	38	Right	V1	−25.1	UK
S11c	F	27	Right	V1 +	−28.8	BR
S12c	M	54	Left	V1	−16.9	UK

HVF Mean deviation scores are given, averaged over the affected hemifield in each eye

have acquired damage post-natally, however the damage would have occurred very early in life. In congenital patients the field defect is often picked up by chance at a sight test, not infrequently during adulthood. It is therefore not necessarily possible to determine the exact period at which damage was sustained. Since there is no obvious event causing the damage, and patients are generally unaware of the field deficit, it is reasonable to assume that damage is likely peri-natal. Furthermore, given the absence of any suggestion of birth trauma or an injury or illness in early life such as encephalitis, it is likely to be predominantly pre-natal. The majority of the congenital patients included had damage to striate cortex (n=6), with the other patients having damage to either the LGN (n=1) or the optic radiations (n=2).

2.1.3 Patients with posterior cortical atrophy

All investigations of PCA patients are reported together in Chapter 6 and so further details of these patients will be given there. In addition to the PCA patients and older

healthy controls, twelve patients with typical Alzheimer's disease were also included for comparison with PCA patients.

2.2 Perimetry

Humphrey visual fields (HVF) were acquired using a Zeiss Humphrey Field Analyzer, using the central 24-2 threshold test and SITA-FAST strategy. Fields for all included patients showed a substantial field loss (incomplete hemianopia was accepted, with a minimum loss requirement of a quadrantanopia) in the hemifield contralateral to the lesion site. The grey-scale overview of the field loss is used for display purposes, however the mean deviation for each patient was used for analyses, and is given in Tables 2.1 and 2.2. Visual fields for the left eye of each subject can be found in Appendix B, and two example fields are given in Figure 2.1. Humphrey perimetry was not available for R4c and S8c.

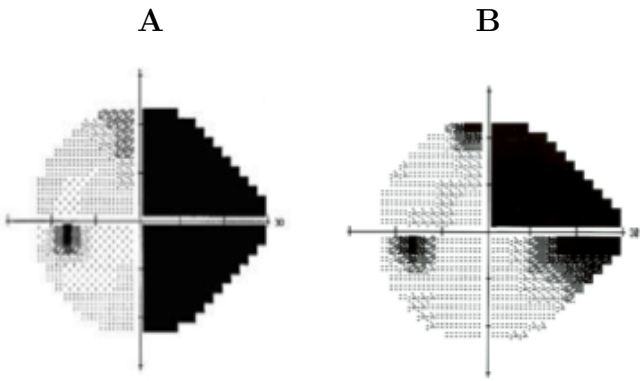

Figure 2.1: Examples of Humphrey visual fields. A: Right hemianopia (S2a). B: Right superior quadrantanopia, extending slightly into the inferior quadrant (L1a). Left eyes are shown.

2.3 Image acquisition and pre-processing

Functional, diffusion weighted and high-resolution structural scans were acquired for all participants. Details of how images were acquired and the stimuli used for functional scans follow. All MRI images were pre-processed and analysed using Oxford Centre for Functional MRI of the Brain's (FMRIB) software library (FSL; Smith et al. (2004)), unless otherwise stated. Scans in both the UK and Brazil were acquired on 3 T scanners, and protocols were designed to be as similar as possible, while maximising the quality of scans acquired. For many of the analyses carried out, no difficulties would be incurred by the use of different scanners, as analyses compared the lesioned and intact hemispheres in the same patient, rather than comparing across subjects directly.

2.3.1 Structural imaging

Scans acquired in the UK
Data was acquired using a 3 T Siemens TIM Trio at the Oxford Centre for Clinical Magnetic Resonance Research (OCMR).
T1-weighted structural scans were acquired axially at a resolution of 1 mm^3, 192 slices, TR = 2.04 s, TE = 4.7 ms

Scans acquired in Brazil
Data was acquired using a 3 T Achieva-Intera Philips scanner.
T1-weighted structural scans were acquired sagittally at a resolution of 1 mm^3, 180 slices, TR = 7 ms, TE = 3.2 ms.

T1-weighted structural scans were skull stripped using the FMRIB brain extraction tool (BET), and used primarily for registration purposes in addition to optic tract analysis (Chapter 3). Except in the case of patients with very small subcortical lesions (for example to the optic tract), lesion masks were created using patients' structural

scans, with the aid of T2-weighted scans where they were available. Lesion masks were hand drawn using FSLView, covering all brain regions where brain tissue was either visibly damaged, abnormal or absent. A number of registration steps were undertaken using each subject's structural scans. Brain extracted structural images were linearly registered to the MNI standard 2mm brain using FLIRT (Jenkinson and Smith, 2001). Using the FLIRT registration as an input, structural scans were then non-linearly registered to standard space, with the inverted lesion mask used to exclude the lesioned area from registration. The standard parameters for non-linear registration of a T1 image to the 2mm standard brain were input using the FSL configuration file. Invwarp was used to create the reverse registration matrix, from the standard brain to structural space.

Structural scans were also processed using recon-all, Freesurfer's automated reconstruction tool (http://surfer.nmr.mgh.harvard.edu/). This produces inflated brain surfaces on which to display data, together with segmentations which enable identification of different brain structures, and a number of statistics for measures of different brain structures, including, for example, cortical thickness and grey matter volume. Where patients had large lesions or marked atrophy, the automated output from Freesurfer was manually edited to correct errors relating to misinterpretation of lesions.

2.3.2 Functional MRI

Functional magnetic resonance imaging (fMRI) is a type of magnetic resonance imaging which allows us to identify the parts of the brain which are active during different

mental processes, and to investigate the time-courses over which these activations occur. This is achieved by measuring increases and decreases in blood oxygenation levels (the BOLD response) over time. This gives an indirect measure of neural activity in an area, by measuring how much energy is being used in specific regions of the brain, as inferred by changes in blood volume and deoxyhaemoglobin content. In this study, fMRI was primarily used to identify the brain regions involved in different aspects of visual processing, in order to identify differences in cortical organisation between hemianopia patients and healthy controls. While other non-invasive techniques for measuring brain activity such as electroencephalography (EEG) may have better temporal resolution than fMRI, which has a temporal resolution of seconds rather than milliseconds, fMRI has the advantage that it can give high spatial resolution. Spatial resolution for fMRI is on the level of a few millimetres at 3 Tesla, and can therefore be used to investigate reorganisation and activity in different regions of the visual cortex. The BOLD response is slow in comparison to the rapid speed of neural firing, as it is dependent on the speed of cerebrovascular reactivity, or changes in blood flow. However in this study, this was not a crucial factor as stimuli were presented for relatively long periods of time, and the haemodynamic response speed was modelled in the fMRI analysis.

FMRI consisted of two scans with similar motion stimuli presented in different locations. Both scans utilised a block design, with each stimulus (and rest periods) being presented for 16 seconds. Scan one (central motion) stimuli consisted of a circular patch of black dots presented centrally on a white background, generated using a VSG 2/5 graphics card (Cambridge Research Systems). The dots were either stationary or

fMRI Protocol for UK scans
Scans 1 and 2 were carried out
Scan 1 stimuli were generated using a VSG 2/5 graphics card
Scan 2 stimuli were initially programmed in presentation,
(From 06/12 reprogrammed in MATLAB due to computer compatibility issues)
Resolution of 3 mm^3 (48 transverse slices, TR = 4 s, TE = 30 ms)
For images acquired after 06/12, TR = 2 s, TE= 49 ms

fMRI Protocol for Brazil scans
Scan 2 was carried out, with stimuli programmed using Eprime
Resolution of 3 mm^3 (40 transverse slices, TR = 2 s, TE = 30 ms)

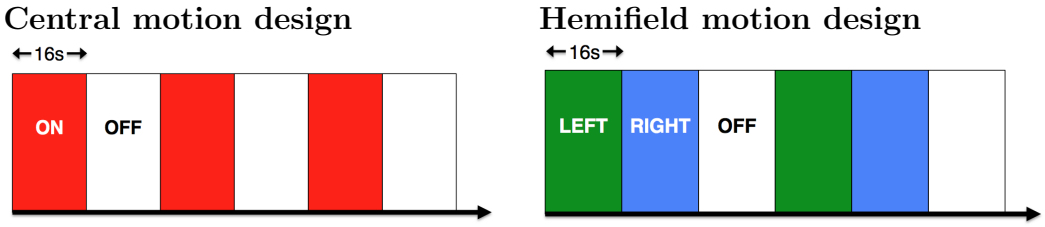

Figure 2.2: Time course of fMRI scans

moving radially at a speed of 30 deg/s, reversing direction every second. 8 cycles of the stimuli were presented, each lasting for 32 seconds, 16 seconds each for moving and stationary blocks. In the second scan (hemifield motion), an oval patch of dots moving outwards from a central point was presented either to the left or right of fixation (see Figure 2.3 for an example). The dots were visible for 16 seconds in each location, and alternated between left, right, and a 16 second rest period with no stimulus, repeated 6 times to make a total of 18 blocks. In both fMRI scans, subjects were instructed to fixate a central point for the duration of the scan.

Due to changes in available equipment, stimuli for scan two were reprogrammed part way through acquiring data. Initially, the stimuli were programmed in presentation, and they were reprogrammed using MATLAB. The presentation software used a pre-

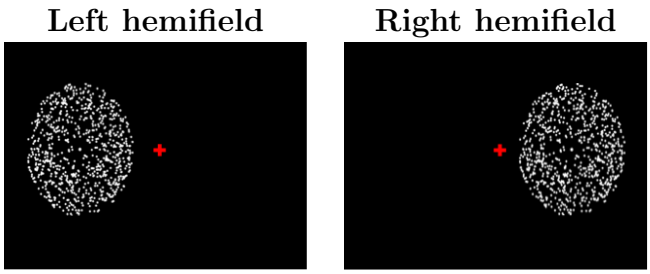

Figure 2.3: Screenshot of the moving dot stimuli presented in scan two: hemifield motion.

made video clip of the motion stimuli. Due to compatibility issues, it was not possible to import this clip into MATLAB, and so the stimulus was remade from scratch. Every effort was made to ensure that the new stimulus was as close as possible to the original stimulus. Patients scanned after this change included the last scans for T2a and L1a, R5c, S8c, S9c, S10c, S12c, and all PCA patients. At the time this change was made, the protocol for fMRI scans was also changed to halve the TR from 4 s to 2 s, and the TE was changed from 30 ms to 49 ms. The original values for TR and TE had been used to be consistent with earlier scans acquired, however it was decided that it would be beneficial to change these, to improve the quality of the data acquired.

fMRI data was primarily analysed using FMRIB's FMRI expert analysis tool (FEAT). General linear model (GLM) analysis was applied to identify voxels which were significantly more active during stimulus blocks than during rest periods. For display purposes, statistical maps produced from this analysis were projected onto inflated brains produced using Freesurfer. Further details of these analyses can be found in Chapter 4.

DTI Protocol for UK scans
Two sets of whole brain diffusion weighted data were acquired.
The diffusion weighting was isotropically distributed along 60 directions b-value 1000 s/mm^2, 65 slices; 2 mm^3 voxels; TR = 9.3 s, TE = 94 ms.
Volumes without diffusion weighting (b-value 0 s/mm^2) were acquired for both sets of data.

DTI Protocol for Brazil scans
One set of whole brain diffusion weighted data was acquired.
The diffusion weighting was isotropically distributed along 32 directions b-value 1000 s/mm^2, 70 slices; 2 mm^3 voxels; TR = 8.5 s, TE = 61 ms.
Volumes without diffusion weighting (b-value 0 s/mm^2) were acquired throughout the sequence.

2.3.3 Diffusion-weighted imaging

Diffusion tensor imaging (DTI) measures the diffusion of water molecules in different directions through the brain. In the absence of any barriers to diffusion, as in cerebrospinal fluid, diffusion occurs at the same rate in all directions, giving an isotropic pattern of diffusion. However, the diffusion of water molecules in white matter is constrained by the fibre bundles present, as water can diffuse more freely along the direction of a fibre bundle than in the perpendicular direction. This results in anisotropic diffusion in voxels containing white matter. The level of anisotropy, and the principal direction of diffusion, are influenced by a number of factors, including fibre density, fibre diameter, and the extent of myelinisation of fibres, each of which can increase the amount of coherent diffusion (Beaulieu, 2002). The integrity of white matter can therefore be estimated by computing fractional anisotropy (FA), which measures the level of anisotropy in each voxel in the brain, which ranges from completely isotropic diffusion (0) to diffusion along one axis only (1).

Diffusion images were first corrected for distortions resulting from eddy-currents and

head movements. Images were skull stripped using the brain extraction tool (Smith, 2002). For data acquired in Oxford, the two sets of data were averaged to increase the signal noise ratio. Diffusion tensor models were applied using DTIFIT, part of FDT (FMRIB's diffusion toolbox) to obtain images of fractional anisotropy (FA) and mean diffusivity (MD) levels. BedpostX was then run on the DTI data for each subject in order to create the files necessary to run probabilistic tractography.

Chapter 3

Quantifying the pattern of optic tract degeneration in human hemianopia

3.1 Abstract

Objective To quantify the dependence of human trans-synaptic retrograde degeneration (TRD) on lesion location and size in a large population of hemianopic subjects with either acquired or congenital damage.

Methods T1-weighted structural and diffusion-weighted images were obtained for 26 patients with hemianopia and 12 age-matched controls. The optic tract (OT) was defined and measured in both the structural and DTI images, and degeneration assessed by comparing the integrity of tracts in the lesioned and undamaged hemisphere.

Results Human patients with hemianopia show a similar pattern of TRD following post-chiasmal lesions to that seen in non-human primates. Optic tract degeneration was found in all patients with established lesions, regardless of lesion location. In patients with acquired lesions, the larger the initial lesion, the greater the resulting trans-synaptic degeneration. However, this was not the case for congenital patients, who generally showed greater degeneration than would be predicted by lesion size. A better predictor of TRD was the size of the visual field deficit, which showed significant correlation with degeneration across all patients. Interestingly, although DTI is more frequently used to examine white matter tracts, for this study the T1-weighted scans gave a better indication of the extent of tract degeneration.

Interpretation TRD of the optic tract occurs in both acquired and congenital hemianopia, is correlated with visual field loss in all cases, and is most severe in congenital cases. Understanding the pattern of TRD may help to predict effects of any visual rehabilitation training.

Note An edited version of this chapter has been accepted at the Journal of Neurology, Neurosurgery, and Psychiatry.

3.2 Introduction

Trans-synaptic (also known as trans-neuronal) retrograde degeneration (TRD) in the optic tract has recently been demonstrated in patients with damage to the visual cortex. However, the time-course of this degeneration is unknown, as is the role of lesion

extent on the severity of TRD. The current study used evidence from T1-weighted and diffusion-weighted MRI to quantify optic tract degeneration in a heterogeneous cohort of patients with substantial visual field deficits.

3.2.1 Potential for recovery in hemianopia

In cases where a hemianopia has not resolved within the first few months, the likelihood of a patient recovering any of the lost visual field is low. With varying degrees of success, a number of different therapies have been proposed which aim to improve visual function in hemianopia. Some, such as vision restoration therapy (Mueller et al., 2007) and Neuro-eye therapy (Sahraie et al., 2010), aim to restore vision in the affected hemifield. In the event that the visual system has already undergone significant degeneration prior to attempts to introduce these therapies, the potential for them being effective may be limited by the loss of fibres in the visual pathway. It is therefore important to understand the time scale and extent of degeneration, as well as the impact of size and location of the damage.

3.2.2 TRD in non-human primates

TRD of retinal ganglion cells (RGCs) following the destruction of axonal target locations has been investigated extensively in monkeys. Weller and Kaas (1989) found both LGN degeneration and RGC loss in infant monkeys as early as 3.5 weeks after V1 ablation. Lesions made in adolescents also led to evidence of cell loss, although to a lesser extent than in infants. In contrast however, TRD was absent in adult New

World Monkeys, suggesting the degeneration was limited to a certain developmental time window. Cowey et al. (1999, 2011) have demonstrated that retinal ganglion cell counts in the fovea are lower in the area corresponding to the blind hemifield than in adjacent unaffected regions of hemianopic monkeys, most of whom were between 2 and 5 years old when lesioned. This effect was present in all monkeys tested, with the greatest rate of RGC loss between 1-3 years after the damage, after which ganglion cell number appeared to be more stable. Furthermore, Cowey et al also found that RGC loss was greater in monkeys with larger cortical ablations. Where TRD does occur, the degeneration results in around 80% loss of RGCs in the affected foveal regions following complete ablation of striate cortex, predominantly cells that would have projected to the parvocellular layers of the LGN (Cowey et al., 1989), which enable fine spatial discrimination and colour opponency in the visual system.

3.2.3 TRD in the human visual system

In contrast to the literature from the macaque, whether TRD exists in the human visual system has been more controversial, with some reports of RGC loss in human patients criticised for not examining pure cases of hemianopia. However, various studies have found evidence of TRD in patients, including histological evidence of RGC loss in patients with optic tract or optic chiasm damage (Kupfer 1963), and occipital lobe resection (Beatty et al 1982). The advance of non-invasive human imaging approaches have now enabled several studies to show conclusive evidence in multiple hemianopic patients (reviewed by Bridge and Plant (2012)).

More recently, optic tract measurement has been used to assess TRD, using the ratio of the tract on the two sides. This method has been employed both in monkeys (Cowey et al., 2011) and in humans (Bridge et al., 2011; Cowey et al., 2011). The latter authors found that optic tract ratios in monkeys (measuring the area of the tracts in multiple cross sections post mortem) were significantly correlated with RGC ratios, with the monkeys showing the greatest loss of RGCs also showing the largest reduction in ipsilesional optic tract volume. Both measurements were similarly related to survival time, showing the greatest decline one to three years post ablation. The authors extended the technique to measure OT ratios in hemianopic humans, measuring absolute OT volume in structural MRI images. The affected OT had a reduced volume in three out of four patients, all of whom had long established lesions. A fourth patient, whose lesion was under one year old, did not show evidence of a reduction in the optic tract, supporting the view that the degeneration occurs over time, and is not a result of the initial insult.

Similarly, Bridge et al. (2011) used structural MRI to investigate whether the optic tract in the damaged hemisphere showed evidence of degeneration in a number of hemianopic subjects with damage to different locations in the visual pathway, including damage to the tract itself, the LGN, and occipital cortex. By comparing the area and volume of the affected and unaffected tracts at a range of intensity thresholds in each patient, the authors found evidence of reduced optic tract size and integrity in all patients with longstanding lesions. As this atrophy was detected in patients with damage beyond the optic tract (for example, in V1), and was greatest in those patients

with longer established lesions, this is good evidence for TRD.

Optical coherence tomography (OCT) provides further evidence for TRD in the human visual system. The retinal nerve fibre layer (RNFL) is reduced in patients with congenital and acquired hemianopia (Jindahra et al., 2009), indicating loss of retinal ganglion cells following damage to the post-chiasmal visual pathway. Furthermore, the RNFL thickness decreases over time following injury (Jindahra et al., 2012a) and can be demonstrated in patients with quadrantanopia secondary to occipital lobe damage (Jindahra et al., 2012b).

3.2.4 Aims of the present study

This study aims to determine whether the pattern of TRD demonstrated elegantly in the macaque is also present in human patients. Here dependence of human TRD on lesion location and size is quantified in a large population of hemianopic subjects, some with acquired, and others with congenital, damage.

Although the study of non-human primates indicates that the extent of TRD is related to a number of factors, including lesion size, and time since lesion acquisition, the relationship between TRD and these factors has not been addressed in human subjects. The aim of the present study was to address this, by investigating optic tract degeneration in a larger group of patients than has been previously investigated, using an adaptation of the technique used by Bridge et al, and extending this to include diffusion-weighted imaging. The cohort includes patients with a variety of lesion sites and sizes, ranging from patients with pure LGN damage to those with full occipital

cortex resections; enabling analysis of the effect of lesion size on TRD. Furthermore, a number of patients were scanned more than once since injury, allowing investigation of whether degeneration of the optic tract increases over time, and the time period over which this occurs.

3.3 Methods

3.3.1 Subjects

Twenty-six subjects with substantial unilateral visual field deficits were recruited, together with twelve age-matched controls. Patients were recruited and scanned in both Brazil and the UK. Key details for each patient are given in Table 3.1, further details can be found in Chapter 2 (Table 2.1 and 2.2). Subjects described as congenital (n=9) may in some cases have acquired damage post-natally, however the damage would have occurred very early in life. All seventeen acquired subjects sustained visual pathway damage in adulthood, with the exception of S3a whose lesion was acquired at age 8. Humphrey perimetry was not available for R4c and S8c, and DTI data was not collected for S3a. Data from 5 of the subjects presented here were included in a previous study (Bridge et al., 2011).

Six subjects were scanned more than once (starred in Table 3.1). The first scan took place within eighteen months of lesion acquisition, and the final scan took place at least one year later. Age and lesion duration details in Table 3.1 refer to the latest scan acquired.

Table 3.1: Characteristics of hemianopic subjects

	Damaged hemisphere	Lesion location	Duration (y)	Mean Deviation HVF
T1a*	Right	optic tract	3	−31.7
T2a	Left	optic tract	3.5	−30.8
T3a	Left	optic tract/radiation	1.5	−30.0
T4a*	Right	optic tract/radiation	4	−32.6
L1a*	Left	LGN	3	−22.1
R1a	Right	radiation	3	−30.2
R2a	Right	radiation	5	−31.3
R3a	Right	radiation (Meyer's loop)	2.5	−16.6
S1a	Left	V1+	18	−23.2
S2a	Left	V1+	5	−29.3
S3a	Left	V1+	45	−31.5
S4a*	Right	partial V1	2	−15.6
S5a*	Left	partial V1+	3	−17.2
S6a*	Right	partial V1	3	−16.0
O1a	Right	full visual cortex	7	−32.2
O2a	Left	full visual cortex	7	−30.8
O3a	Right	full visual cortex	6	−30.9
L2c	Left	LGN/radiation	congenital	−20.8
R4c	Left	radiation/V1	congenital	NA
R5c	Right	radiation/extrastriate cortex	congenital	−12.6
S7c	Left	V1	congenital	−34.0
S8c	Right	V1	congenital	NA
S9c	Left	V1	congenital	−24.3
S10c	Right	V1	congenital	−25.1
S11c	Right	V1 +	congenital	−28.8
S12c	Left	V1	congenital	−16.9

3.3.2 Data acquisition

Diffusion-weighted and T1-weighted structural scans were acquired using either a 3T Siemens Trio (UK) or a 3T Achieva-Intera Philips scanner (Brazil). Standard protocols for T1 and DTI acquisition were used, with T1-weighted scans acquired at a resolution of 1x1x1mm^3, and DTI scans with 2mm^3 isotropic voxels. See Chapter 2 for full parameters used for each scanner. As analyses focused on within subject comparisons, no issues were incurred by the use of two different scanners.

Visual fields for all patients were acquired using a Zeiss Humphrey Field Analyzer, using the central 24-2 threshold test and SITA-FAST strategy. All patients showed a substantial field loss in the hemifield contralateral to the lesion site (incomplete hemianopia was accepted, with a minimum loss requirement of a quadrantanopia). The mean deviation for each patient is given in Table 3.1.

3.3.3 Analysis of degeneration using T1-weighted imaging

Definition of the optic tract

To ensure that optic tract definition was not affected by head orientation in the scanner, T1-weighted structural scans were reoriented using FSL image analysis software so that the optic tract was parallel to the Anterior Posterior axis in standard space, and then resliced parallel and perpendicular to the optic tract. The optic tract was measured using an adaptation of the technique used by Bridge et al. (2011). Masks of equal size were hand drawn over the optic tract in FSLview, starting at the optic chiasm and continuing until the optic tract was no longer distinct from surrounding structures.

For analysis of optic tract volume and integrity, voxels in the masked region were thresholded according to their T1-weighted signal so that only voxels containing white matter were included in analysis. Intensity thresholds ranged from a minimum of 25% of the greatest intensity in either tract (the least conservative measurement used), to a maximum of 85% (leaving only voxels with high white matter integrity), rising in increments of 5%. The number of voxels included in the mask was reduced as the intensity inclusion criterion rose, and in this way, optic tract size could be compared

between the two hemispheres at different levels of white matter integrity.

A laterality index (LI) was computed to quantify the difference in volume and integrity between the left and right optic tracts at each white matter threshold. The LI ((contralesional - ipsilesional)/(contralesional + ipsilesional)) was computed using the tract volumes for all intensity threshold levels. In control subjects, the LI was calculated in a similar manner, with LI = (right - left)/(right + left); there was no reason to expect control subjects to have any difference between right and left optic tract, and indeed 7 showed an average positive index, while 5 showed an average negative index. Patient LIs were compared to controls by computing z statistics ((patient score - control mean) / control standard deviation) at each threshold.

Quantification of lesion size in patients with occipital lobe lesions

In order to assess whether optic tract degeneration was related to the extent of damage to the visual cortex, the volume of the lesion within the occipital lobe was measured in subjects with established cortical damage. T1-weighted structural scans were used to identify regions containing abnormal or absent tissue within the occipital lobe, and a mask of this region was created manually using FSLview. A second mask, encompassing the entire occipital lobe in the lesioned hemisphere, was also drawn and a comparison of the sizes of these masks was used to determine the proportion of occipital damage.

3.3.4 Analysis of degeneration using diffusion-weighted imaging

The optic tract was identified for analysis in the diffusion-weighted images using a two-stage process. Probabilistic tractography (Behrens et al., 2003b, 2007) estimates the likelihood that a pathway exists between pre-determined locations, based on the probability distribution of different fibre directions at each voxel. In control subjects, this method was used to trace the optic tract from a mask drawn in a single plane of the optic chiasm to the LGN. The LGN was defined using the Juelich histological atlas (Bürgel et al., 2006), and thresholded to approximately 120 mm^3, corresponding to reported average LGN size (Andrews et al., 1997). Restrictive exclusion masks were used to ensure that only the optic tract appeared in the resulting tract, with rejection of pathways that crossed hemispheres or appeared outside of the area where the optic tract could be clearly visualised on a coronal slice. 50000 samples were tracked from each voxel in the chiasm and only tracts reaching the LGN were retained. An example subject is shown in Figure 3.1a. As probabilistic tractography depends on a recognisable white matter tract existing between the seed and target locations, this method was not used to define the optic tract in patients, where the degenerated optic tract may not have high enough FA throughout to be detected. The results of tractography in T1a are shown in Figure 3.1b. Here the optic tract has been defined in the left hemisphere, however no pathway was found between the optic chiasm and the LGN in the lesioned right hemisphere. Thus a group optic tract mask was created in each hemisphere by transforming the tracts into standard space and summing across

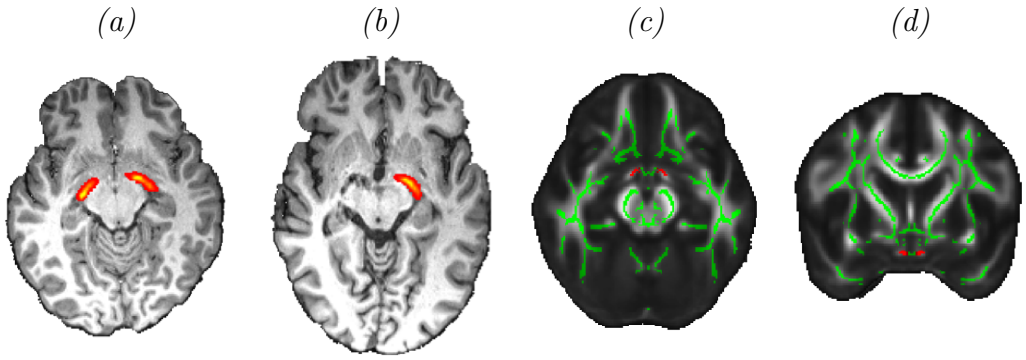

Figure 3.1: Examples of optic tract ROIs. Optic tract ROIs defined using tractography are shown for a control subject (a) and patient T1a (b), projected into individual subject structural space. For display purposes, tracts have been thresholded at 1% of the total tracts reaching the target mask. The averaged optic tract ROIs used for analysis of FA are shown in axial (c) and coronal (d) views, projected into the average FA image. The mean FA skeleton is shown in green.

subjects. The masks were thresholded at 75% overlap in participants, binarised, and flipped in the x-axis and summed to ensure masks were of equal size in each hemisphere. The resulting masks formed the optic tract region of interest (ROI) for further analysis (see Figure 3.1).

In the second stage, Tract-Based Spatial Statistics (TBSS; Smith et al. (2006)), which allows voxelwise comparisons across individual subjects, was used to project fractional anisotropy (FA) and mean diffusivity (MD) images for all subjects onto a symmetrical mean FA tract skeleton in MNI standard space. This skeleton was then masked by the optic tract ROI produced by the probabilistic tractography to leave only the skeleton of the optic tract. Voxels within these regions were then thresholded for each individual subject according to signal intensity in the raw T2 image, so that lesion voxels with minimal T2 signal were not included. Mean FA and MD were calculated for the optic tract in each hemisphere of each subject.

3.4 Results

The aim of this study was to assess optic tract degeneration in a larger group of patients than has been previously investigated, using an extension of the technique used by Bridge et al. (2011). The cohort includes patients with a variety of lesion sites and sizes, ranging from patients with pure LGN damage to those with full occipital cortex resections; enabling analysis of whether TRD is greater in patients with bigger lesions, as shown with monkeys. Furthermore, a number of patients have been scanned more than once since injury, which will allow investigation of whether OT degeneration increases over time, and enable elucidation of the time period during which this occurs.

3.4.1 TRD is present in all patients with stable adult-onset hemianopia

Patients were divided into groups depending on the lesion location: optic tract, LGN, optic radiation, primary visual cortex and occipital lobectomy. Figure 3.2 shows an example from each patient group and a control. In each case the affected side is indicated with a white arrow. Patients were considered to have stable lesions if the damage had occurred more than 2.5 years prior to the scan.

Optic tract degeneration was assessed by computing a laterality index (LI) for each patient, whereby the optic tract in the lesioned hemisphere was compared to the optic tract in the unaffected hemisphere. The LIs from patients with stable lesions, grouped according to lesion location, are shown in Figure 3.3a. The V1 group was subdivided

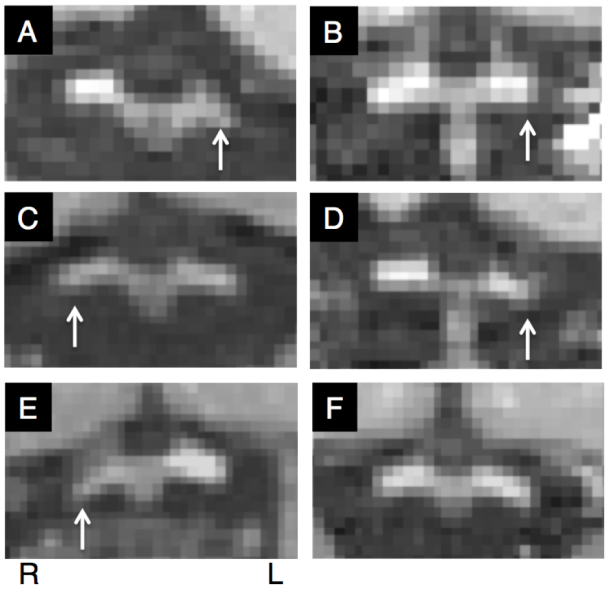

Figure 3.2: Examples of optic tract degeneration in patients with hemianopia. The slices, perpendicular to the optic tract, are approximately 3mm posterior to the optic chiasm. Images A-E show patient T2a (optic tract), L1a (LGN), R1a (optic radiation), S1a (striate) and O3a (occipital) respectively. Image F shows a control subject. Scans are oriented radiologically. Arrows show the tract in the damaged hemisphere.

into hemianopia and quandrantanopia. Although patient T3a was only 17 months post damage, the data were used as the Wallerian degeneration from optic tract damage has a rapid effect on LI. Including patients with optic tract damage allows us to determine the maximum damage likely to be measured, as the site of the lesion is close to the measured region. Controls did not show any difference in optic tract size between hemispheres, with LIs varying only slightly around zero (black line in Figure 3.3a).

A Mann-Whitney U test showed a significant difference between controls and patients ($U_{(36)} = 7.50$, $z = -4.669$, $p < 0.001$). Indeed, optic tract degeneration was present in all patients with established lesions, and all patients showed significant higher LIs than controls ($z > 2.44$, $p < 0.01$). Patients with occipital lobe resections or damage to the tract itself showed the largest LIs while those with partial occipital

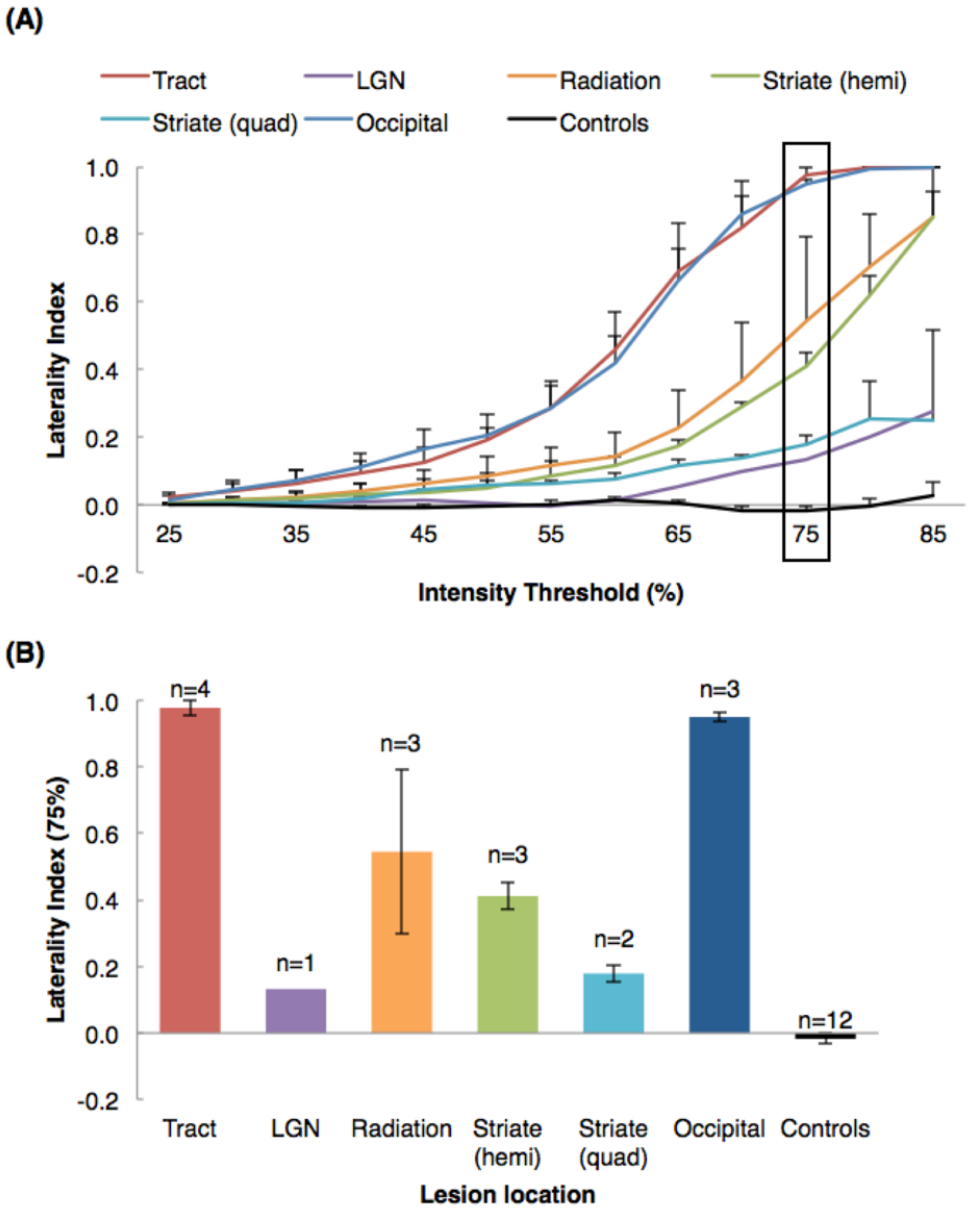

Figure 3.3: Plots of laterality indices (LIs) for patients with acquired damage. A: LIs of patients with established acquired lesions over the range of intensity thresholds, grouped according to lesion location. Locations of damage include the optic tract, LGN, optic radiation, full occipital resection, and striate cortex, split into hemianopia and quadrantanopia. The average LI for controls is shown in black. B: Laterality index at 75% intensity threshold, as indicated by the black box in A. Standard errors across subjects are shown.

damage or optic radiation damage showed lower LIs. Damage to LGN and lesions resulting in quadrantanopia had the lowest LIs of all the patients. In order to quantify the damage, the LI at an intensity value 75% of the maximum signal from the T1-weighted image was extracted for each individual. These values are shown for the group in Figure 3.3b.

3.4.2 Optic tract degeneration is a result of processes beyond the effects of the initial insult

The previous analyses were focussed on the patients with stable lesions, acquired at least 2.5 years prior to imaging. In addition to the stable cases, a further 7 cases with more recent damage were also studied. These patients also have damage to different locations of the visual pathway (V1, optic tract, LGN or optic radiation). In order to quantify the rate of degeneration, patients in this group were scanned on multiple occasions. The laterality indices for this group are shown in Figure 3.4, grouped according to lesion location. Controls scanned twice, with a year between scans, showed no significant difference in LIs between scans.

Table 3.2: Details of patient scanned on more than one occasion

	Lesion	VF Deficit	Scan 1	Scan 2	Scan 3
T1a	optic tract	Hemianopia	11m	22m	44m
T4a	optic tract	Hemianopia	16m	3.5yr	4yr
L1a	LGN	Quadrantanopia	3m	22m	41m
S4a	V1	Quadrantanopia	3m	2yr	
S5a	V1	Quadrantanopia	8m	22m	3yr
S6a	V1	Quadrantanopia	18m	3yr	

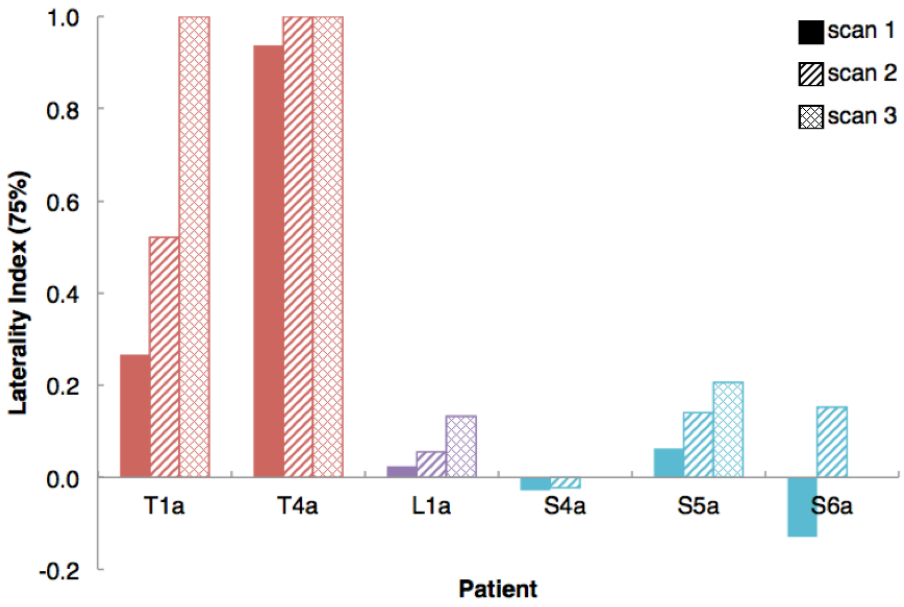

Figure 3.4: Increases in LI over time. LIs are compared across time for patients who have been scanned twice or more. The result from the earliest scan is illustrated by the solid bar, the second scan by the bar containing diagonal lines and the third scan (where it exists) by the bar containing cross-hashing.

The location of damage clearly affects the rate of degeneration with the greatest change seen in T1a who suffered damage to the optic tract directly, 11 months prior to the first scan. The LI increased rapidly to a value close to one almost 3 years after the damage, indicating that the tract is severely compromised. Two patients with striate cortex damage (S5a, S6a) also show an increase in atrophy of the ipsilesional optic tract, over a period of 2.5 years in S5a, with the initial scan at 8 months after surgical resection, and 1.5 years for S6a (beginning at 18 months post stroke). Only one of these patients did not show an elevated LI relative to controls (S4a), and the lesion in this case was to V1, resulting in quadrantanopia. The most recent scan was at 2 years from damage, and it is likely that the degeneration is ongoing in this case.

3.4.3 Congenital hemianopia leads to a significant decrease in white matter integrity

Each of the 9 congenital cases is shown separately in Figure 3.5a, coloured according to lesion location. The majority of lesions in the congenital group are to V1 (n=6), with two cases having lesions to the optic radiation, and one with LGN damage. As for the acquired cases, LIs are highest for the V1 lesions resulting in hemianopia, and smallest for patients with quadrantanopia following post-geniculate damage. The patient with damage to the LGN (quadrantanopia) has a similar LI to patients with hemianopia following V1 damage, but since this quadrantanopia is due to a large arteriovenous malformation it may be that other thalamic structures such as the pulvinar and potentially the optic radiation are also affected.

3.4.4 Optic tract degeneration is proportional to amount of occipital damage in acquired, but not congenital, hemianopia

To determine the relationship between optic tract degeneration and lesion size, only patients with occipital damage were considered, a total of 14 patients. The lesion size for the group of patients varied considerably, ranging from minimal damage affecting just a portion of striate cortex in several congenital patients, to full occipital lobectomy in one hemisphere (100% damage) in O1a, O2a and O3a. Figure 3.6a shows the relationship between the laterality at 75% and occipital lesion size for the patients with acquired

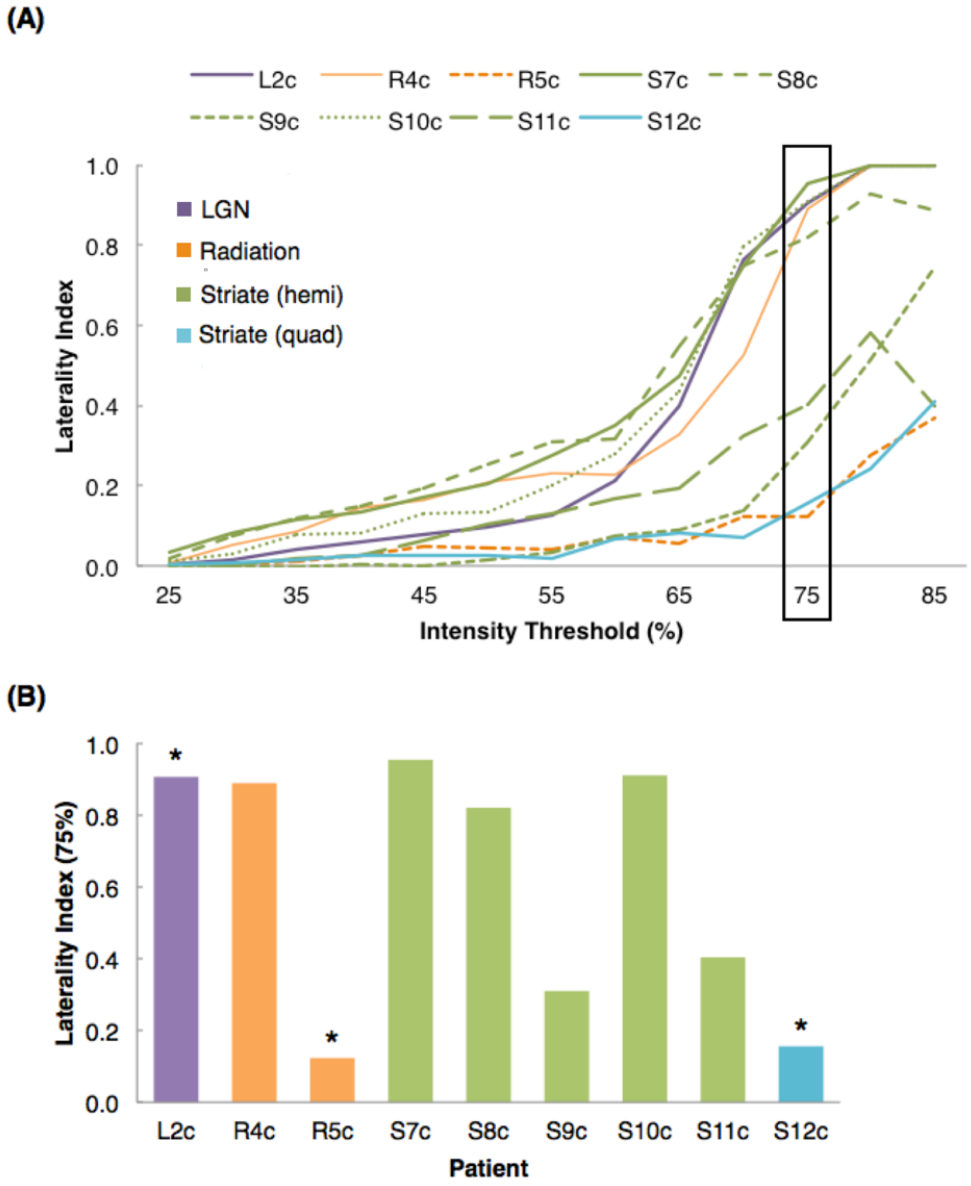

Figure 3.5: Plots of laterality indices for congenital patients. A: LIs of patients with congenital lesions over the range of intensity thresholds, coloured according to lesion location (as with acquired cases). LGN lesions are shown in purple, V1 lesions are either in green (hemianopia) or light blue (quadrantanopia), and optic radiation damage is shown in orange. B: LIs at the 75% intensity threshold for each patient. Asterisks identify patients with quadrantanopia.

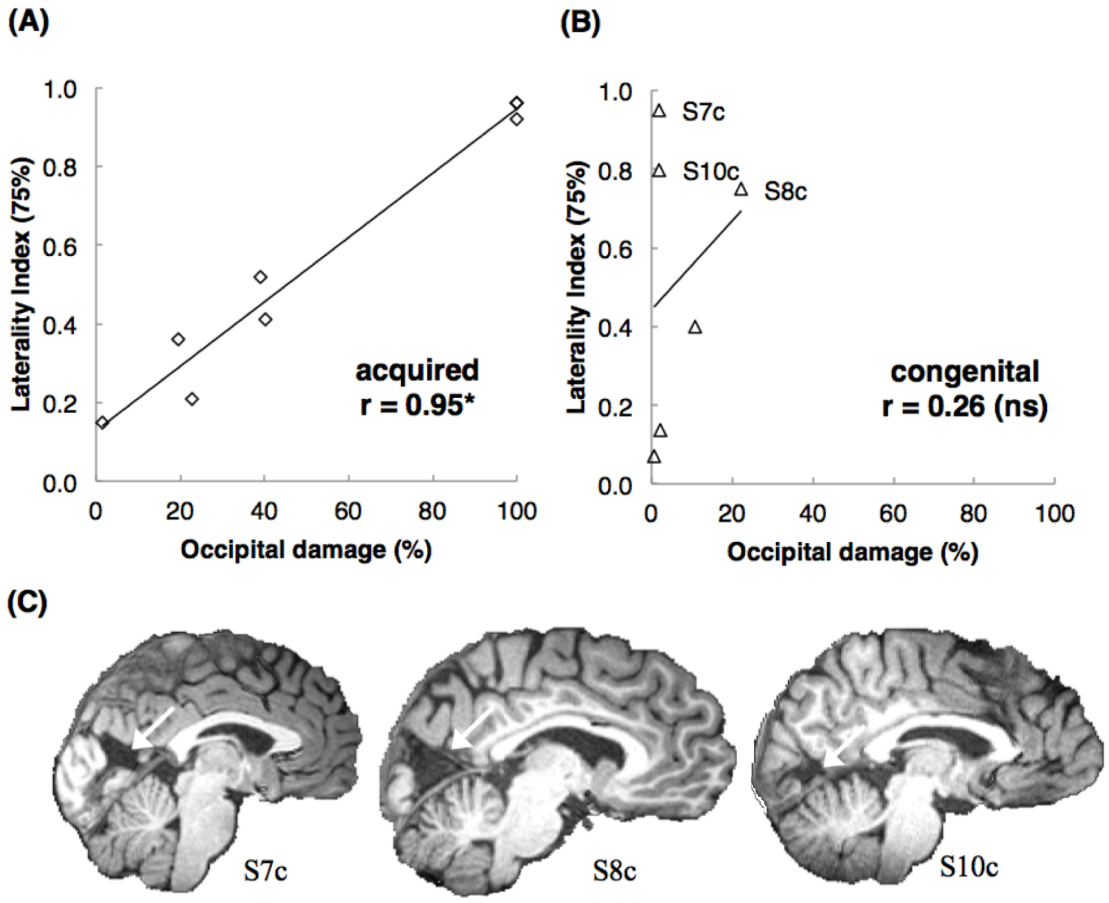

Figure 3.6: Relationship between optic tract atrophy and lesion size. A-B: Plots showing the correlation between the degree of optic tract degeneration (intensity threshold 75%) and the extent of occipital damage in the patients with acquired (left, diamonds) and congenital (right, triangles) cortical lesions. C: T1-weighted images showing the lesion location (indicated by the white arrows) in three congenital subjects with high optic tract laterality.

damage. The highly significant correlation ($r = 0.95$; $p < 0.005$; one-tailed Pearson correlation) is clear from the plot, as the greatest LI occurs in the largest lesions. In contrast, the congenital hemianopic subjects do not show this strong correlation and, in fact, do not show a significant correlation ($r = 0.26$; $p = 0.31$). Figure 3.6b shows the relationship between these values in the congenital cases. It is clear from the graph that in general lesion size is considerably smaller in this group, with the maximum damage around 20%. However, these small lesions can clearly have a significant effect on the white matter integrity in the affected hemisphere. The labelled cases show a higher LI for the lesion size than would be predicted from the graph of the acquired subjects. These small lesions are located specifically within V1 (Figure 3.6c), and have therefore damaged neurons relatively early in the visual pathway, and of critical importance for visual function.

The LIs were also correlated to the visual field loss, as quantified using Humphrey perimetry. Figure 3.7a shows this significant relationship in the patients with acquired lesions ($r = 0.81$; $p < 0.01$), while the congenital cases are shown in Figure 3.7b. Although the correlation is high in the congenital cases ($r = 0.72$), the smaller number of patients in this category means that this is not a significant correlation ($p = 0.090$). Moreover, the regression line for the two groups of hemianopic patients is remarkably similar, indicating a similar relationship in the two groups.

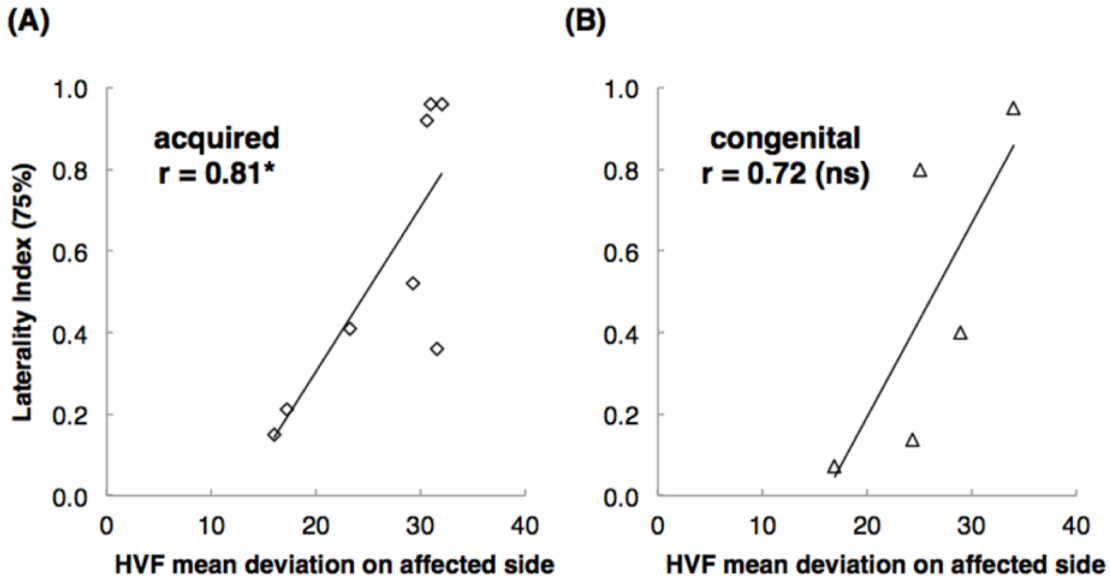

Figure 3.7: Relationship between optic tract atrophy and size of the visual field deficit. Plots showing the correlation between optic tract laterality and the HVF mean deviation on the hemianopic side. Acquired patients are shown on the left (diamonds) and congenital patients on the right (triangles).

3.4.5 Diffusion-weighted measures can provide measures of laterality

Since diffusion-weighted imaging can quantify white matter integrity in fibre bundles, analysis of fractional anisotropy (FA) and mean diffusivity (MD) extracted from these images was used in two ways. Firstly a LI comparable to the analysis from the T1-weighted images was undertaken, in order to ensure correlation between the two approaches. Secondly, the mean FA and MD values within the affected optic tract were correlated with the structural and diffusion-extracted LI. MD was not found to be a good predictor of tract degeneration, and so results focus on FA. Correlations are given in Table 3.3.

One of the major points to make is that, unlike the structural measurement, the diffusion measures were often difficult to extract. Because FA is so sensitive to partial voluming, accurate identification of the tract is critical, and the tract cannot impinge on surrounding grey matter or CSF. Using tractography between the optic chiasm and LGN was a suitable approach in control subjects, but this was not effective in lesioned hemispheres as the decrease in white matter integrity makes it difficult to fit a diffusion vector. Therefore values were extracted using a white matter skeleton that projects FA values from the centre of an individual tract to the centre of that tract in standard space.

Figure 3.8 shows the relationship between the LI derived from the T1-weighted images and FA images. While there is a significant correlation in the acquired patients, the graph clearly shows that there is considerable variability, particularly in the cases showing a large structural LI. Indeed, the DTI derived LIs are much lower than the structural values in general, presumably because the range of values of FA found within

Table 3.3: Correlations between DTI and structural measures of tract degeneration

		Correlations		
	N	LI (struct) LI (FA)	LI (struct) Mean FA	LI (FA) Mean FA
ALL PATIENTS				
All	25	0.36*	-0.16	-0.67**
Acquired	16	0.43*	-0.19	-0.68**
Congenital	9	0.26	-0.12	-0.54 (p=0.07)
OCCIPITAL PATIENTS				
All	14	0.38 (p=0.11)	-0.15	-0.79
Acquired	8	0.50 (p=0.10)	-0.21	-0.87
Congenital	6	0.39	-0.07	-0.35

*Mean FA is the average FA in the damaged tract

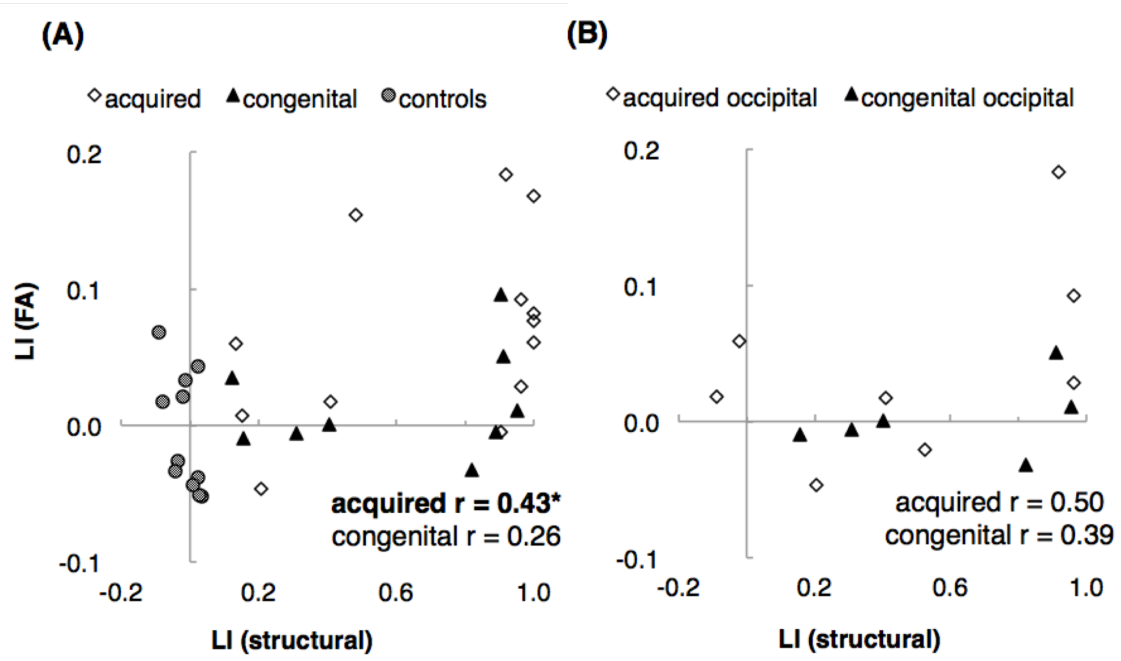

Figure 3.8: Comparison of the laterality indices for structural and DTI measures of optic tract integrity. Scatterplots show the correlation between DTI LI and structural LI for all patients (A), and for patients with damage restricted to the occipital lobe (B).

white matter, whether damaged or intact is reasonably low. Therefore, while structural LI can reach almost 1, the highest DTI LI was less than 0.2. Plots showing the correlations between mean FA and both structural and FA LIs are shown in Figure 3.9.

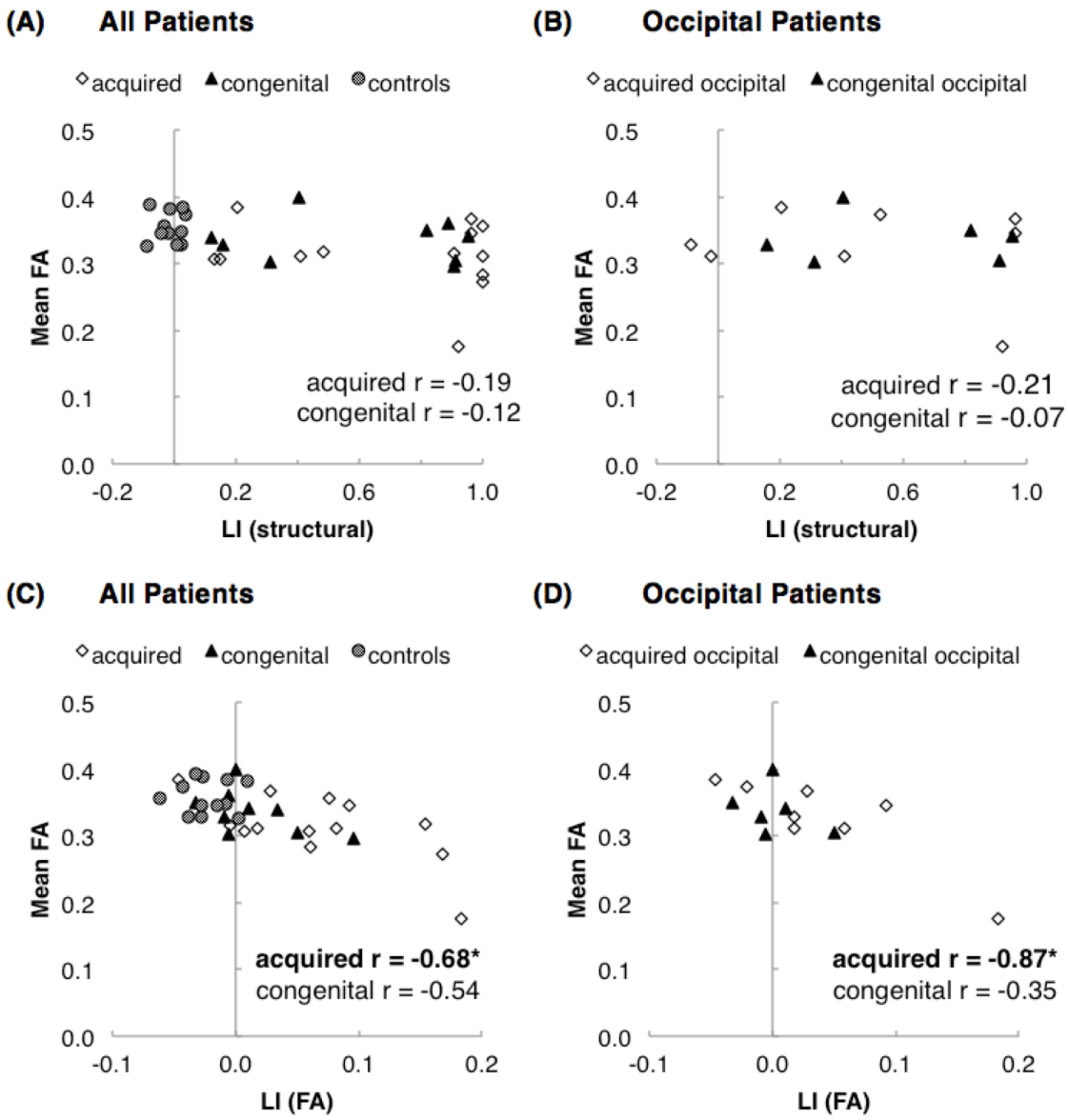

Figure 3.9: Comparison of the laterality indices for mean FA in the damaged tract and the structural and DTI laterality indices. Scatterplots show the correlation between mean FA in the damaged tract and structural LI for all patients (A), and for patients with damage restricted to the occipital lobe (B). The same data is shown for the laterality measure derived from the DTI data in (C) and (D).

3.5 Discussion

The large number of patients with hemianopia scanned in this study has allowed a quantification of the effect of both lesion size and location. Retaining the integrity of the optic tract is clearly crucial to visual perception, and therefore a measure of its degeneration can be used for long-term prognosis and may be of importance in predicting the outcome of vision restoration therapies.

3.5.1 Human TRD appears to follow a similar pattern to non-human primate

Based on the extensive literature on TRD in the visual system of non-human primates, a number of predictions may be made with respect to optic tract degeneration in hemianopia. Degeneration should be most extensive when the occipital lesion is acquired in childhood (Weller and Kaas, 1989), increase with size of the occipital lesion (Cowey et al., 1999), and have the greatest rate of cell loss within the first 1-3 years, thereafter becoming relatively stable (Cowey et al., 1999, 2011). Optic tract atrophy in the cohort of patients studied, as defined by the laterality index derived from T1-weighted structural imaging, was compatible with all of these predictions. Furthermore, following adult-onset lesions, the time-course of the degeneration shown by this methodology is in agreement with the results shown using OCT in humans (Jindahra et al., 2012a).

3.5.2 TRD is extensive in cases where a hemianopia was acquired pre-natally

Investigation of non-human primate TRD suggested that animals in which V1 was lesioned when they were juveniles had the most severe disruption of the optic tract (Weller and Kaas, 1989). The current study, by investigating both acquired and congenital damage, also appears to suggest that this is the case in humans. Over half of the congenital patients studied have LIs approaching 1 at the highest white matter thresholds, indicating severe axonal loss, including patients with LGN, radiation, and restricted V1 damage. Patients with lesions in similar locations acquired in adulthood do not generally show optic tract degeneration to the same extent.

There are however some difficulties inherent to the study of patients with reportedly congenital lesions. The field defect is often picked up by chance at a sight test, not infrequently during adulthood. It is therefore not necessarily possible to determine the exact period at which damage was sustained. Since there is no obvious event causing the damage, and patients are generally unaware of the field deficit, it is reasonable however to assume that damage is likely peri-natal. Furthermore, given the absence of any suggestion of birth trauma or an injury or illness in early life such as encephalitis, it is likely to be predominantly pre-natal.

At least in the patients studied here the congenital lesions tend to be smaller, but result in comparable field deficits to patients with acquired damage. It is often posited that damage occurring early in life when the brain is still within the critical period ought to have less effect on function (Hoyt, 2003). At this early stage, it is

thought to be possible for lesions to lead to different forms of reorganisation, and there is therefore potential for greater input from subcortical structures that bypass V1. However, this does not appear to be the case when damage is within the visual pathway. Any reorganization which occurs in these patients does not appear to be sufficient to minimise visual field loss or to prevent TRD.

3.5.3 Lesion size and field deficit correlate significantly with LI in patients with acquired damage

Previous work in non-human primates has suggested that TRD is more extensive in cases with larger occipital lesions (Cowey et al., 1999), although this had not been systematically addressed in humans. Here, a highly significant correlation between lesion size and LI exists for patients with acquired lesions. While the major visual pathway to the cortex is through the LGN to V1, various smaller projections that bypass V1 are also present. Indeed, these pathways have been posited to underlie the ability of some of these patients to make unconscious guesses about visual stimuli (blindsight (Cowey and Stoerig, 1991)). Thus, where damage is specific to V1, any projections from the LGN or the pulvinar (Warner et al., 2012) that may project to V2 (Schmid et al., 2010), V5/MT (Bridge et al., 2008; Sincich et al., 2004) or other extrastriate regions may still be intact, and therefore optic tract fibres are preserved. As the lesion size is increased within the occipital lobe, the additional pathways are also affected, and therefore there is no longer a useful function for the optic tract.

A further predictor of TRD in this patient group was the size and density of the

visual field deficit. Intuitively, the relationship is perhaps unsurprising, as more dense field loss is likely a direct result of extensive damage in the visual pathway, whether to the optic tract or to axonal targets later in striate cortex. As perimetry is readily available and generally becomes stable soon after a hemianopia occurs, it may be possible to use computerized visual field testing to predict the amount of degeneration likely to occur in patients with occipital lesions.

In congenital patients however, LI was not significantly correlated with either the extent of occipital damage or the visual field deficit. With respect to the visual field deficit, the pattern of results are suggestive that in fact the relationship in congenital patients is the same as that of acquired patients, and it is likely that increasing the sample size would give a significant result with a similar slope. However, the relationship between lesion size and LI is markedly different between acquired and congenital patients. A number of the congenital patients had relatively small cortical lesions combined with dense visual field deficits and extensive optic tract degeneration, more so than would be anticipated when compared with patients with lesions acquired in adulthood. However, this is in agreement with the literature on TRD in primates, where retinal ganglion cell loss has been shown to be more extensive the earlier in life a lesion is acquired (Weller and Kaas, 1989).

3.5.4 Diffusion-weighted imaging is less reliable than structural measures

Since diffusion-weighted imaging is a relatively direct surrogate measure of white matter integrity, it was expected to provide a sensitive measure of degeneration in the optic tract. However, in this study, the FA appeared to provide a less sensitive measure of optic tract integrity than the structural measure taken from the T1-weighted image. While the structural and diffusion measures were correlated in patients with acquired hemianopia, there was a substantial overlap in the range of diffusion LIs for controls and patients, making it unlikely that optic tract degeneration could be identified from this measure. This is in stark contrast to the structural LI, where patients and controls were easily distinguishable. Previous attempts to use DTI to assess white matter degeneration in the optic tract have had mixed results. Dasenbrock et al. (2011) found optic tract FA to be related to RNFL measures in optic neuritis, but found no significant reduction in optic tract FA compared to controls, nor any relationship between DTI measures and visual acuity. In contrast, a study of patients with Leber's hereditary optic neuropathy, where RGC degeneration causes loss of central vision, did find a significant correlation between FA in the optic tract and visual acuity in patients, together with a group-wise effect of reduced FA and increased MD in the optic tract (Milesi et al., 2012). Results from studies such as these suggest that it is possible to use diffusion-weighted imaging to assess optic tract damage, however it is questionable whether the measure as used up to now is adequately sensitive for such a small tract, and in a region that is highly susceptible to distortions during image acquisition.

In the present study, there could be several reasons for the lack of sensitivity compared with the structural analysis. The most likely reason may be due to the technical difficulties of identifying the tract in the diffusion-weighted data. Whereas in the high-resolution T1-weighted images the optic tract can be immediately identified visually, the diffusion-weighted images are lower resolution, with 2mm isotropic voxels rather than 1mm, and, as echo-planar images, they are more susceptible to distortion. Furthermore, the laterality measure used on the structural images takes into account any partial voluming at the border of the optic tract, while this cannot be accomplished with diffusion-weighted images. It may be possible to improve the sensitivity of diffusion measures of optic tract integrity, either by acquiring higher resolution images using a higher field strength, or by using a protocol designed to reduce distortions in the regions around the anterior components of the visual pathway, for example that used effectively by Hofer et al. (2010) to reconstruct the visual pathway from the optic nerve to the occipital cortex.

As a decrease in FA in a white matter tract due to neurodegeneration is generally accompanied by an increase in MD (Bridge et al., 2010; Milesi et al., 2012), the lack of correlation with the structural measure was unexpected. In subjects with direct damage to either the region of interest or a neighbouring area, i.e. the optic tract, LGN, and potentially also the anterior optic radiation, this could be due to T2 signal loss in regions with bleeds from the initial insult (Fazekas et al., 1999), which would give low FA and MD values. Thresholding the DTI images to remove areas of low T2 signal was intended to combat this, however it is possible that some affected areas remained

in the analysis. Nonetheless, this does not explain lack of correlation in subjects with lesions more distal to the optic tract. It is possible that this is also connected to partial voluming, with a more detrimental effect on MD than FA occurring. This type of issue is less problematic when all tracts are within the white matter, rather than surrounded by CSF.

3.5.5 Conclusion

This large imaging study of patients with acquired and congenital hemianopia has confirmed that the human brain shows a similar pattern of trans-neuronal retinal degeneration to that seen in the macaque monkey. The subjects with congenital damage show the greatest TRD, while lesion size also determines the amount of TRD.

Chapter 4

Motion processing in hemianopia

4.1 Abstract

Objective To investigate motion processing in patients with acquired and congenital hemianopia with lesions in different visual pathway locations, and to relate residual motion processing with activity in the motion area MT.

Methods Activity in area MT was measured using fMRI while patients and healthy control subjects viewed moving dot stimuli in their blind and sighted hemifields. Half of these patients were also tested on the ability to discriminate the direction of luminance and colour defined moving stimuli in the blind field.

Results Motion stimuli activated both striate cortex and area MT in patients and control subjects, with patients generally showing reduced activity in both the lesioned and, to a lesser extent, the intact hemisphere. While there was a large degree of

variability between patients, there was no clear effect of lesion location or size on activity in ipsilesional MT, and BOLD activity in patients with adult acquired and congenital hemianopia did not significantly differ. There was however a suggestion of a relationship between residual visual function and activity in MT, as some of the patients who were able to discriminate motion in the blind field did show greater levels of activity in area MT than was found in other patients.

Interpretation Neural activity in response to motion stimuli is highly variable among patients with hemianopia, and the pattern of activity cannot easily be predicted based solely on the type of lesion present.

4.2 Introduction

Residual vision in the blind hemifield of patients with damage to striate cortex has been a topic of investigation for almost a century, following Riddoch (1917)'s account of spared motion perception in patients with gunshot wounds to the occipital cortex. Extensive investigation of the properties of blindsight, the ability to respond to visual stimuli without consciously perceiving them, has been carried out since then (reviewed by Cowey et al. (1989)), with the observed properties ranging from simple localisation of stimuli (Weiskrantz et al., 1974) through to discrimination of emotional faces (Pegna et al., 2005).

4.2.1 Motion perception in the blind hemifield

While there are a range of aspects of the visual scene that can be detected in blindsight, moving stimuli are considered to be the easiest to detect, with patients often reporting some level of perception of the stimulus, although they still cannot 'see' it as presented (Azzopardi and Cowey, 2001; Weiskrantz, 1986). In traditional 'type 1' blindsight, the patient is completely consciously unaware of the stimulus in the blind field, however this is not always the case. Having some level of knowledge that a stimulus is present in the blind field without consciously perceiving it is known as type 2 blindsight; specific awareness of motion in the absence of perception is known as the Riddoch phenomenon (Zeki and Ffytche, 1998).

That moving stimuli in the blind field appear to be more accessible to hemianopia patients than other stimuli suggests that pathways to area MT, the motion area, survive the loss of V1 and the primary visual pathway. Investigations into the limits of this motion processing show that patients can detect the presence of motion in a wide range of stimuli, including random dot kinetograms, plaids, and gratings. Patients appear to be more limited at discriminating direction of movement, and Azzopardi and Cowey (2001) found patients were only able to do this with single bars. It has also been suggested that patients may be able to process colour defined motion stimuli, however Alexander and Cowey (2013) found that this was only possible when there was a luminance difference between the moving stimulus and the background.

4.2.2 Neuroimaging evidence for function in MT

Several fMRI studies have investigated MT activity in patients with regions of cortical blindness. In a patient with bilateral damage to V1, resulting in complete cortical blindness, Bridge et al. (2010) found evidence of activity in MT in the absence of any striate activation. In this cases, there must therefore be functioning pathways to MT which do not pass through striate cortex. Investigations of hemianopia patients have also found activity in area MT following disruption of the visual pathway. Goebel et al. (2001) found responses in ipsilesional MT in a patient with damage to striate cortex, and in another with a lesion affecting the optic radiation. As in the patient with bilateral V1 damage, this activity occurred in spite of a complete absence of activity in striate cortex in the lesioned hemisphere. In the striate patient (GY), the activity found in MT was comparable to that found in contralesional MT, however activity was considerably lower in the optic radiation patient, illustrating the variation in function that can be found in hemianopia. This variation in the pattern of responses in different patients with hemianopia was further demonstrated by Morland et al. (2004). In patients able to discriminate the direction of a drifting grating, responses were found in ipsilesional MT. However, while in GY this activity in MT was in the absence of any striate activation, consistent with the study by Goebel et al. (2001), in the other patient studied, spared regions of V1 were still functioning. MT may therefore, in some cases, be receiving some input from the usual route through striate cortex.

While the main input to area MT usually comes from the striate cortex, results from patient studies where MT is active in the absence of striate activation provide

evidence for alternative pathways to MT, although it is unclear whether these are pre-existing pathways, or the result of cortical reorganisation. It has been shown that presentation of very high contrast motion stimuli results in comparable MT activity in the two hemispheres, a finding that is not replicated in V1, nor at lower stimulus contrast in MT, where ipsilesional activity is reduced in comparison to the unaffected hemisphere (Radoeva et al., 2008). Subcortical connections to MT have been suggested to underlie this response to high contrast motion stimuli in area MT, and indeed there are pathways from both the LGN and the pulvinar which are known to project directly to area MT (Sincich et al., 2004; Warner et al., 2010). Studies in patient GY suggest that, in some cases, reorganisation has occurred that has resulted in atypical connections to area MT. Investigation of connectivity in GY using diffusion tensor imaging has shown cortico-cortico connections between MT bilaterally, and contralateral connections between LGN and area MT (Bridge et al., 2008). Further evidence of this functional reorganisation in GY has come from investigation of activity in the striate cortex and area MT, using transcranial magnetic stimulation (Silvanto et al., 2009). Stimulation of area MT in the lesioned hemisphere affected the appearance of phosphenes induced from contralateral striate cortex, an effect not seen in controls. GY is, however, often considered a special case, having acquired his hemianopia at a young age, and having undergone countless hours of stimulation in his blind field in the course of investigating blindsight. It is unclear, then, whether this finding of substantial remaining function in area MT is common to all patients with hemianopia, or whether it is dependent on factors such as lesion size and location, and the age at

which the hemianopia occurred.

4.2.3 Aims of the present study

The extent to which area MT is able to process motion stimuli in patients with hemianopia stemming from different causes was investigated using a combination of neuroimaging and forced-choice discrimination tests. Functional MRI was used to measure the level of activity in area MT and striate cortex when patients were presented with motion stimuli in the blind and sighted visual fields, in order to ascertain whether any processing of stimuli in the blind field was being carried out. Patients were also tested on their ability to discriminate the direction of luminance and colour defined motion stimuli in the blind field, to ascertain whether patients with more activity in area MT had a greater capacity to process and respond to visual stimuli in the blind field. In addition to these questions being of interest in themselves, the data will be used as explanatory factors in conjunction with later structural analyses.

4.3 Methods

4.3.1 Subjects

Functional imaging was acquired for all hemianopia patients described in Chapter 2, with the exception of S3a. All patients scanned in the UK underwent two fMRI scans, while subjects scanned in Brazil underwent the hemifield motion scan only. Of the patients recruited in the UK, 12 also performed some motion discrimination tasks

Table 4.1: Patients tested for visual motion processing

	Damaged hemisphere	Lesion location	Duration (y)
T1a	Right	optic tract	3
T2a	Left	optic tract	3.5
L1a	Left	LGN	3
R2a	Right	radiation	5
S1a	Left	V1+	18
S2a	Left	V1+	5
S4a	Right	partial V1	2
S6a	Right	partial V1	3
R4c	Left	radiation/V1	congenital
R5c	Right	radiation/extrastriate cortex	congenital
S7c	Left	V1	congenital
S12c	Left	V1	congenital

outside of the scanner, as detailed in Table 4.1. Twelve healthy controls were also scanned (age range 21-74, mean age 46, 6 females).

4.3.2 Functional imaging

Central motion scan

In the central motion scan, a block design was employed with subjects being presented with alternating blocks of moving and stationary dots. Stimuli were generated on a VSG 2/5 graphics card (Cambridge Research Systems), and projected using a Sanyo projector. Stimuli were viewed through mirrors, with the projected screen covering a visual field with a diameter of approximately 26°. An 8° circular patch of black square dots was presented centrally on a white background. During motion blocks, the dots moved radially at a speed of 30 deg/s, reversing direction every second. The dots then remained on the screen, motionless, during rest blocks. 8 cycles of the motion and

rest blocks were displayed, with each cycle lasting for 32 seconds, 16 seconds each for motion and rest blocks. Three cycles are shown in Figure 4.1. Subjects were instructed to maintain gaze on a central fixation spot, a red square. Images were acquired at a resolution of 3 mm x 3 mm x 3 mm, with a TR of either 4 s or 2 s, and a TE of 30 ms or 49 ms, depending on whether subjects were scanned before or after June 2012 (further explanation of this is given in Chapter 2).

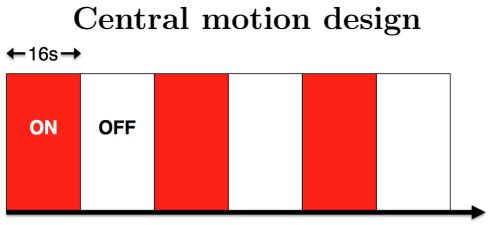

Figure 4.1: Time course of the central motion scan

Hemifield motion scan

For patients scanned in the UK, the same projector and viewing set up were used as for the central motion scan. For subjects scanned in Brazil, Invivo's Eloquence system was used, with patients viewing stimuli on a screen with a total field of view of 30°. In the hemifield motion scan, a block design was again employed. Here, instead of stationary dots, the rest blocks were a blank black screen with just a central red cross for fixation. Subjects were instructed to fixate this cross at all times. In motion blocks, an 8.5° circular patch of white dots moving outwards from a central point was presented on a black screen. The dots were displayed either to the left or right of fixation, with the centre of the stimulus being horizontally aligned with the fixation point. The nearest

edge of the stimulus was 3° from fixation. An example of the stimulus location in the left and right hemifields is given in Figure 4.2. 6 cycles of the motion and rest blocks were displayed, with each cycle lasting for 48 seconds, with 16 seconds each for left motion, right motion, and rest blocks. Two cycles are shown in Figure 4.2. Images were acquired at a resolution of 3 mm x 3 mm x 3 mm. As with the central motion scans, initial scans acquired in the UK had TR = 4 s, TE = 30 ms, while later scans had TR = 2 s, TE = 49 ms. All scans acquired in Brazil had TR = 2 s and TE = 30 ms.

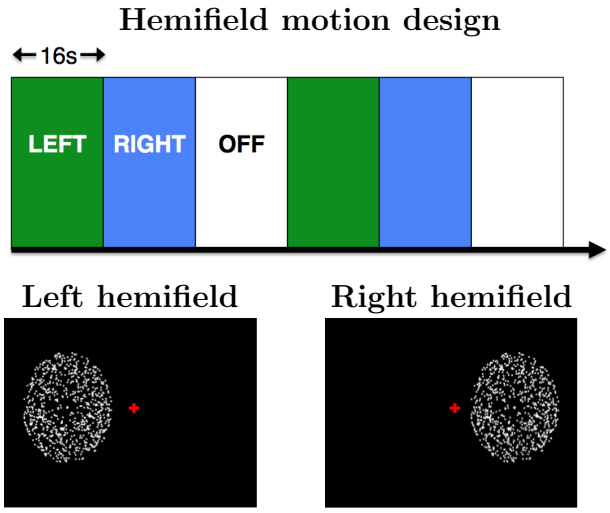

Figure 4.2: Hemifield motion scan design. The time course of the hemifield motion scan is shown, with examples of moving dot stimuli shown in each hemifield (not to scale).

Structural images

T1-weighted images were collected for registration purposes, at a resolution of 1x1x1 mm^3, as described in Chapter 2.

fMRI data analysis

Functional data were analysed using FEAT, from the FSL toolbox. Images were motion corrected using MCFLIRT, spatially smoothed with a Gaussian kernel FWHM of 5 mm, and highpass temporal filtering was applied. FILM prewhitening was used for first-level analysis to increase statistical validity, using standard motion parameters. Functional images were initially registered to the individual subject's T1-weighted structural image. This image was then registered to standard space with FNIRT, using the T1-weighted MNI 152 2 mm structural image.

General linear model (GLM) analysis was applied to identify voxels which were significantly more active during stimulus blocks than during rest periods. For the central motion scan, the only explanatory variable (EV) was motion vs stationary stimuli. In the hemifield motion scan, there were two EVs, left and right stimulus presentation. A higher level FEAT analysis was performed on control subjects, to create a group mean BOLD activation map for each EV, using FLAME 1+2. To create these maps of activity in the control group, Z-statistic images were thresholded at $z > 2.3$, with a cluster correction threshold of $p < 0.05$. For group comparisons, the resulting Z-statistic images for each EV were also thresholded at $z > 2.3$, with a cluster correction threshold of $p < 0.05$. Z-statistic maps for the control group were projected onto the inflated brain surface using Freesurfer for display purposes, in order to look for different overall patterns of activation.

Finally, ROIs were identified for further investigation: striate cortex (V1) and area MT in each hemisphere. Area MT was identified using the Juelich Histological Atlas

(Malikovic et al., 2007; Wilms et al., 2005), and was thresholded at 20% to remove voxels with a lower probability of being part of MT. As the Juelich V1 mask (Amunts et al., 2000) covers a reasonably large region, a smaller V1 mask was used, that was specifically created to correspond to the V1 regions that respond to stimuli in the central visual field. In order to create this mask, Bridge (2011) retinotopically mapped V1 in 16 healthy subjects, registered these maps to an average brain in Freesurfer using surface-based registration, and summed them. For this study, these masks were thresholded to include regions where the portion of V1 mapped overlapped in at least 30% of subjects.

The mean percentage BOLD change in striate cortex and MT was computed using the Featquery tool in FSL, using non-binarised ROI masks, such that voxels with a higher probability of being in the mask contributed more to the signal. In addition to this, the number of voxels where $z > 2.3$ following cluster correction was computed, in order to ascertain the extent of regions of activity within each ROI.

4.3.3 Motion discrimination tasks

Subjects were seated in front of the apparatus and a head rest was used to restrict head movement and standardise distance to the stimulus across the session and between subjects. All subjects carried out two motion discrimination tasks, one with luminance defined motion, and one with colour defined motion. Tasks were carried out separately in each hemifield, with the good hemifield being tested first, followed by testing in the blind hemifield.

Motion stimuli for both luminance and colour defined motion tests were presented on a square background of checks, varying in luminance to give rise to the perception of noise. The square filled the majority of the upper quadrant of the screen, either on the left or right hand side depending on which hemifield was being tested. Where subjects had an inferior quadrantanopia, stimuli were presented in the bottom half of the screen instead of the top half. Stimuli were positioned such that the nearest edge of the test stimulus was 5 ° from fixation both horizontally and vertically.

Luminance stimuli

Stimuli were presented on a grey background with a luminance of $24cd/m^2$, and chromaticity 0.305, 0.323 (CIE-(x,y) chromaticity chart). In the stimulus background, three levels of static noise were used, 12%, 24%, and 45%. In each trial, a square, defined by luminance contrast, appeared in one of the corners and moved diagonally to the opposite corner. The luminance of the square varied, and a staircase procedure was used to find the contrast threshold at which motion could just be detected.

Colour stimuli

Detection of colour defined motion was tested using an adaptation of the colour assessment and diagnosis test (CAD, (Barbur and Connolly, 2011)). Stimuli were presented on a grey background with a luminance of 26cd/m^2, and chromaticity 0.305, 0.323. Luminance contrast signals were masked by the use of dynamic noise instead of static noise in the background square. During a trial, a small colour defined box appeared in one corner of the background noise (examples of each colour are shown in Figure 4.3),

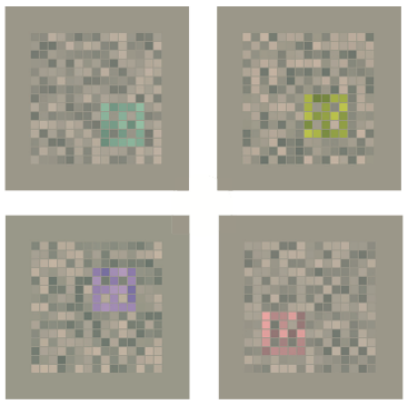

Figure 4.3: Colour defined motion test stimuli. Examples of each of the four stimulus colours are shown (image taken from Barbur and Connolly (2011)). Stimuli were all shown in the upper half of the screen, filling the majority of the upper quadrant of the the screen in the hemifield being tested.

and moved to the opposite corner. The use of dynamic contrast noise renders the coloured box effectively isoluminant, meaning that the ability to detect the direction is dependent on chromatic processing. The coloured stimuli had the following hue angles: 62° (yellow), 158° (green), 242° (blue), and 338° (red). A staircase procedure was used to find the smallest difference between the chromaticity of the target and the background where the direction of motion could be discriminated.

Procedure

A fixation cross appeared which was shown throughout each trial. The large background square then appeared, followed by the moving stimulus, which started at one corner of the background square and moved diagonally to the opposite corner. The moving stimulus was shown for 860 ms. The end of each trial was signified by a bleep, after which subjects indicated the direction of motion of the stimulus using a button box. Subjects were instructed to guess the direction of motion when they were unsure

or had seen no stimulus. Some catch trials were included where no moving stimulus appeared, so all subjects had to guess for some trials. Subjects were questioned about their perception of stimuli in the blind field at the end of each test.

4.4 Results

Both the centrally presented and hemifield motion stimuli were successful in activating striate cortex and area MT in the control group. Centrally presented motion stimuli activated the visual cortex consistently in both hemispheres (Figure 4.4). When hemifield motion stimuli were shown, the pattern of activation in the contralateral hemisphere was very similar to that shown for motion spanning both hemifields. In contrast, there was relatively little activity in the visual cortex in response to ipsilateral motion stimuli (Figure 4.5). Paired samples t tests showed that for the control group, neither percentage BOLD change nor the number of significantly active voxels differed across hemispheres in areas V1 or MT. This was the case for central, ipsilateral, and contralateral motion stimuli. Therefore results for controls were averaged across hemispheres when comparing with patients.

4.4.1 Hemianopia patients have reduced activity bilaterally when viewing centrally presented moving dots

To ascertain whether activity in V1 and MT differed in patients compared to controls, ANOVAs were performed on indicators of functional activity, with patient hemispheres

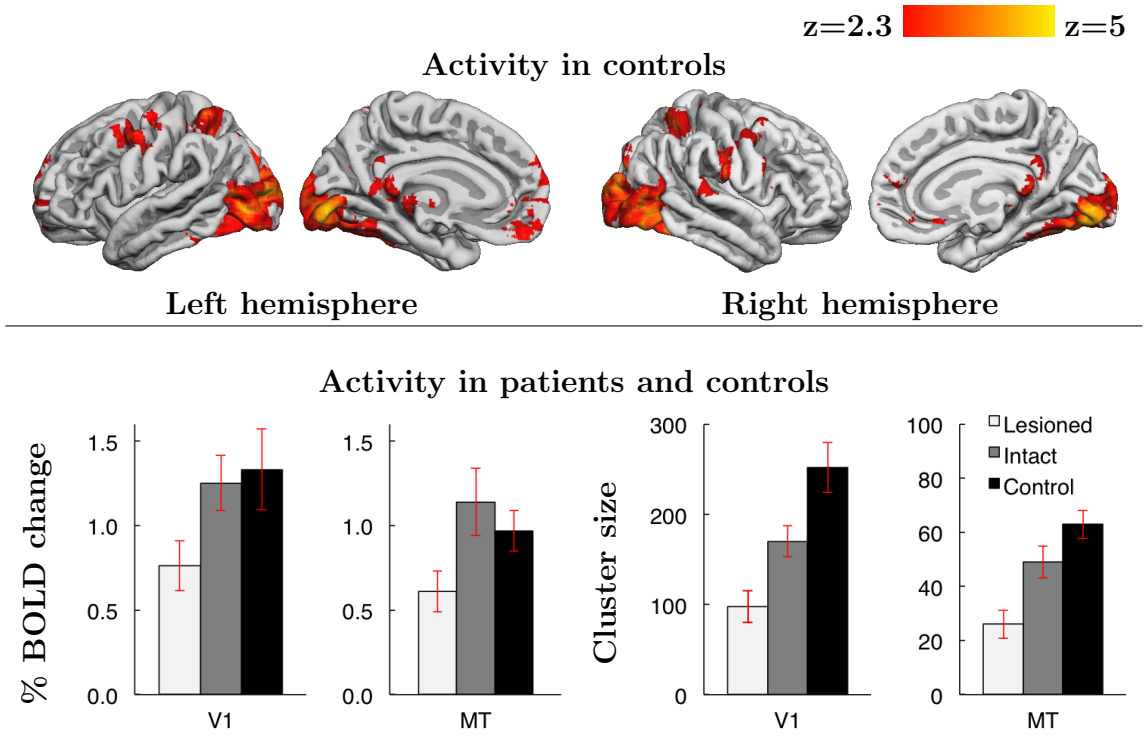

Figure 4.4: Activation in response to central moving dot stimuli. The average BOLD response in controls to moving dots presented centrally spanning both hemifields is shown. V1 and MT were activated in both hemispheres to a similar degree. For each of the visual areas, the number of significantly active voxels and the percentage BOLD change are shown. For patients, two means are shown, one for the undamaged hemisphere, and one for the lesioned hemisphere, while results for the control group are averaged across hemispheres. Standard errors are shown for each group.

separated into lesioned and undamaged groups. Mean BOLD activity and cluster size for each group are shown in the bottom panel of Figure 4.4. When moving dots were presented spanning both hemifields, there was no significant difference in the percentage BOLD change between the lesioned hemisphere, undamaged hemisphere, and controls in either V1 ($F_{(2,43)}$=3.076, p=0.056) or MT ($F_{(2,43)}$=3.093, p=0.056). Both effects approached significance however, probably due to smaller changes in BOLD activity in the lesioned hemisphere of patients in comparison to controls. Interestingly, on average patients had slightly greater activity in MT in the undamaged hemisphere than

controls, perhaps compensating for the reduced activity in the lesioned hemisphere, however this difference was not statistically significant.

While the differences in BOLD activity averaged across the ROIs were minimal, there were group differences in the size of clusters of activity within these regions, calculated as the number of voxels where $z > 2.3$ following cluster correction. In V1, there was an overall effect of group ($F_{(2,43)}$=13.59, $p < 0.001$), and comparison of groups, using Bonferroni correction for multiple comparisons, showed that cluster size in patients was significantly smaller than in controls in both the lesioned ($p < 0.001$) and intact ($p < 0.05$) hemisphere, and that cluster size in the lesioned hemisphere of patients was lower than in the undamaged hemisphere ($p < 0.05$). Paired samples t tests comparing the lesioned and undamaged hemisphere in patients confirmed that the extent of the activated region is smaller in V1 in the lesioned hemisphere ($t_{(16)}$=4.476, $p < 0.001$). In MT, there were again differences in cluster sizes between groups ($F_{(2,43)}$=5070.92, $p < 0.001$). However, while cluster size in the lesioned hemisphere of patients was reduced in comparison to both the undamaged hemisphere ($p < 0.05$, paired t test) and controls ($p < 0.001$), in MT cluster size in the undamaged hemisphere of patients was not different from in control subjects. Paired samples t tests showed that clusters were smaller in the lesioned hemisphere than in the undamaged hemisphere of patients ($t_{(16)}$=3.695, $p < 0.01$).

4.4.2 Hemianopia patients have reduced activity bilaterally when viewing hemifield motion stimuli

Functional activity in response to contralateral and ipsilateral motion stimuli was initially analysed using repeated measures ANOVAs. Bold activity was compared between the lesioned and undamaged hemisphere in patients, and against control subjects. Additionally, activity in each hemisphere (contralateral or ipsilateral) was compared within subjects. Mean BOLD activity and cluster size for each group are shown in Figure 4.5. In striate cortex, across all subjects the percentage BOLD change during the presentation of motion stimuli was greater in the contralateral hemisphere than in the ipsilateral hemisphere ($F_{(1,59)}$=38.15, $p < 0.001$), and there were a greater numbers of voxels showing significant activation ($F_{(2,59)}$=65.26, $p < 0.001$). This was also the case in area MT, both for levels of BOLD activity ($F_{(1,59)}$=27.42 $p < 0.001$) and cluster size ($F_{(1,59)}$=47.29, $p < 0.001$). This pattern of high activity in the contralateral hemisphere and low activity in the ipsilateral hemisphere is as would be expected, since the majority of processing of visual stimuli is carried out in the hemisphere contralateral to stimuli, due to the crossing of nasal fibres at the optic chiasm.

While the ipsilateral/contralateral difference in activity was consistent across V1 and MT for both measures of functional activity, patterns of activity differed across groups, as did the extent of the ipsilateral/contralateral difference in BOLD activity. In V1, there were significant differences in cluster sizes between all groups (all $p < 0.01$, main effect $F_{(2,59)}$=21.49, $p < 0.001$), and in overall BOLD activity between control subjects and the lesioned hemisphere in patients ($p < 0.01$, main effect $F_{(2,59)}$=6.25,

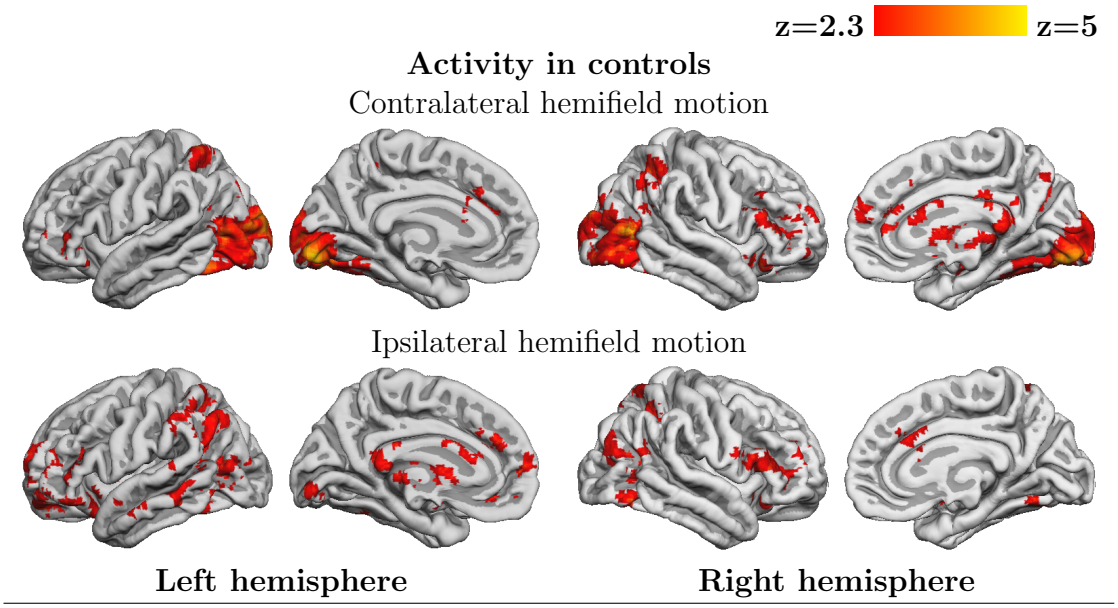

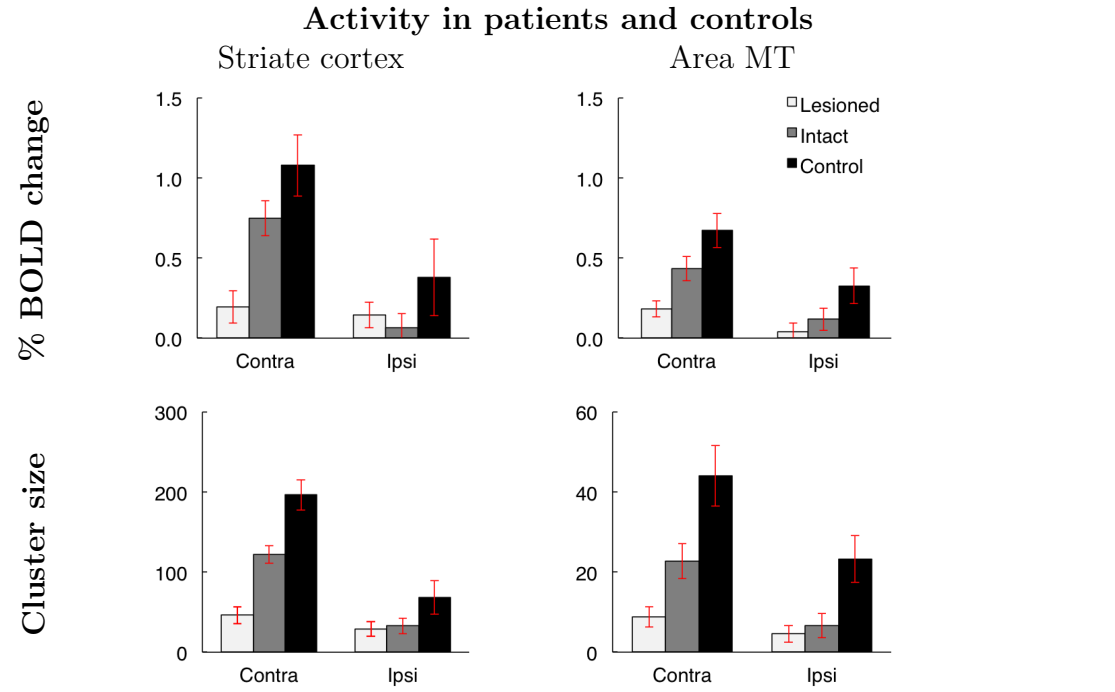

Figure 4.5: Activation in response to hemifield moving dot stimuli. The average BOLD response in controls to moving dots presented in the ipsilateral and contralateral hemifields are shown (group FEAT analysis). Consistent with expected activation patterns, the majority of activity was in response to contralaterally presented stimuli. For each of the visual areas, the % BOLD change and active cluster size are shown, for ipsilateral and contralateral stimuli. For patients, means for the intact and lesioned hemispheres are shown separately, while control group results are averaged across hemispheres. Standard errors are shown for each group.

$p < 0.05$). There was also a significant interaction between hemifield and group for cluster size ($F_{(2,59)}$=11.55, $p < 0.001$), and level of BOLD activity ($F_{(2,59)}$=9.24, $p < 0.001$). Comparison of the means shown in Figure 4.5 suggests that this is likely due to small differences between ipsi- and contralateral activity in the lesioned hemisphere, in comparison to greater differences between these in the undamaged hemisphere and controls.

In area MT, there was less variation in patterns of activity between the groups. While there was a main effect of group for both cluster size ($F_{(2,59)}$=14.19, $p < 0.001$) and percentage BOLD change ($F_{(2,59)}$=7.19, $p < 0.01$), post hoc comparison of groups using Bonferroni correction showed no significant differences in functional activity between the lesioned and undamaged hemisphere in patients, however both percentage BOLD activity and cluster size were lower in the lesioned hemisphere of patients in comparison to controls (both $p < 0.01$), with the latter also being significantly greater in controls than in the undamaged hemisphere of patients ($p < 0.01$). For cluster size, there was an interaction between hemisphere and group ($F_{(2,59)}$=3.74, $p < 0.05$), and as with striate cortex, this is likely mediated by the relative consistency between cluster sizes in response to ipsi- and contralateral stimuli in the lesioned hemisphere, where there is a reduction in activity in the ipsilateral hemisphere in controls and the undamaged hemisphere of patients. Unlike in the central motion scan, here there was no evidence of patients having greater activity in MT in the undamaged hemisphere than in control subjects.

To further investigate differences in activity in the lesioned and undamaged hemi-

spheres of patients, repeated measures ANOVAs were run, with ipsi/contralateral hemifield and ipsi/contralesional hemisphere included as within subject factors. As would be expected in hemianopia patients, in both V1 and MT for both indicators of functional activity, there was significantly lower functional activation in the lesioned hemisphere of patients ($F_{(1,24)} > 7.26$, $p < 0.05$ in all cases), and less activation in the ipsilateral hemisphere than the contralateral hemisphere ($F_{(1,24)} > 14.89$, $p < 0.001$).

Across the entire patient group, when presented with moving dot stimuli in either the sighted or blind visual field, or centrally spanning both fields, patients showed reduced activity in both V1 and MT in the affected hemisphere. A large number of the patients included have lesions directly affecting V1, and in some cases there was in fact no intact V1 remaining. MT however, was present in all patients with the exception of those who had had extensive resections for epilepsy (01a-3a). Further analysis investigating how functional activity differs between patients will focus on area MT, in those patients where it was intact.

4.4.3 Impact of lesion location on activity in area MT

If any reorganisation occurs in hemianopia in order to increase the ability of the visual system to process motion stimuli in the blind field, it would need to result in increased connectivity to ipsilesional MT via a non striate route, enabling activation in area MT in response to stimuli in the blind field. Alternatively, the usually small ipsilateral response in area MT to stimuli would need to increase. In order for the former to happen, some functional visual pathway would need to be present in the lesioned

hemisphere. It was expected therefore that activity in ipsilesional MT would be greatest in patients with damage to striate cortex, and lowest in patients with optic tract or LGN damage, due to the earlier disruption of the visual pathway in these patients. ANOVAs however showed no significant effects of lesion location on either cluster size or percentage bold change in area MT. As group sizes are small when grouped according to lesion location, mean BOLD activity was plotted for each lesion location (Figure 4.6)

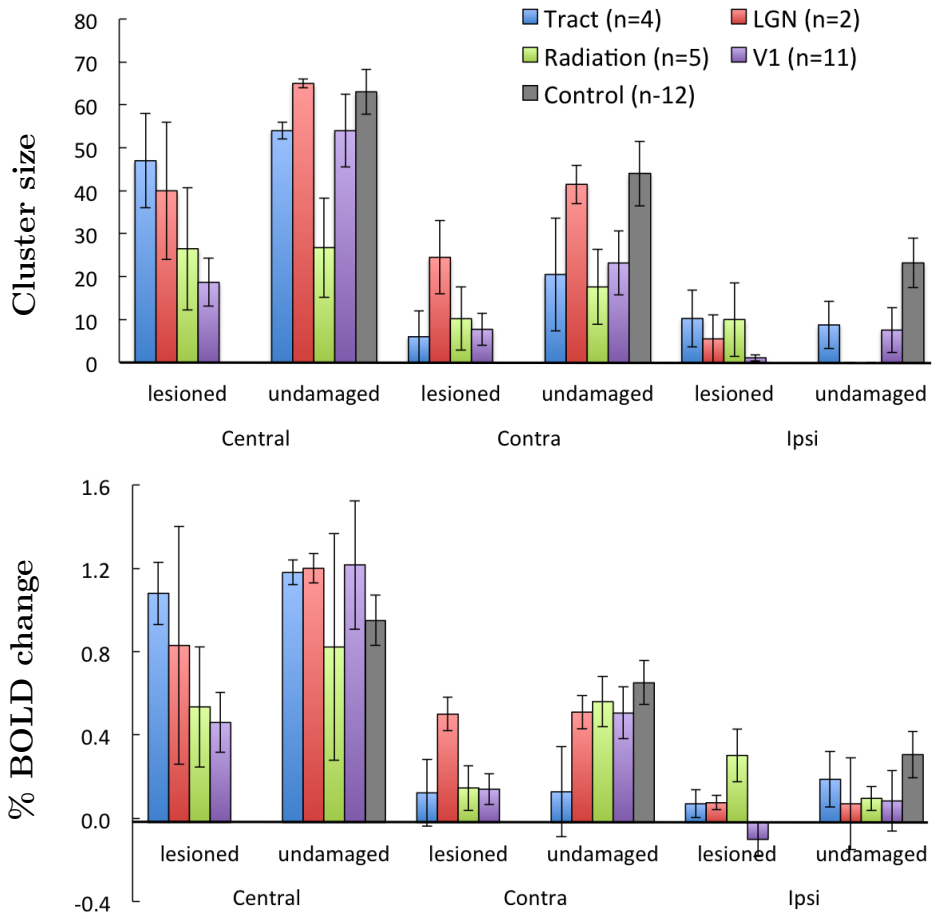

Figure 4.6: BOLD activity in area MT in patients with different lesion locations. Activity in area MT varies widely for patients with different lesion locations, however there is no systematic pattern of MT activity being affected by how early in the visual pathway the damage occurred. Standard errors are shown for each patient group, indicating variability within the lesion groups themselves.

to see whether any trends existed which did not reach significance. The only cases where there was a consistent effect of lesion location was however in the opposite direction to that predicted. For both cluster size and percentage BOLD change, activity in ipsilesional MT to centrally presented moving stimuli in fact was higher when lesions were earlier in the visual pathway. However, conclusions from this graph should be made with caution, as results varied between subjects with the same lesion location, as evidenced by the large standard errors of the mean in many cases.

4.4.4 Impact of lesion size on activity in MT

It was hypothesised that the extent to which motion stimuli activated area MT would be influenced by lesion size, in patients with damage affecting the cortex. In the lesioned hemisphere, it was expected that activity in area MT would reduce with lesion size. Therefore the percentage of the ipsilesional occipital lobe that was damaged

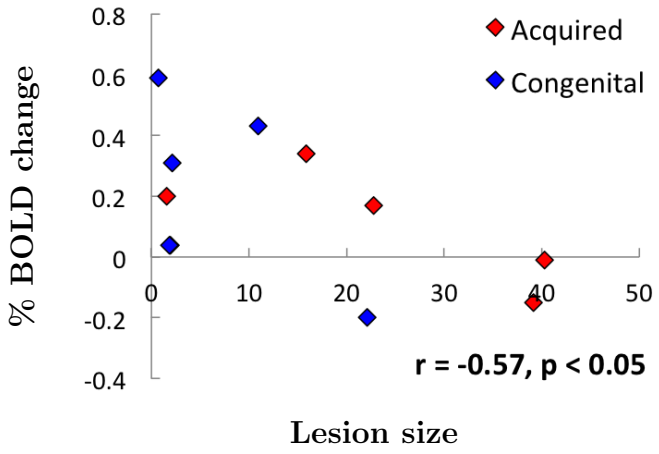

Figure 4.7: Relationship between Lesion size and BOLD activity in ipsilesional MT. Activity in MT in the lesioned hemisphere is lower in patients with large lesions in comparison to those with smaller lesions.

was correlated with activity in MT. Pearson correlations showed that there was no significant relationship between lesion size and BOLD activity in MT in the undamaged hemisphere, or for BOLD activity in response to ipsilateral activity in the lesioned hemisphere. There was a significant negative relationship between lesion size and the percentage BOLD change in the lesioned hemisphere in response to contralaterally presented motion stimuli ($r = -0.57$, $p < 0.05$, 1 tailed pearson correlation). This relationship is shown in Figure 4.7, with patients colour coded according to whether they had congenital or adult acquired hemianopia. For acquired patients in particular there appears to be a strong relationship where BOLD activity decreases as the lesion size increases. This would be expected, as in cases where a large lesion in present, there is a lower likelihood of functioning pathways to area MT existing.

4.4.5 Activity in area MT does not differ between patients with acquired and congenital hemianopia

As the visual system has a greater capacity to reorganise and compensate when damage occurs early in life, congenital patients might be expected to show greater activity to motion stimuli in ipsilesional MT than acquired patients, and greater activation in response to ipsilaterally presented stimuli, both of which could aid perception. However, there were no significant differences in MT activity between patients with acquired or congenital hemianopia. In fact, while not significantly different, in the lesioned hemisphere, congenital patients seem to have slightly less activity than acquired patients (Figure 4.8). Even if this difference were significant however, it could be argued that

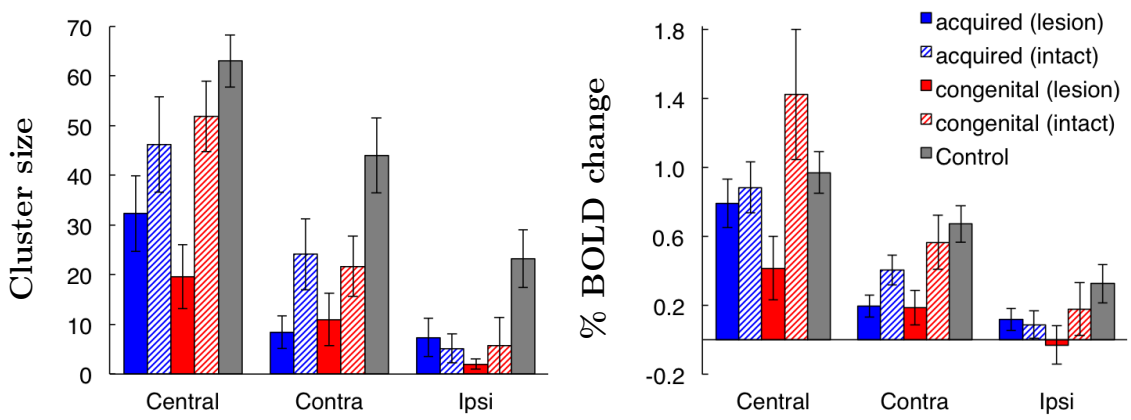

Figure 4.8: Comparison of MT activation in acquired and congenital hemianopia. For both acquired and congenital patients, activity is reduced in the lesioned hemisphere in response to central and contralaterally presented stimuli; ipsilateral responses are uniformly low. While congenital patients appear to have a greater difference between activity in the lesioned and intact hemisphere than acquired patients, the groups were not found to be significantly different.

this was not an effect of when the lesion was acquired, but rather a consequence of the lesion location, as previous analyses have suggested that MT activation is lower in patients with striate cortex damage, which is the case in the majority of congenital patients. As the patients studied vary on a number of different factors, there are issues with disentangling the exact cause of differences between groups.

4.4.6 Motion discrimination tasks

During the motion discrimination tasks, patients were questioned on the extent to which they perceived stimuli in their blind fields. For many patients, a floor effect occurred, where patients were unable to discriminate the direction of motion at even the highest possible contrast levels. In all cases where this occurred, the patient denied any knowledge of stimuli being present in the blind field. Where patient performance

did not show a floor effect, responses were more variable, as will be discussed below. Where patients did not have visual field loss that covered the entire quadrant being tested, or where macular sparing existed, efforts were made to adjust the stimulus location such that the entirety of the stimulus fell in the blind field for every patient.

Luminance defined motion

The majority of patients were unable to identify the direction of motion in the luminance defined motion task, and acknowledged no awareness of any stimuli being present in the blind field. However, a small number of patients were able to perform this task, correctly identifying the direction of motion when the contrast was sufficiently high (Figure 4.9). These patients all had lesions affecting the visual pathway before V1; either the optic radiation, LGN, or the optic tract. That the patient with optic tract damage could discriminate motion direction in his blind field was surprising, as it should be necessary for the optic tract to be intact for any residual processing to take place. It is possible that assuming the result was not attributable to experimental error (which will be discussed later), that if the damage affects the posterior regions of the tract, some fibres may reach the cortex via a non geniculate route, as must presumably be the case in the patient with damage to the LGN. When questioned on their perception of motion in the blind field, all patients reported some degree of conscious perception of the motion stimuli. L1a reported the motion as being like a line going in a certain direction, although she could not see the square stimuli; for colour defined motion stimuli the patient reported seeing a 'blue blur' at times, although she could

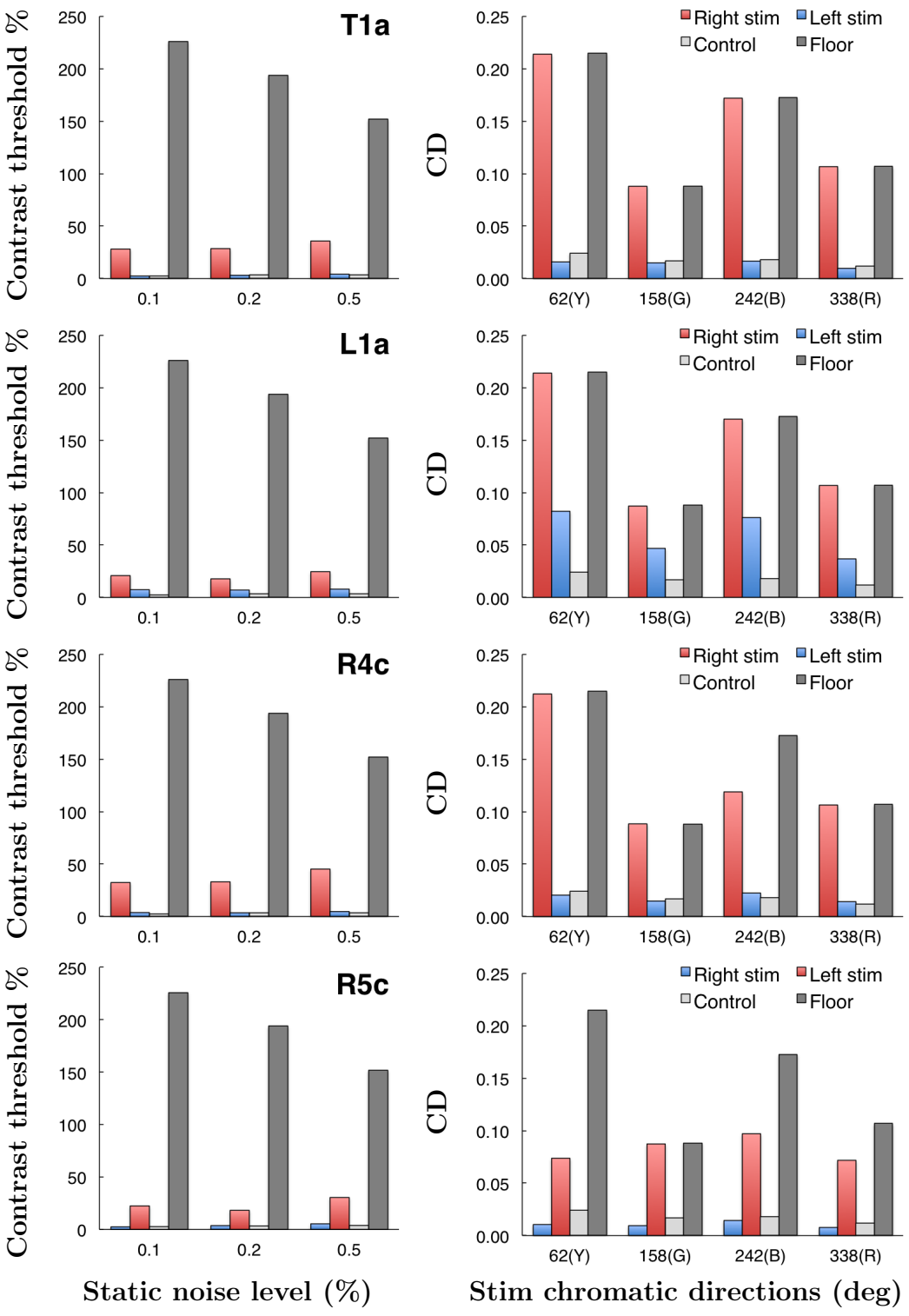

Figure 4.9: Motion discrimination in the blind field. Four patients discriminated the direction of luminance defined motion in their blind field (red bar). Two of these patients also showed some evidence of colour defined motion discrimination. Patient detection thresholds are shown for left and right VFs, with a control subject and the floor value for comparison. CD: chromatic displacement

not tell the direction of motion. T1a reported that he is aware of motion in his blind field in every day life, although it is indistinct and blurred; when the coloured stimuli were shown he reported a 'shimmer' as being present, with no perception of motion direction. Both R4c and R5c made similar reports. As the patients are consciously aware of the motion stimuli, this would be termed Riddoch phenomena.

Colour defined motion

The colour defined motion task was performed at floor by almost all of the patients tested, including the two patients with acquired lesions who could discriminate luminance defined motion. In the congenital subjects who could discriminate luminance defined motion however, there was also some evidence of an ability to process colour defined motion, in particular with blue stimuli. In R4c, performance was at floor for red, green and yellow stimuli, however he was able to discriminate direction of movement of the blue stimulus when it was at a high enough contrast. R5c performed similarly to R4c on the blue stimulus, and was also able to perform the task with the yellow stimulus, and to some extent the red stimulus. It is notable that neither subject was able to perform the task at all when the green stimulus was shown, making it unlikely that their performance was solely mediated by eye movements into the blind field, as this should improve performance for all colours. There was also no instance, for either the luminance or the colour defined motion tasks, where patients performed as well in their blind field as in the sighted field, where performance was generally similar to that of a healthy young control.

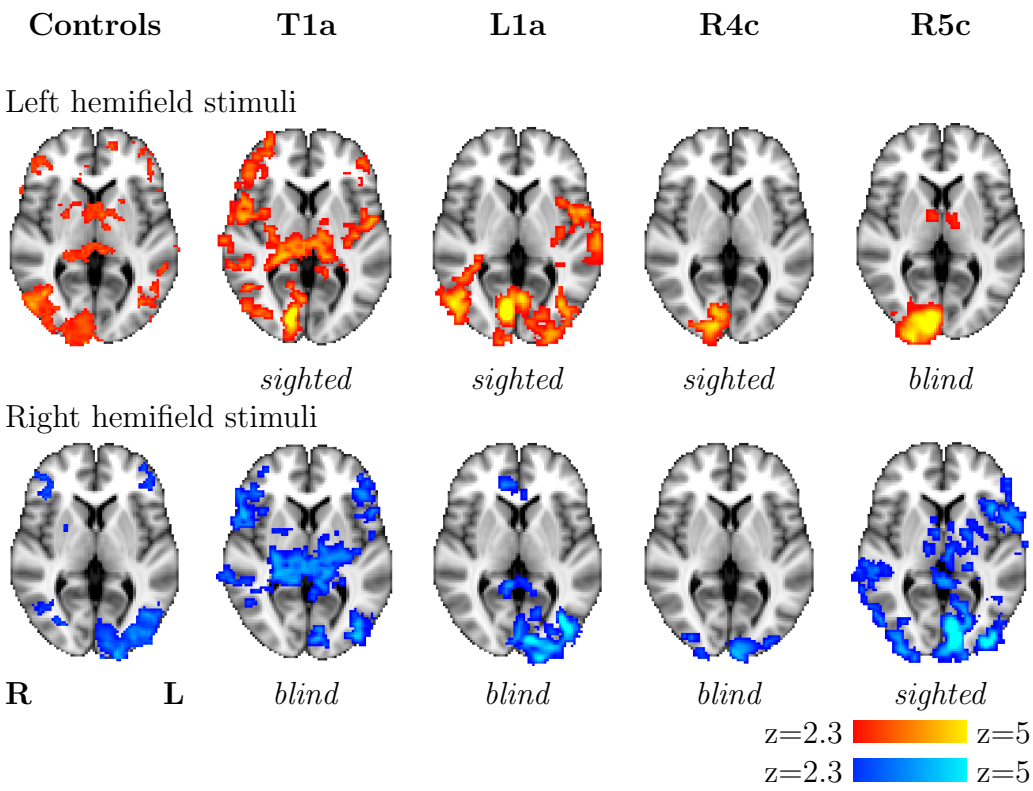

Figure 4.10: fMRI results for patients able to discriminate motion in the blind field. BOLD responses to stimuli presented in the left (top row) and right (bottom row) hemifields are shown for the control group, and for each patient. The axial slices (z=4, MNI coordinates) shown show the levels of activity in both V1 and MT. Asterisks show activation in response to stimuli in the blind field for patients.

fMRI activity in patients able to discriminate motion in the blind field

To understand why these patients are able to process stimuli in the blind field, results from the fMRI hemifield motion scan were investigated for each of the four patients. The results were mixed, with evidence of blind field stimuli being processed by area MT present in T1a and L1a, but not in either of the congenital patients (R4c and R5c). In T1a, patterns of activity in V1 and MT look to be similar to the control subjects, although reduced in magnitude, with the exception that there is no ipsilateral response to motion stimuli in the blind field. Motion stimuli in the blind hemifield

is therefore being processed to some degree by MT in both the lesioned and undamaged hemispheres. L1a shows an unusual pattern of activity, with substantial BOLD activation in the lesioned hemisphere in response to ipsilateral motion stimuli. Again, there is activity in ipsilesional area MT in response to motion stimuli in the blind field. R5c shows widespread activity in response to stimuli presented in the sighted field, in contrast to very localised activation in striate and extrastriate cortex for stimuli in the blind (left) hemifield. There were no significantly active voxels in area MT in either hemisphere in response to stimuli in the blind hemifield. In contrast to the other three patients investigated, R4a shows little or no activity in what would usually be considered to be area MT in either hemisphere. There is however evidence of blind field stimuli being processing bilaterally, in contrast to stimuli in the sighted field, which provokes contralateral activity only.

4.5 Discussion

4.5.1 Hemianopia patients have reduced activity in the visual cortex when viewing motion stimuli

Following a lesion to the post-chiasmal visual pathway, whether in V1 or elsewhere, patients show reduced activity in the occipital cortex when viewing moving dot stimuli designed to activate V1 and the motion area MT. This reduction in activity is greater in the lesioned hemisphere, as would be expected, however the reduction in activity also appears to affect the undamaged hemisphere, although to a lesser extent. This

latter result conflicts with the study by Goebel et al. (2001), who reported comparable activation between controls and the intact hemifield of patients when viewing stimuli in the good hemifield. However, the difference between groups in this study is likely small, as only the extent of the activated region differed between controls and the intact hemisphere of patients, and not the overall BOLD percentage change for the region.

4.5.2 Activity in MT cannot easily be predicted according to the type of lesion present

Activity in area MT was variable from patient to patient, however the predicted effects of lesion location, size, and age on MT activity did not in general occur. Activity in area MT in the lesioned hemisphere of hemianopia patients presumably relies on non-striate input to MT, possibly through a direct route from either the pulvinar or the koniocellular layers of the LGN. The exception to this is in patients with some activity remaining in spared regions of striate cortex, as described by Morland et al. (2004). It was expected therefore that patients with damage early in the visual pathway would have less activity in area MT than those with striate or perhaps optic radiation lesions, as in these cases where the damage is later, subcortical pathways to MT are more likely to exist. There was however no evidence of this. Indeed in many cases, the striate patients appeared to show lower MT activity than other patients.

There was, however, a relationship between lesion size and the level of BOLD activity in the lesioned hemisphere of patients with occipital damage. As the patients with cortical damage tended to have significantly larger lesions than those with damage

to the optic tracts, LGN, and in some cases, the radiations, this lack of a clear pattern may be due to conflicting impacts of lesion size and location. The lack of a difference in activity between congenital and acquired patients may also be related to group differences in lesion locations and size, as two thirds of patients in the congenital group had direct V1 damage, in contrast to less than half of the acquired group. The heterogeneity of the group makes it difficult to interpret the differences found. Furthermore, it may be that in order to understand the different patterns of activity in patients with different lesions, an understanding of the presence of both plasticity and degeneration in the pathways of individual patients would be required, as these could be considerably different even in patients with apparently similar lesions.

4.5.3 Problems with measuring the neural response to motion stimuli with fMRI

There are a number of potential problems with the acquisition of imaging data which may impact on results. First and foremost, eye movements were not recorded during the collection of functional imaging data. When motion stimuli were presented centrally, this is less important, however it is possible that responses to stimuli presented in the blind field were the product of eye movements into this region. In a minority of the congenital subjects in particular, this may have been a factor, as some of these subjects reported during behavioural testing that they found it very difficult not to automatically look into the blind field, as it was a heavily ingrained compensatory technique. In the majority of these patients however, this is unlikely to have been a

large issue, as they were accustomed to performing similar tasks having taken part in similar previous experiments. Indeed the twelve patients who took part in the motion testing outside of the scanner also completed a further task where their pupils were recorded while they were required to fixate a central point for long periods while being shown peripheral stimuli, and all of these patients showed good fixation.

As the data were collected over the course of a three year period, hardware upgrades meant that it was not possible to maintain the exact same stimuli for all subjects. Every effort was made to ensure that any stimulus changes were minimal, and additionally, the stimulus used was a relatively coarse one, designed purely to activate the motion area as strongly as possible. It is unlikely therefore that extensive differences in MT activation would occur as a result of any stimulus differences that persisted.

Beyond these technical issues, there may also be limitations relating to the use of fMRI to quantify brain activity in patients with atypical physiology, due to, for example, stroke. fMRI is not a direct measure of neural activity, and it depends on a range of neurophysiological events, which may be abnormal in patients (Iannetti and Wise, 2007). In stroke patients in particular, vasculature is atypical, and thus baseline measures in these patients will already be different from those in healthy controls, making a comparison between groups difficult. In the cohort studied, hemianopia arises from a range of different pathologies, including tumours, strokes, epilepsy, and trauma, all of which may impact on the baseline BOLD measurement in different ways. It may be that arterial spin labelling (ASL) would be a better measure of neural activity in a cohort such of this, as this technique gives an absolute measure of blood flow, and is

therefore less heavily compromised by pathological changes in underlying physiology.

4.5.4 Patients demonstrating strong residual motion processing did not have V1 damage

The majority of patients were not able to perform the motion discrimination task in their blind field. This is perhaps not surprising, as it has been shown that the ability to discriminate the direction of motion can be difficult to elicit when anything but the simplest of stimuli are used (Azzopardi and Cowey, 2001). In spite of this, four patients were able to discriminate the direction of luminance defined motion stimuli. A higher contrast between the stimulus and the background was required than in the good field, where most patients performed similarly to a healthy control subject. Two of these patients were unable to perform the task when the motion stimulus was colour defined, making it unlikely that the performance was based on eye movements into the blind field. It was anticipated that patients with the ability to process motion in the blind field would have cortical damage, however, these two patients had damage to the LGN and the optic tract. The performance in the patient with LGN damage could be due to visual information reaching area MT via a pulvinar route, however it is unclear how a patient with optic tract damage could show residual function. The patient reported that he is frequently aware of moving stimuli in his blind field, in spite of the complete left hemianopia shown by Humphrey perimetry. It is possible that some fibres may have left the tract prior to the location of the damage, or that a few diffuse fibres have survived the damage, which could carry sparse information to the visual cortex.

However, this would need to be the subject of further investigation.

The two congenital patients with residual motion perception also had damage outside of the striate cortex, in this case in the white matter, affecting the optic radiations, together with some grey matter damage. These patients were also able to discriminate the direction of colour defined motion for some colours. For patient R4c, this ability was restricted to blue stimuli, suggesting that the ability might be mediated by the direct route from the koniocellular layers of the LGN to area MT, which contains cells which receive input from the short wavelength cone cells, and thus respond best to blue stimuli. R5c was also able to respond to blue stimuli, and in addition to this, yellow stimuli (which are also processed by the koniocellular pathway), and also, to some extent, red stimuli. It is unlikely that these results were due to eye movements into the blind field, as for both patients, there were colours of stimuli that they were unable to process under any conditions. The advantage for processing blue stimuli is notable, in particular when it is considered that although unable to discriminate motion direction, L1a reported being aware of blue flashes in her blind field. The koniocellular pathway provides a possible candidate for underlying this capacity for awareness of, and ability to respond to, motion stimuli in the blind field.

4.5.5 Conclusion

Activity in the visual cortex is reduced in the lesioned hemisphere in hemianopia. The extent to which activity is reduced, and the relative amounts of activation to ipsilateral and contralateral stimuli, vary from patient to patient, although not in a

systematic fashion that can easily be attributed to the underlying pathology. Residual motion processing is possible in patients with damage to earlier locations in the visual pathway than striate cortex, some of which may be due to a functioning pathway existing between the koniocellular layers of the LGN and area MT.

Chapter 5

Non-striate vision: investigating connectivity between the pulvinar and motion area MT using diffusion imaging

5.1 Abstract

Objective To investigate the existence of a direct pathway from the pulvinar to area MT in hemianopia, and to assess whether this pathway is stronger in patients with congenital hemianopia.

Methods Diffusion tensor imaging was used to segment the pulvinar according to its connectivity with area MT, primary visual cortex, and two non visual areas, primary

somatosensory cortex and auditory cortex.

Results The pulvinar was successfully segmented according to its cortical connectivity, with more extensive connections between the pulvinar and MT being found in the lesioned hemisphere of patients in comparison to in the contralesional hemisphere and controls. This increased connectivity to area MT was particularly evident in those patients with the ability to detect motion stimuli in their blind hemifield. Contrary to predictions from the literature, there was no evidence of greater reorganisation of pulvinar connectivity in patients with lesions acquired congenitally.

Interpretation The non-striate pathway from the pulvinar to area MT is a candidate for the 'blindsight' pathway, as evidenced by its increased strength in hemianopia, particularly in patients who can process motion stimuli in their blind field.

5.2 Introduction

The projection from the retina to the primary visual cortex via the LGN, the retino-geniculo-striate pathway, is widely agreed to be the major pathway through which visual information is processed. From the primary visual cortex, or V1, visual information is relayed to higher visual areas along either the dorsal or ventral streams for 'how' and 'what' information respectively Goodale and Milner (1992). However, evidence of intact residual visual processing in hemianopia patients in the absence of V1 has demonstrated that other visual pathways must exist (reviewed by Cowey and Stoerig (1991) and Cowey (2010)). It is unclear which pathways underlie this visual function,

and whether they are the product of the strengthening of existing visual pathways, or new pathways being created as a result of cortical reorganisation.

While evidence for degeneration of the visual pathway following damage to V1 and other locations has been conclusively shown, the existence of plasticity and reorganisation of the visual system after damage remains controversial. Damage sustained very early in life, either pre- or peri-natally, has been shown to result in considerable reorganisation of the visual system (Hoyt, 2003), with some children showing relatively normal visual fields in the absence of striate and prestriate cortex (Werth, 2006). However, with a few exceptions, evidence for cortical reorganisation following adult acquired damage has been limited. Where plasticity has been found, as in Dilks et al. (2007), where a stroke patient showed distorted visual perception following a stroke, reorganisation has not approached the level of alteration found in children. The exception to this is the often reported blindsight patient GY, who has been shown to have atypical cortical connections to the motion area MT (Bridge et al., 2008; Silvanto et al., 2009), and reorganisation of cortical maps in extrastriate visual areas (Baseler et al., 1999).

5.2.1 Visual pathways exist which bypass V1

A number of pathways have been reported which relay information from the optic tract through to extrastriate visual cortex, bypassing the primary visual cortex. The first pathway is the geniculo-extrastriate pathway, which relays information from the retina to the koniocellular layers of the LGN, and then projects directly to extrastriate cortex

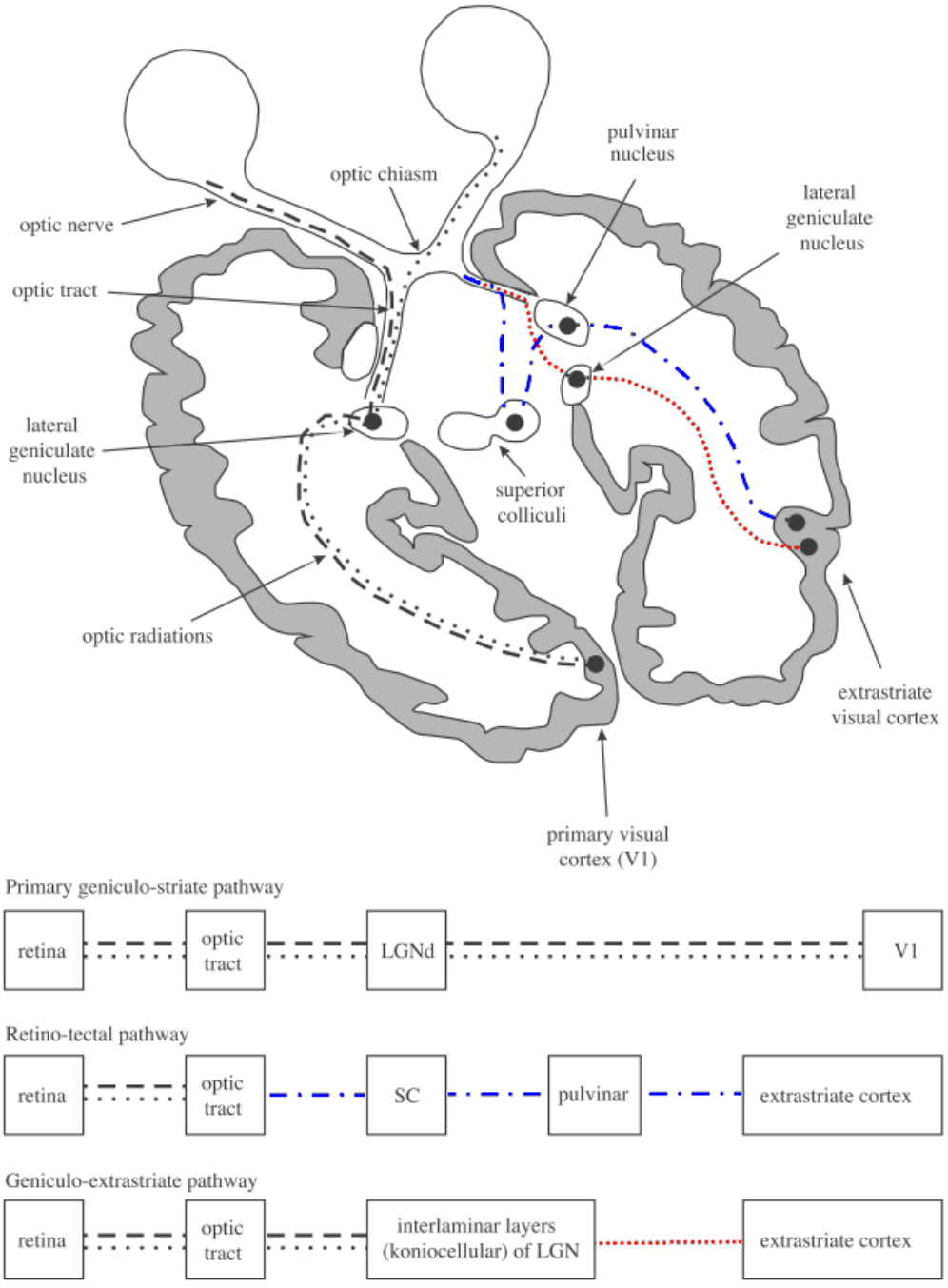

Figure 5.1: Depiction of the striate and extrastriate visual pathways. The pathways which bypass V1 have been outlined in blue (the pulvinar pathway) and red (the koniocellular pathway). Figure adapted from Danckert and Rossetti (2005).

(Sincich et al., 2004). Other pathways project from the retina to the pulvinar, either directly (Warner et al., 2010) or through the superior colliculus (Harting et al., 1973),

and then to the extrastriate cortex. Evidence for the existence of these pathways has come almost exclusively from anatomical studies in non-human primates. Recently, cells have been found both in the pulvinar and the koniocellular layers of the LGN that project to area MT in marmoset monkeys (Warner et al., 2010). In the LGN, these are located in the K1 and K3 layers, while pulvinar projections to area MT are located specifically in the medial portion of the inferior pulvinar nucleus (PIm), an area which is adjacent to, but distinct from, the posterior inferior pulvinar nucleus (PIp) and the central medial inferior pulvinar nucleus, regions which receive input from the superior colliculus (Stepniewska et al., 2000). Investigation of the anatomy underlying blindsight has found evidence for involvement of both the pathway through the LGN (Schmid et al., 2010), and the colliculo-pulvinar pathway (Leh et al., 2006b). When these pathways are inaccessible to patients, either due to inactivation (e.g. of the LGN) or due to the specific choice of visual stimuli, patients no longer exhibit the same level of residual visual function in the blind field. Having already been the subject of DTI investigation in hemispherectomy patients (Leh et al., 2006a), it is the pulvinar route that will be investigated here.

5.2.2 Cortical connections of the pulvinar

In addition to its connections to the visual cortex, the pulvinar is also connected to a wide range of other brain regions, including cortices involved in the processing of other sensory stimuli (Figure 5.2). The pulvinar can be subdivided into a number of separate regions according to its cortical connections as follows. The anterior region

of the pulvinar (also called the oral pulvinar (Grieve et al., 2000)) is connected to the primary somatosensory cortex, including Brodmann areas 2 (Pons and Kaas, 1985), 3a (Huffman and Krubitzer, 2001), and 3b (Darian-Smith et al., 1990; Krubitzer and Kaas, 1992). The auditory cortex receives input from the pulvinar, with the medial portion of the pulvinar projecting to the superior temporal gyrus including the parabelt, which forms part of the auditory cortex (Kaas and Hackett, 2000). Finally, the pulvinar input to the visual cortex is primarily located in the inferior and lateral pulvinar, with projections to V1 and V2 originating in these regions (Shipp, 2003). Connections to area MT are typically found in similar locations, together with an extra area of connectivity in the medial part of the inferior pulvinar, extending into the medial pulvinar (Standage and Benevento, 1983).

Evidence from studies of visual pathway development in marmoset monkeys have suggested that while in adults the V1 projection to MT is far greater than that from the pulvinar, early in development, connectivity to area MT is very different (Warner et al., 2012). In neonates, the greatest input to area MT comes from PIm, with V1 input gradually increasing over time, and the pulvinar input reducing with maturation. In the absence of input from V1, as may be found in patients with congenital hemianopia, it is possible that this pathway may be stronger than in healthy subjects, potentially underlying the residual vision demonstrated in those patients with blindsight. This has recently been found to be the case in marmoset monkeys where V1 was lesioned very early in life (James Bourne, personal communication, unpublished data). In cases of adult acquired hemianopia, some reorganisation may also be possible, however as the

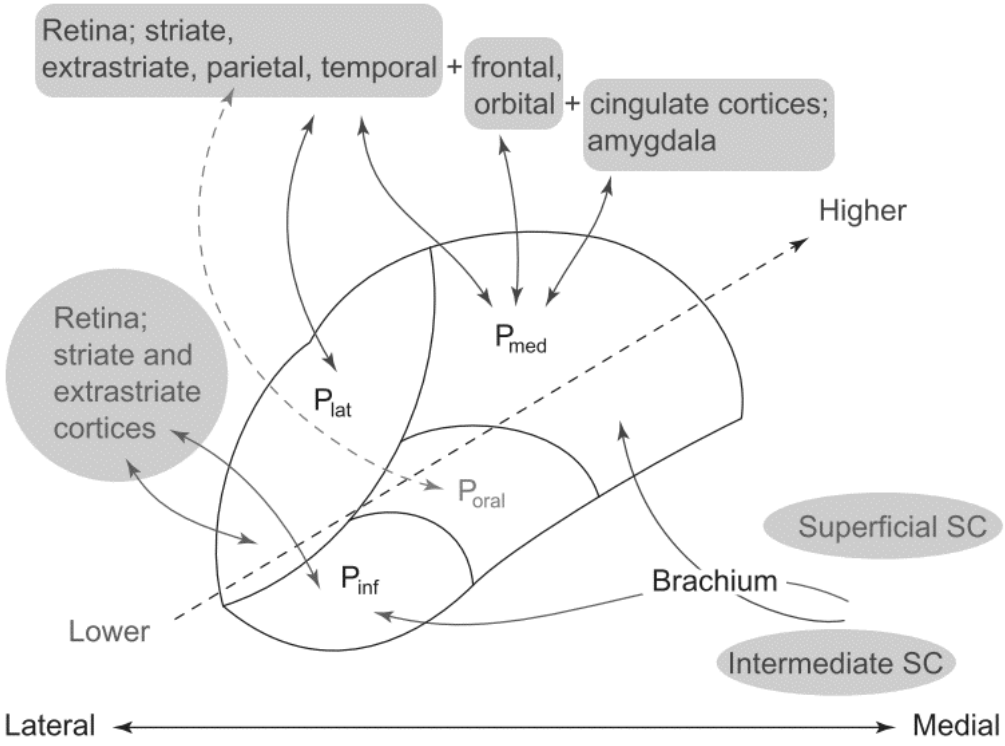

Figure 5.2: Cortical connections of the pulvinar. The different regions of the pulvinar are shown as follows: P_{inf} inferior pulvinar, P_{med} medial pulvinar, P_{lat} lateral pulvinar, P_{oral} oral or anterior pulvinar. The arrows show some of the known cortical connections with the pulvinar, and the regions where they connect. Figure adapted from Grieve et al. (2000).

visual system is not as plastic in adulthood, reorganisation in congenital subjects may be more likely to occur.

5.2.3 Investigating connectivity using DTI

While most studies investigating the visual pathways have necessarily involved non-human primates, diffusion tensor imaging provides a means of investigating reorganisation of the pulvinar's cortical connections in human patients. Leh et al. (2007) demonstrated that DTI can be used to investigate the pulvinar's cortical connections, finding connectivity consistent with the animal literature. Specifically, connections

were found to prefontal cortex, the frontal eye fields, posterior parietal association areas, and a range of visual areas including V1, V2, and MT. The relative strengths of these connections were not reported, however it is notable that a pathway to area MT was found in healthy controls. Additionally, techniques exist which can identify specific regions within a brain structure that are connected to different brain regions. For example, DTI has been used successfully to segment the thalamus, including the pulvinar, according to its cortical connectivity (Behrens et al., 2003a; Johansen-Berg et al., 2005). It may therefore be possible to employ DTI to assess the strength of connectivity between area MT and the pulvinar in hemianopia patients, to see whether greater connectivity exists between these regions in the lesioned hemisphere.

5.2.4 Aim of the present study

This study aimed to determine whether the pathway between the pulvinar and area MT is strengthened in the absence of a functioning primary visual pathway. The cortical connections of the pulvinar were investigated in a group of patients with either congenital or adult acquired hemianopia, as well as in a group of healthy controls. Diffusion tensor imaging was used to quantify the level of connectivity between the pulvinar and the main sensory cortices (primary visual cortex, primary somatosensory cortex, and primary auditory cortex) and area MT. In addition to this, the extent of connectivity between the pulvinar and area MT was correlated with residual visual function in patients, to ascertain whether any strong pathways found have a functional benefit to patients.

5.3 Methods

5.3.1 Subjects

13 patients with acquired hemianopia, and 9 with congenital hemianopia were included in this study, together with twenty control subjects. Details for each included patient are shown in Table 5.1, and they are labelled consistently with elsewhere in the thesis. Patients with extensive occipital resections were not included in this DTI study, as tractography would not be possible due to the extent of the damage to grey and white matter. Control subjects were included from both Brazil (n=8, mean age 47, range 30 to 54 years) and the UK (n=12, mean age 41, range 21 to 74 years).

5.3.2 Image acquisition

Diffusion-weighted images were acquired for all subjects, together with high-resolution T1-weighted structural images for registration purposes. Diffusion images were acquired at a resolution of 2x2x2 mm^3, and T1-weighted images were acquired at a resolution of 1x1x1 mm^3. Further details of protocols for the acquisition of these images are described in Chapter 2.

5.3.3 Image preprocessing

Diffusion images were first corrected for distortions resulting from eddy-currents and head movements. Where more than one repeat was acquired, data were averaged to increase the signal to noise ratio. Images were skull stripped using the brain extraction

Table 5.1: DTI study patient details

	Damaged hemisphere	Lesion location	Duration (y)
T1a*	Right	optic tract	3
T2a*	Left	optic tract	3.5
T3a	Left	optic tract/radiation	1.5
T4a	Right	optic tract/radiation	4
L1a*	Left	LGN	3
R1a	Right	radiation	3
R2a	Right	radiation	5
R3a	Right	radiation (Meyer's loop)	2.5
S1a*	Left	V1+	18
S2a*	Left	V1+	5
S4a*	Right	partial V1	2
S5a	Left	partial V1+	3
S6a*	Right	partial V1	3
L2c*	Left	LGN/radiation	congenital
R4c*	Left	radiation/V1	congenital
R5c*	Right	radiation/extrastriate cortex	congenital
S7c*	Left	V1	congenital
S8c	Right	V1	congenital
S9c	Left	V1	congenital
S10c	Right	V1	congenital
S11c	Right	V1+	congenital
S12c*	Left	V1	congenital

* subjects who were tested for ability to discriminate motion in the blind field

tool (Smith, 2002). Diffusion tensor models were applied using DTIFIT, part of FDT (FMRIB's diffusion toolbox), to obtain images of fractional anisotropy (FA) and mean diffusivity (MD) levels. BedpostX was then run on the DTI data for each subject in order to create the files necessary to run probabilistic tractography.

5.3.4 Creation of ROIs

An existing mask was utilised for the pulvinar ROI, which had been created as follows. The pulvinar was identified on anatomical images with reference to the Morel atlas

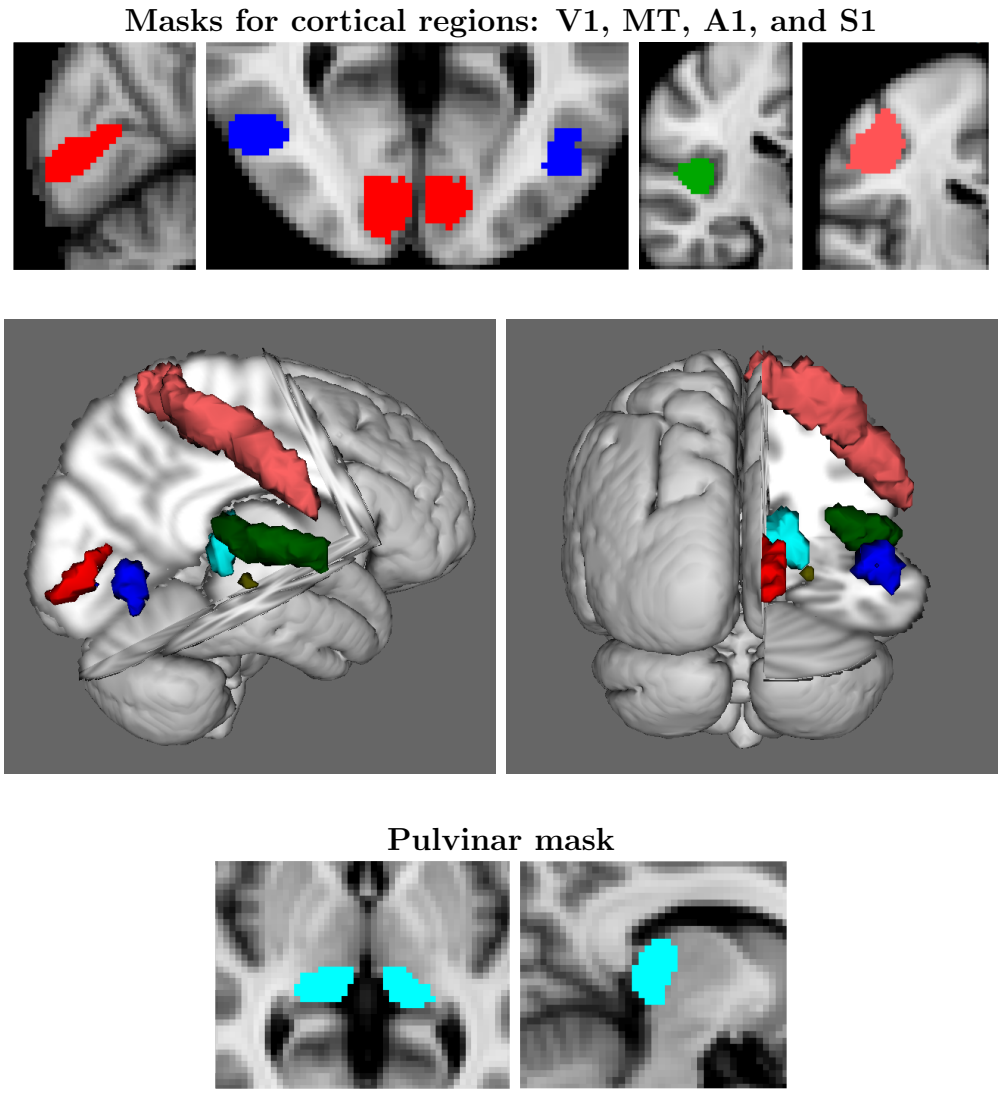

Figure 5.3: Regions of interest used in tractography. Cortical target regions are shown on the top line, and the subcortical seed mask is shown on the bottom row. For the cortical targets, V1 is shown in red, MT in blue, A1 in green, and S1 in pink. The pulvinar is shown in cyan. The same colour key is used in the depictions of the relative positions of the masks in 3D space.

(Morel et al., 1997) and publicly available histological data (http://brainmaps.org). The mask was created by manually drawing the pulvinar on sagittal slices on T1-weighted scans registered to standard space, before refining the edges in the other two principal directions (J. Klein).

V1 was also defined manually, in a manner similar to that used for the pulvinar mask. The calcarine sulcus was manually drawn on sagittal slices on the T1-weighted 2 mm standard brain. Masks for A1, S1, and MT were defined using the Juelich histological atlas. A1 was created by combining areas TE1.0, TE1.1 and TE1.2 (Morosan et al., 2001) This mask extends outside of primary auditory cortex, including the core, belt, and parabelt regions of the auditory cortex, however it will be referred to as A1. Area S1 is generally described as Brodmann areas (BA) 1, 2, 3a, and 3b. It has however been argued that BA3b alone should be considered to be the primary somatosensory cortex, on the basis of the different thalamic inputs and neural response properties of these areas, which favour BA3b as the homologue to monkey S1 (Kaas, 1983). As area S1 is in any case substantially larger than areas MT, V1 and A1 (the areas against which S1 would be compared), the S1 mask created was defined as BA3b (Geyer et al., 2000).

A1 and S1 masks were thresholded at 25% in order to have a big enough mask that still excluded voxels that had a lower likelihood of being part of the required region. MT (Malikovic et al., 2007; Wilms et al., 2005), as a smaller and more variably located region compared to the other regions, was thresholded at 20%. After thresholding, all masks were binarised. Figure 5.3 shows example slices with these masks in standard space, together with a 3D representation of the masks in order to see their relative locations. In addition to these ROI masks, a mask of the corpus collosum was also created manually, to serve as an exclusion mask in tractography. Once complete all masks were non-linearly registered to subject space using FNIRT.

5.3.5 Probabilistic tractography

Probabilistic tractography (Behrens et al., 2003b, 2007) was used to identify and investigate the connections between the pulvinar and areas MT, primary visual cortex, primary somatosensory cortex, and primary auditory cortex.

Probabilistic tractography works by estimating the probability that neighbouring voxels are connected in a tract on the basis of their principal diffusion directions. Analyses were run in subject structural space, with linear transformation to diffusion space utilised. In the first instance, the pulvinar mask was employed as a seed mask, and S1, V1, A1 and MT masks were included as classification targets. In order to quantify the connectivity between voxels in the pulvinar and the target locations, 5000 streamline samples were drawn through probability distributions on each fibre direction from seed voxels in the pulvinar, to estimate connectivity distributions from each seed voxel. Voxels whose principal diffusion directions align to a great enough extent are considered part of the tract. For each of the four target masks, the number of samples reaching the target from each voxel of the pulvinar seed mask is recorded, such that the level of connectivity from the pulvinar to each target location is quantified, and the regions of the pulvinar with the strongest connections to the target are identified.

Hard segmentation of the classification output was run on the tractography outputs, where each voxel in the pulvinar was segmented according to which classification target they were most strongly connected to. This technique has been effectively used previously to segment the thalamus (Johansen-Berg et al., 2005). In order to create a probabilistic map of pulvinar connectivity, outputs for control subjects showing

connectivity between the pulvinar and each target were non-linearly registered into standard space, and summed. A further hard segmentation was performed on the resulting maps. The same process was repeated for patients, with lesioned and unlesioned hemispheres being analysed separately.

To assess the extent to which the regions of the pulvinar that project to different cortical regions overlap, the output of the seed classification from tractography was converted into proportions, according to the relative likelihood of a voxel projecting to each cortical mask. This was achieved for each voxel by summing the total samples reaching any target mask from that voxel, and then calculating the proportion of the total samples which reached each target. Therefore a connectivity map of the pulvinar was created for each target for each subject with values from 0 (no samples reaching the specific target) to 1 (some number of samples reaching the target mask from the voxel, and zero samples from that same voxel reaching any other target location). These maps were thresholded to include only voxels with at least a 25% chance of connection to the target, binarised, and individual maps were then summed together in standard space to create group maps showing the regions of the pulvinar that connected to each target.

5.3.6 Function in area MT

To see whether changes in connectivity between MT and the pulvinar have any functional consequence, relationships between tractography results and BOLD activity in area MT in response to motion stimuli were investigated. fMRI previously acquired

and analysed to investigate functional activation in the visual cortex were utilised, as discussed in Chapter 4. Ten out of the 22 patients included had been tested for the ability to discriminate motion in the blind field (starred in Table 5.1), as described in Chapter 4. Those patients who showed evidence of residual visual function (T2a, L1a, R4c and R5c) were prioritised for investigation due to their enhanced perception of motion stimuli in comparison to the other patients.

5.4 Results

5.4.1 Segmentation of the pulvinar in healthy controls

The use of probabilistic tractography to quantify the cortical connections of the pulvinar produced probabilistic maps of the connection strength between the pulvinar and each cortical target for each voxel in the pulvinar. The strongest connectivity found was between S1 and the pulvinar, with, on average in controls, 2520 seeds reaching S1 from the pulvinar voxel with the greatest connectivity. In contrast, the maximum seeds reaching the other cortical targets are lower, with the mean maximum number of seeds reaching V1 (775), A1 (457), and MT (149) from any single voxel in the pulvinar being far lower than for S1 across control subjects. Examples of maps of the different distributions of connectivity for each cortical target are shown for a single control in Figure 5.4. Here, the regions of maximal connectivity are very different between S1 and the visual areas, however the regions of the pulvinar that project to V1 and MT are more similar. Connections to A1 appear to be in between these two regions.

Using these connectivity maps, the pulvinar was segmented according to the relative strength of its connections to S1, A1, V1, and area MT. Previous studies have shown that projections to these different regions of the cerebral cortex originate in different regions of the pulvinar, with the anterior pulvinar connected to S1, medial pulvinar to A1, and inferior and lateral pulvinar connected to V1 and MT, with additional connections to MT from medial areas. To identify these regions in the pulvinar in these subjects, a hard segmentation was applied to the results from the tractography, with each voxel in the pulvinar being classified according to which target the voxel had the highest probability of being connected to, as measured by the number of seeds reaching each cortical target region. The results of this segmentation can be seen in

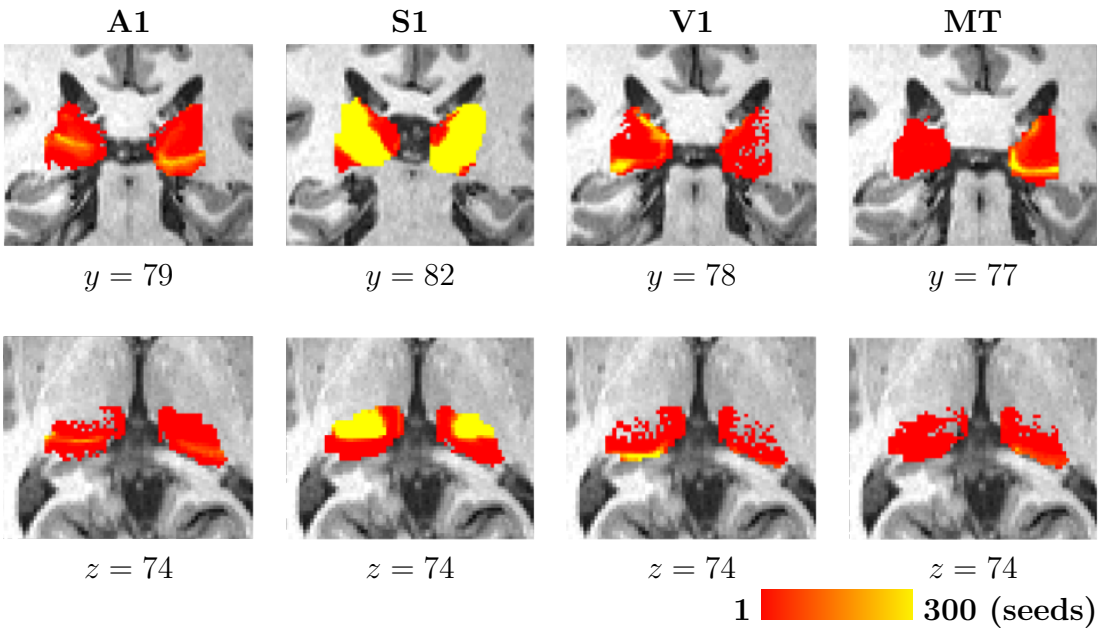

Figure 5.4: Seeds reaching the cortex from the pulvinar in a single subject. The number of seeds reaching cortical targets from each pulvinar voxel are shown, on a scale from red (1) to yellow (300). For coronal slices along the top row, the slice closest to the centre of gravity of the cluster is shown. Axial images all show the same slice, so that the different connectivity maps can be compared. Slice numbers are given to show the relative positions of the slices.

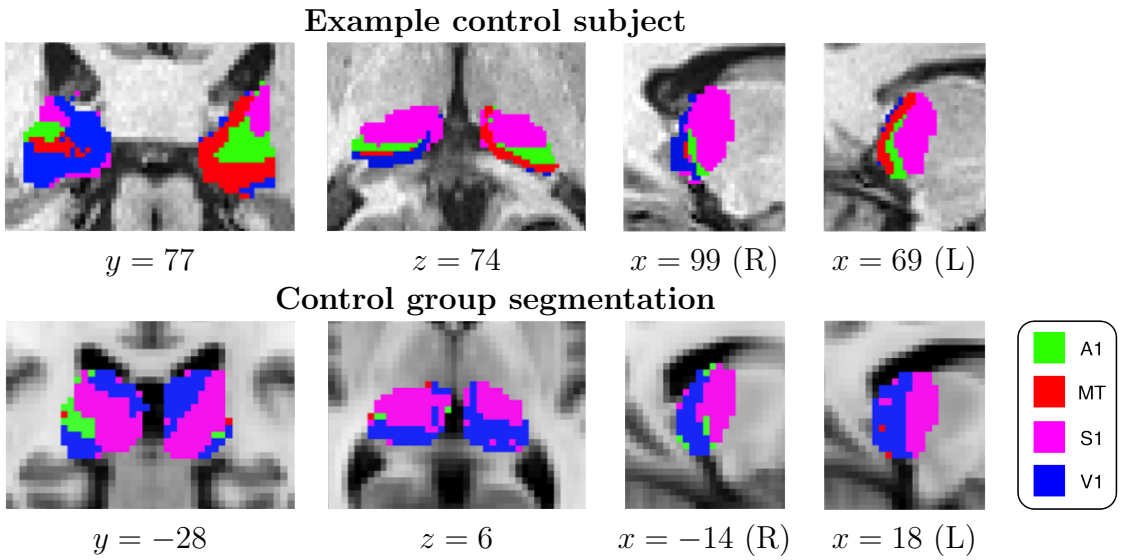

Figure 5.5: Segmentation of the pulvinar in healthy controls.. The top row shows the segmentation in a single control subject, and the bottom row shows the segmentation for the control group. The segmented regions for V1 (blue) and S1 (magenta) are large and similarly located between the individual and group maps. MT (red) and A1 (green) connections are smaller and more variable. Slice numbers are given for the individual subject, and for the group map voxel coordinates are in MNI standard space.

Figure 5.5, both for a single subject (the same subject is shown in Figure 5.4) and for the group average. Approximately half of the pulvinar connects most strongly to S1 (59% in the left hemisphere, 45% in the right). Most of the remaining voxels connect to the primary visual cortex (40% left, 49% right), with only a small proportion projecting to the auditory cortex, accounting for 5% of the pulvinar in the right hemisphere, and just 1% in the left. The smallest connection is to area MT, accounting for just 0.5% of the segmented pulvinar in controls. It is noteworthy however, that even though the region MT projecting to area MT is small, as with the regions segmented as connecting to S1 and V1, there is a high level of concordance both between the individual subject shown and the group map, and with the expected locations of connectivity according to the literature.

5.4.2 Cortical connections of the pulvinar in hemianopia

As with the control subjects, group connectivity maps of the pulvinar were created for patients, by summing the seed connectivity maps in standard space, and performing a hard segmentation on this. The lesioned and undamaged hemispheres were analysed separately, and as there was an equal number of patients with damage to each hemisphere (n=11 for left and right hemisphere damage), each map contained the summed connectivity for 11 subjects (Figure 5.6). In the undamaged hemisphere, the connections of the pulvinar to the cortical regions investigated were broadly similar to that found in control subjects, both in terms of the regions occupied by connections to each region, and their proportions, with the exception of A1 in the right hemisphere, which is more heavily represented in the patient group. In the lesioned hemisphere however, connections between the pulvinar and the cortex are different. In both the left and right hemisphere, there is a clear increase in the number of voxels that primarily project to area MT, and a decrease in the representation of V1 connectivity. The majority of voxels that project to MT in the lesioned hemispheres appear to be in regions that would usually project to V1. When the number of voxels segmented to each region is quantified in the group maps (see the bar chart in Figure 5.6), this increase in voxels projecting to MT and the reduction to V1 is evident, together with an increase in voxels projecting to A1.

Within individual patients, the extent to which MT projections increase and V1 projections decrease is variable. The cohort is fairly heterogeneous, with patients varying according to location, duration and size of lesion, thus variation is to be expected.

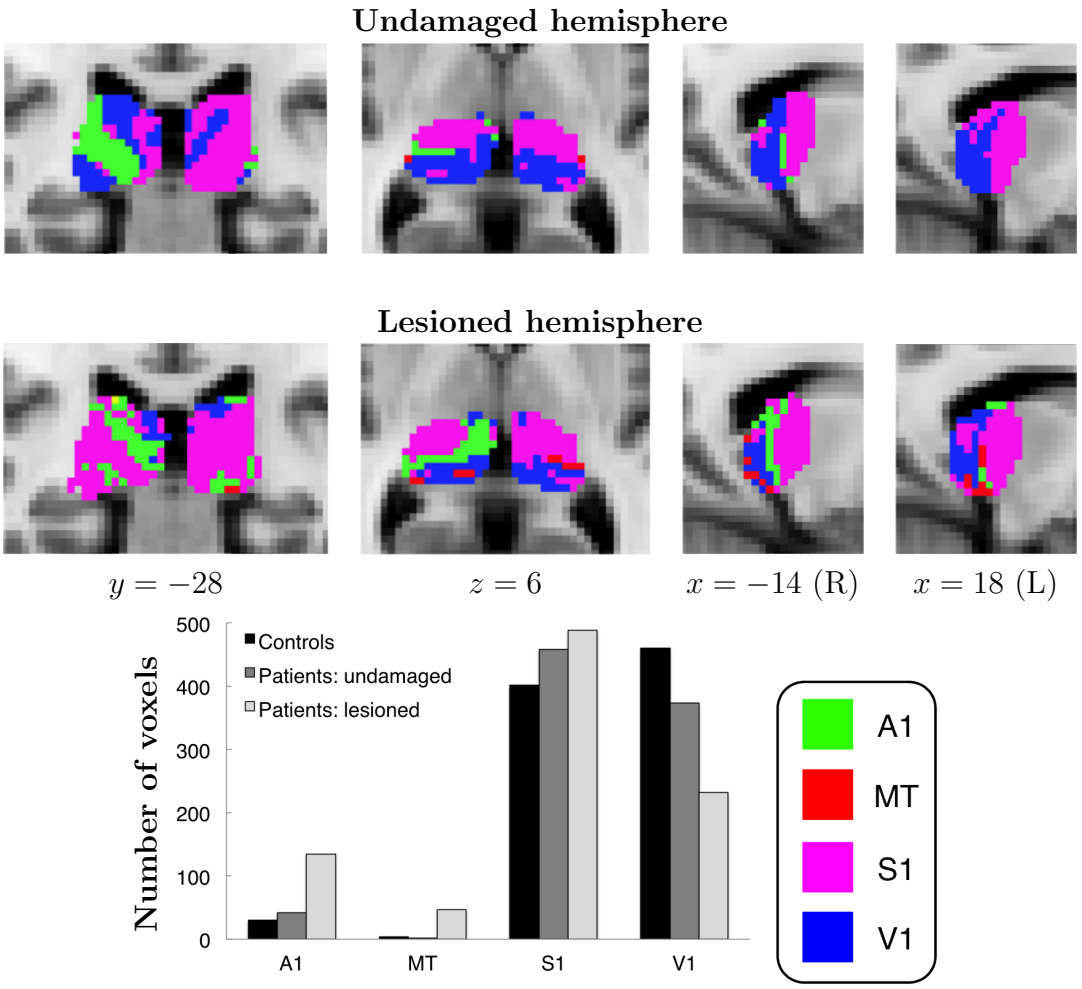

Figure 5.6: Segmentation of the pulvinar in patients. Group segmentations shown were created by summing the seed connectivity maps from each patient, split into lesioned and unlesioned hemisphere, before performing a segmentation on the results. The top line shows this group segmentation in patient undamaged hemispheres, and the second line shows the segmentation for lesioned hemispheres. The number of voxels segmented as connecting most strongly to each cortical trget for each group is shown below in the bar graph. Key for segmentations : V1 (blue), MT (red), S1 (magenta), A1 (green). Voxel coordinates for group maps are in MNI standard space, with the same slices shown for lesioned and undamaged maps.

Two key factors were assessed, the difference between congenital and acquired hemianopia, and reorganisation in patients with the ability to discriminate motion in their blind field.

Comparison of patients with congenital and acquired damage

Studies have shown that reorganisation of the visual system is more likely to occur when damage happens early in life, as in the congenital patients. However, there was little evidence that congenital patients showed greater reorganisation in the pulvinar in comparison to patients with acquired damage. The number of voxels found to connect to each of the visual target areas (MT and V1) in the lesioned and intact hemisphere can be seen for each patient in Figure 5.7. Only three congenital patients show a noticeably larger number of voxels connecting to area MT in the lesioned hemisphere, patients R4c, R5c, and S12c. Of the acquired patients, three patients with striate damage have the greatest MT connectivity in the lesioned side in comparison to the undamaged hemisphere. A further acquired patient, with LGN damage, has unusually large connectivity to area MT in the pulvinar in both hemispheres. Not only is there no clear differentiation between congenital and acquired patients, but there is also no clear pattern with regards to lesion location. Some patients with damage to each lesion location show enhanced connectivity to MT, while others have little or none.

Reorganisation in patients with demonstrated residual visual function

In behavioural testing, 4/12 patients could discriminate the direction of luminance defined movement in their blind field. Two of these patients had adult acquired damage,

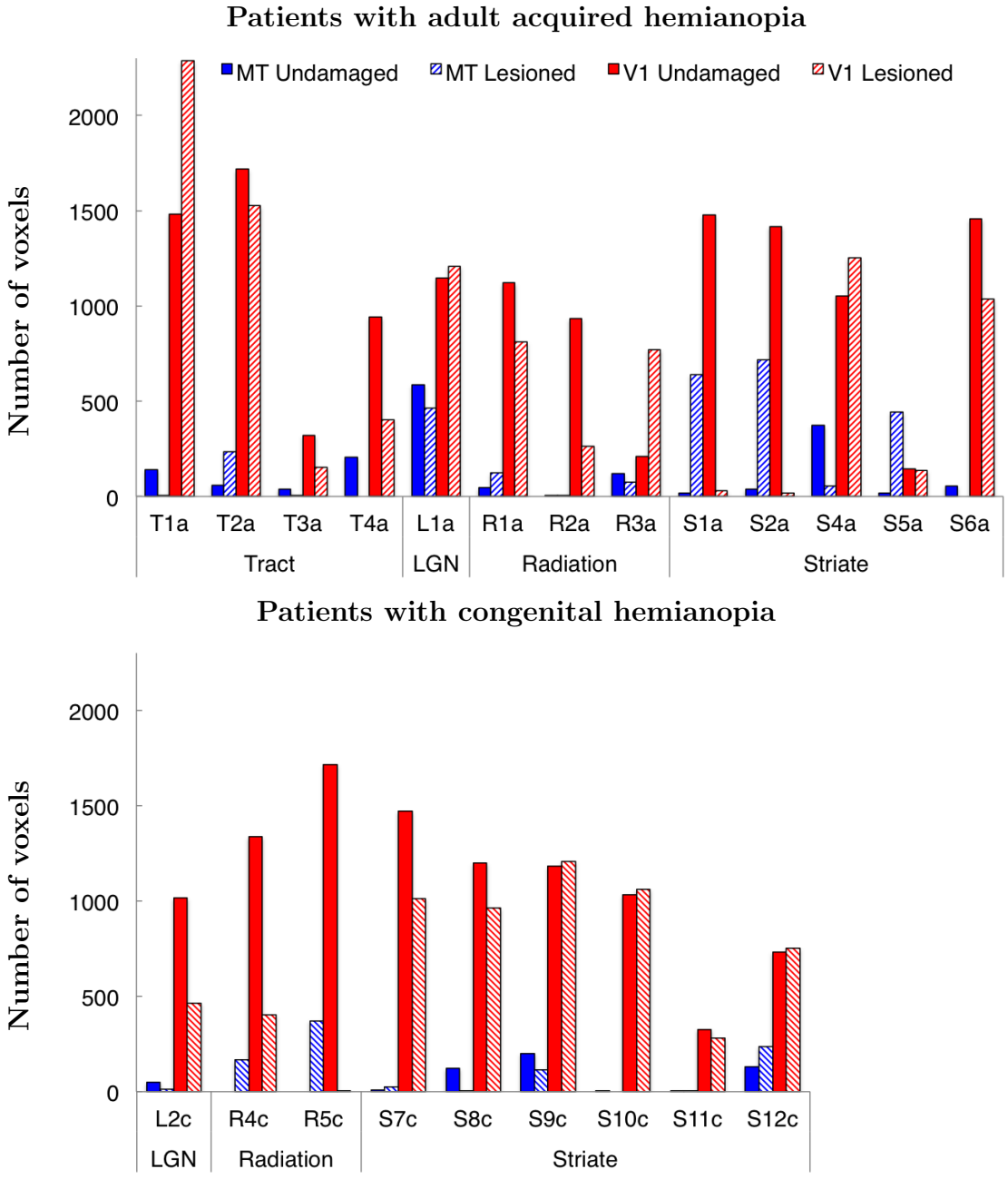

Figure 5.7: Connections between the pulvinar and the visual cortex in patients. Each patient is shown separately, with acquired patients included in the top graph, and congenitals in the bottom graph. Greater numbers of pulvinar voxels connecting to area MT (blue stripes), and a reduced number of pulvinar voxels connecting to area V1 (red stripes) in the lesioned hemisphere in comparison to the undamaged hemisphere are likely to indicate reorganisation.

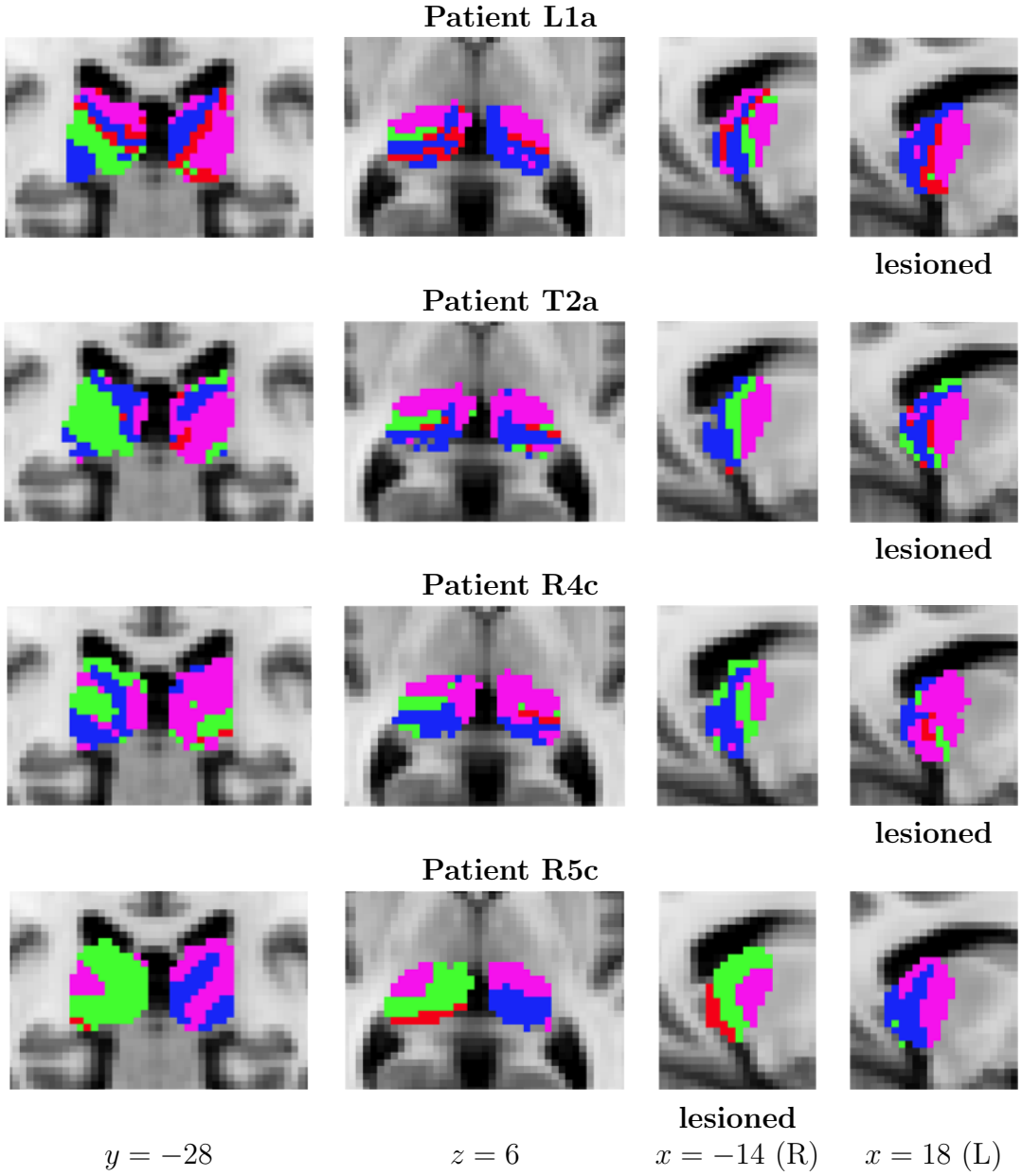

Figure 5.8: Pulvinar segmentation for patients with residual motion perception in the blind field. Coronal, axial, and two sagittal slices show the pulvinar segmentation in each of these patients. In most of these patients, MT connectivity is more heavily represented in the lesioned hemisphere. For comparison, segmentations are shown in standard space and the same slices are shown for each patient. The lesioned hemisphere is noted below the relevant sagittal slice for each patient, which is the left hemisphere for all patients except R5c, shown on the bottom row.

Table 5.2: Number of voxels with maximum projection to either area MT or V1 in patients with residual vision function

	MT		V1	
	lesioned	undamaged	lesioned	undamaged
L1a	464	585	1208	1146
T2a	234	59	1525	1717
R4c	166	0	403	1337
R5c	372	0	4	1714

and two had congenital hemianopia. The pulvinar segmentation for each of these patients is shown in Figure 5.8. The patient with the clearest pulvinar reorganisation was R5c, a congenital patient with damage to both extrastriate cortex and the optic radiation. In this patient, while the undamaged hemisphere was similar to controls, the pulvinar in the lesioned hemisphere had no connection to V1, but a strong connection to area MT. In the other patients, the differences were less striking, however all showed greater connections to MT in the lesioned hemisphere, with the exception of L1a who had strong connections to area MT in both hemispheres. Surprisingly, one of these patients had damage to the optic tract, which should preclude the existence of residual visual function; it is unclear why reorganisation would occur in this case. None of these patients had any direct damage to primary visual cortex, however the size of the regions with predominantly V1 connections varied among them. In the two congenital patients, very little or no connectivity to V1 existed in the lesioned hemisphere. In the acquired patients however, very similar sized regions were found to be connected to V1. Exact numbers of voxels in the regions segmented as connecting to areas MT or V1 for these patients are given in Table 5.2.

5.4.3 Overlap of connectivity in the visual areas

As a hard segmentation cannot account for regions where projections exist to more than one cortical target, further group analysis was applied using a less restrictive approach. For each cortical target, every voxel in the pulvinar was given a value between 0 and 1, according to the proportion of the projections from that voxel which reached each target mask. This was then thresholded for each cortical target to only show voxels with at least a 25% probability of connecting to that target. In this way, secondary connections could be visualised in addition to the biggest projection. After thresholding at >25%, connectivity maps for each control subject were binarised

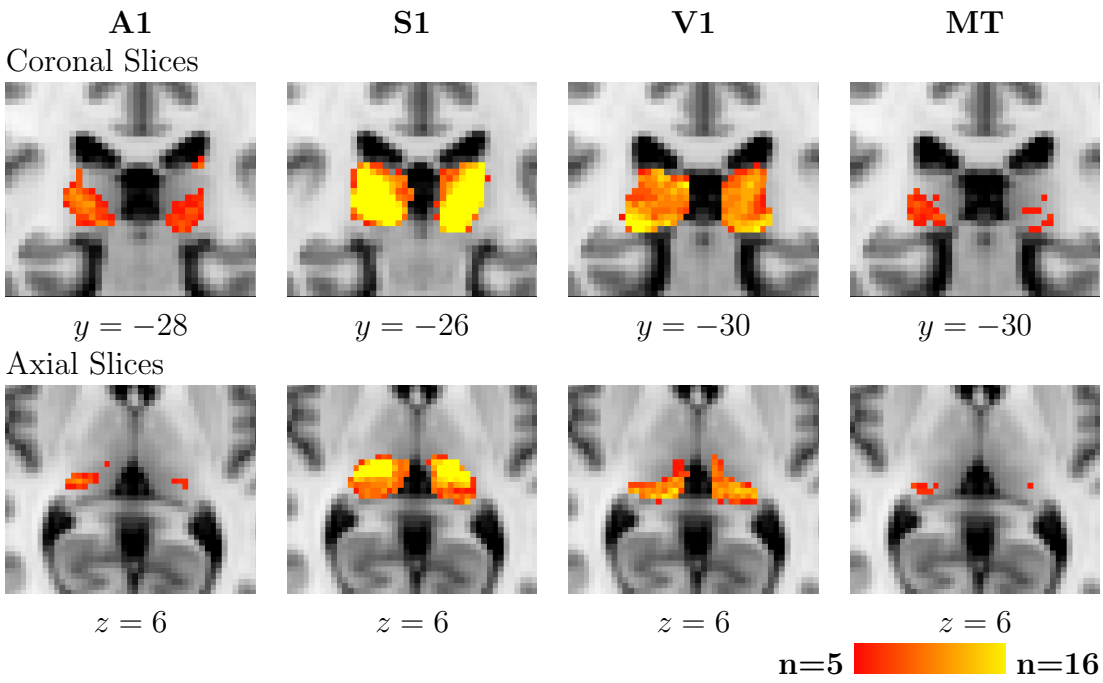

Figure 5.9: Group probability maps for connectivity to each target region. Maps showing the overlap of cortical connection regions across control subjects after thresholding to remove voxels with less than 25% connection probability, on a scale from red (5/20 subjects) to yellow (16/20 subjects). Coronal slices are shown on the top row, with the centre of gravity for each cluster shown. Axial slices are shown on the bottom row, all at the same z co-ordinate. Voxel co-ordinates are given in MNI standard space.

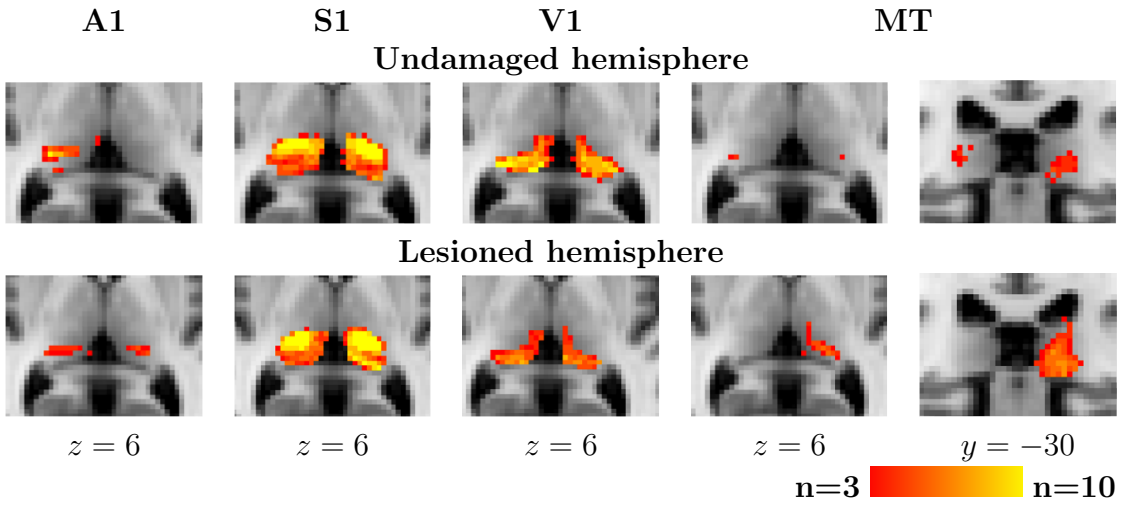

Figure 5.10: Group probability maps for pulvinar connectivity in patients. Maps showing the overlap of cortical connection regions across subjects after thresholding to remove voxels with less than 25% connection probability, on a scale from red (3/11 patients) to yellow (10/11 patients). Probability maps are shown separately for the lesioned and undamaged hemispheres. All slices are the same axial slice, with the exception of the final image in each row, which is a coronal slice showing the centre of gravity for the MT cluster.

and summed together in standard space, to create group probabilistic maps for each target (Figure 5.9). The highest inter-subject concordance was found for areas S1 and V1, with clearly delineated regions in the pulvinar being connected to these targets. Smaller regions of consistent connectivity were found for areas A1 and MT. As in the hard segmentation, the regions with the strongest connectivity to S1 were clearly differentiated from the other regions, which were more similar. The pulvinar area with the greatest connection to MT overlapped the V1 region, with the centre of the cluster falling on the same coronal slice for each. Some overlap was also present between A1 and V1, although strong connections to V1 were more anterior and inferiorly located than to A1.

The same analysis was applied to patients, with lesioned and undamaged hemi-

spheres again analysed separately (Figure 5.10). From the axial slices shown, the pulvinar region that projects most strongly to area MT in the lesioned hemisphere does overlap the region which projects to V1. However, this is also the region which appears to have lost more V1 projection. The more anterior portion of the V1 map has reduced most, and it is in this region that the MT projection appears to be strongest in the lesioned hemisphere of the hemianopia patients.

5.4.4 Relationship between pulvinar connectivity and functional activation to motion stimuli

To investigate whether increased connectivity between area MT and the pulvinar was accompanied by increased functional activity in area MT, the number of pulvinar voxels that were segmented as being connected most strongly to area MT were correlated with indicators of functional activity. Specifically, percentage BOLD change and the size of significantly active clusters in area MT in response to central, ipsilateral, and contralateral stimuli were correlated with the number of voxels showing predominantly MT-pulvinar connectivity in each patient (1 tailed pearson correlations).

It was expected that effects of increased activity in area MT accompanied by increased MT connectivity would be most likely to occur in the lesioned hemisphere, were functional reorganisation to occur. However, in the lesioned hemisphere of patients, there were no significant correlations found between these measures of functional activity in area MT and connectivity between area MT and the pulvinar.

In the undamaged hemisphere, there was some relationship between connectivity

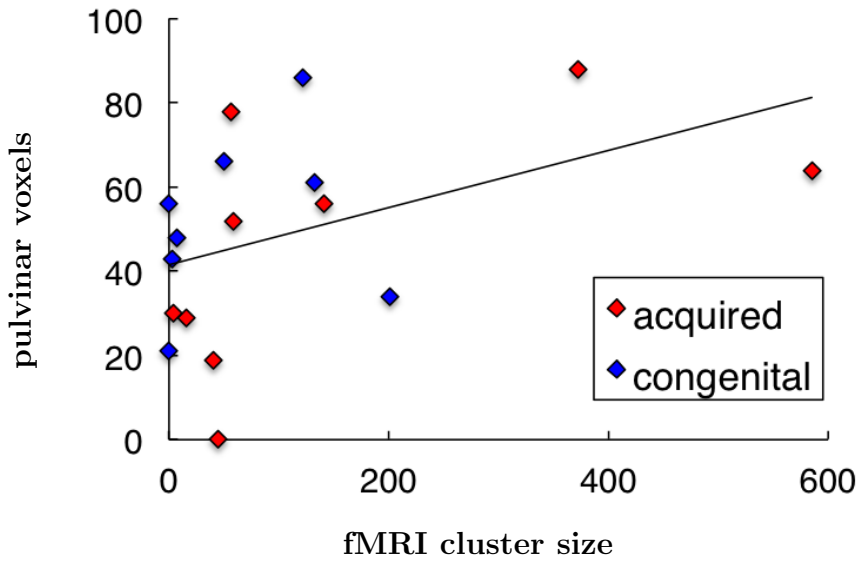

Figure 5.11: Relationship between connectivity and function in area MT. The relationship between activity in area MT in the undamaged hemisphere in response to centrally presented motion stimuli (x axis) and the number of pulvinar voxels segmented as projecting primarily to area MT (y axis) is shown. The trend line shows the positive relationship between these factors ($r = 0.432$, $p < 0.05$) for all patients. Patients are colour coded according to whether their hemianopia was congenital (blue) or acquired (red), showing that the two patients with the greatest functional activity in MT are both acquired patients, which may be driving the correlation.

and function in area MT, with the number of voxels being active in area MT in response to centrally presented motion stimuli being positively correlated with the number of voxels that predominantly connect to area MT in the pulvinar ($r = 0.432$, $p < 0.05$). However, as can be seen in Figure 5.11, there are two patients with acquired damage that have far greater MT activity than the other patients, which may be driving the correlation. There was no relationship for activation in response to ipsi- or contralateral motion stimuli presentation, or for the percentage BOLD change in response to centrally presented stimuli.

5.5 Discussion

5.5.1 The pulvinar can be segmented using DTI

This study shows that it is possible, at least to some extent, to segment the pulvinar according to its cortical connections in the same manner as has been demonstrated by Behrens et al. (2003a) and Johansen-Berg et al. (2005) in the thalamus. Regions projecting to S1 and V1 were clearly identified both in individual control subjects and in group averages, and these regions corresponded to the known projection regions identified in non-human primates. Projection to auditory cortex and area MT were less consistent, as befits the smaller projection from the pulvinar to these areas. However for the most part they too were located in expected regions, with the MT projection generally overlapping the V1 projection region in healthy controls.

5.5.2 Connectivity between the pulvinar and area MT is not greater in congenital than acquired patients

Previous studies of cortical reorganisation in the visual system have tended to find extensive reorganisation in cases where damage has occurred congenitally. In cases where the damage has been acquired in adulthood however, the visual system appears to change to a much lesser extent. Nonetheless, in one of the most famous blindsight cases, GY, plasticity has been demonstrated. However as GY acquired his striate cortex damage in childhood, he may not be the best example of the capacity for the visual system to reorganise once adulthood has been reached.

In line with this, recent work has shown that in monkeys with very early lesions, there is reorganisation of the pulvinar such that a stronger connection from PIm to area MT is formed (James Bourne, unpublished data). However in the current study, there was no evidence for greater reorganisation in congenital patients than in patients with damage acquired as adults. One potential reason for this is that in cases where the visual system has reorganised following congenital or peri-natal damage, the visual system may have recovered to such an extent that the deficit is no longer detectable, and therefore such patients would be unlikely to be included in such a study. As it is, the majority of congenital patients in this cohort are unaware of their VF deficit, frequently discovering it in adulthood following routine vision examinations. In monkeys however, the full range of outcomes following lesions can be investigated, regardless of the level of compensation following the lesion.

In fact, the strongest pattern of increased ipsilesional MT connectivity combined with reduced ipsilesional V1 connectivity was shown in patients with long-standing acquired V1 damage. In the congenital striate patients, relatively little MT connectivity was found. Given that the congenital striate patients are most similar to the monkeys in the Bourne study, this is a surprising result. However, as noted in previous chapters, the congenital patients have much smaller lesions than the patients with acquired damage, and this may impact on the results of the pulvinar segmentation due to methodological issues, as will be discussed later.

5.5.3 The relationship between connectivity and function in area MT is unclear

In instances where stronger connectivity between the pulvinar and area MT exists, it would be expected that there would be an accompanying improvement in motion processing ability. This could be demonstrated either as increased functional activity in area MT as measured in fMRI studies, or by an ability to detect and discriminate motion stimuli in the blind field, both of which could be enhanced by increased connectivity to area MT. In line with this, the patients with the ability to discriminate motion direction in the blind field do show evidence of reorganisation of pulvinar connectivity in the lesioned hemisphere, in a manner which favours connectivity to area MT. It should be noted however, that the testing used was a relatively coarse assessment of motion processing abilities; more thorough testing may well elicit a greater range of residual processing capacities in patients. Where fMRI was concerned, there was no relationship between connectivity and function in the lesioned hemisphere, although there was the suggestion of a relationship in the expected direction in the undamaged hemisphere. It is possible that the lack of a relationship in the lesioned hemisphere may stem from methodological issues, relating to potential difficulties in interpreting tractography in damaged white matter tissue, as will be discussed in greater detail in the next section. The comparison between fMRI and connectivity may also benefit from a more robust protocol for activating MT, as discussed in Chapter 4. Nonetheless, the results are suggestive that increased connectivity to area MT may underlie some residual motion processing in hemianopia.

It may also be the case that other routes to extrastriate cortex can explain some of the variation in the extent to which area MT remains functional, which could be the subject of further exploration in the DTI data. A DTI study by Bridge et al. (2008) focusing on abnormal white matter connections to area MT in patient GY revealed contralateral pathways between LGN and MT, and a cortico-cortico connection between areas MT bilaterally; neither of these pathways were present in controls. These pathways, together with the ipsilateral koniocellular LGN route to extrastriate cortex could be the subject of further exploration in these patients.

5.5.4 Limitations of DTI

The use of diffusion tensor imaging gives rise to a number of methodological limitations that must be considered when interpreting results. The first key issue relates to the pulvinar mask itself, and our ability to dissociate the pulvinar from surrounding thalamic regions. While the pulvinar was drawn on high resolution T1-images, it is possible that on the lower resolution diffusion images (2x2x2 mm^3 as opposed to 1x1x1mm^3), the seed region used may have incorporated nearby non pulvinar regions to some extent. For example, it is possible that the strong connection between the anterior pulvinar and S1 might in part be mediated by seeds reaching the ventral posterior lateral nucleus, a thalamic region lying close to the anterior pulvinar, and from which connection to S1 have been found previously using DTI (Johansen-Berg et al., 2005). In some cases probabilistic tractography can be 'cleaned up' using exclusion masks to prevent pathways entering undesired brain regions, as for example in this

study where samples were prevented from entering the corpus callosum. However, it would not here be possible to use exclusion masks for the surrounding thalamic nuclei, as this would prevent characterisation of pathways that pass through the regions where they are located. The exception to this is the lateral geniculate nucleus. The pathways of interest, in particular from the pulvinar to area MT, should not pass through the LGN. As a relatively small region, it is possible that the LGN could be designated as an exclusion region without making it impossible to trace the pathways to be investigated. This might then be the subject of future work, to confirm that samples reaching the LGN are not mediating increased connectivity where it is found.

Related to this issue is the more general question of whether diffusion tensor imaging with voxels of 2x2x2 mm^3 is sufficient to segment the pulvinar according to its connectivity, and find pathways which are by their nature, relatively small in comparison to other more substantial white matter pathways such as the optic radiations. PIm for example, which has been shown to project to area MT (Stepniewska et al., 2000), and is distinct from the pulvinar region that projects to V1 (Shipp, 2003), is a relatively small area of the pulvinar, and it may be that the resolution of the DTI images used are not sufficiently detailed to make clear definition of this area possible. It may be that the use of higher field imaging, which can enable greater resolution images, may be necessary to identify the small subregions of the pulvinar using this methodology.

A final issue with the use of DTI to identify the connections between the pulvinar and the cortex is specific to the use of patients. It is possible that in regions where the

white matter is degraded, either due to specific lesions or retrograde degeneration, the accuracy of tractography in hemianopia patients might be affected. Supporting this argument, the most substantial reorganisation of the pulvinar in congenital patients was found in those with the largest lesions. It may also be argued, however, that more extensive lesions have a greater likelihood of making cortical reorganisation necessary, and that as the damage was sustained during the critical period, such plasticity is possible. Nonetheless, tractography is most effective and simple to interpret in regions of coherent white matter with minimal fibre crossing. It is unclear to what extent tractography is affected by degraded white matter, and thus it is possible that the extent of the lesions presents problems for the tractography itself.

5.5.5 Conclusions

There is evidence of altered connectivity between the pulvinar and area MT in the lesioned hemisphere of patients with hemianopia, with increased connectivity to area MT and decreased connectivity to V1. The expected increase in reorganisation in congenital patients in comparison to those with adult acquired hemianopia was not found, however there was evidence of increased connectivity to area MT in those patients with the ability to process motion stimuli in the blind field. This supports the idea that a direct pathway between the pulvinar and extrastriate cortex may support some residual visual function.

Chapter 6

The neurological basis of hemianopia in posterior cortical atrophy

6.1 Abstract

Objective To characterise the changes in the brain which differentiate posterior cortical atrophy (PCA) from Alzheimer's disease (AD), and to investigate the pathological basis of hemianopia in PCA.

Methods T1-weighted structural and diffusion-weighted images were obtained for 7 patients with PCA, 12 patients with AD, and 14 healthy older controls. Additional fMRI data was acquired for PCA patients and a subset of the healthy controls to investigate cortical responses to visual stimuli. Grey matter atrophy was assessed

using voxel-based morphometry and by measuring cortical thickness. White matter degeneration was assessed by measuring fractional anisotropy and mean diffusivity across the whole brain, and more specifically in the optic radiations.

Results Reductions in grey matter volume and white matter integrity were found throughout the brain in PCA patients. Differences between PCA and AD were found in both grey and white matter, and consistently showed greater degeneration of posterior brain regions in PCA, in particular in the occipital lobe. This is in contrast to previous studies comparing these patients, where group differences have been less substantial. Perimetry confirmed that 6 out of the 7 PCA patients exhibited visual field deficits, all of which were asymmetric to some extent. Evidence for asymmetric degeneration was found in areas MT and V2, and in the anterior optic radiation, with the hemisphere contralateral to the visual field deficit most affected. Surprisingly, higher visual areas showed greater atrophy than early visual areas, with the primary visual cortex showing relatively little atrophy compared to other areas.

Interpretation PCA patients have considerably greater levels of degeneration in the occipital and parietal cortex than AD patients, consistent with the visual impairment these patients exhibit. While hemianopia is often attributed to V1 damage, in PCA patients it may be that hemianopia results from damage to either the optic radiations or extrastriate visual cortex, rather than damage to V1.

6.2 Introduction

Posterior cortical atrophy (PCA) is a progressive neurodegenerative disease, commonly described as the visual variant of Alzheimer's disease (AD). The disorder is characterized by an early presentation of higher order visual processing deficits and only mild memory impairments, although memory deteriorates with progression of the disease. Neuroimaging in these patients shows marked atrophy of the parietal and occipital lobes. Typically, PCA has an earlier age of onset than AD, with diagnosis usually between 50 - 65 years of age. PCA is thought to account for a small but significant proportion of dementia diagnoses, with a study of 523 dementia patients finding visual processing deficits in 24 patients, 5% of the total cohort (Snowden et al., 2007). However, the exact incidence of PCA is difficult to quantify, as often the condition is diagnosed late or not at all, due to a focus on seeking ophthalmological causes underlying symptoms (Ruis et al., 2012), rooted in a lack of general awareness of the condition.

6.2.1 Common visual processing deficits in PCA

Benson et al. (1988)'s original description of the deficits associated with posterior cortical atrophy include anomia, alexia, Balint's syndrome, agnosia, extinction, and Gerstmann's syndrome, including agraphia and acalculia. All patients retained insight into their condition until late in the course of the disease, and their primary motor and sensory systems remained intact. Primary visual systems were also seen to be intact, with visual fields and visual acuity being normal in all patients. Further suggestions

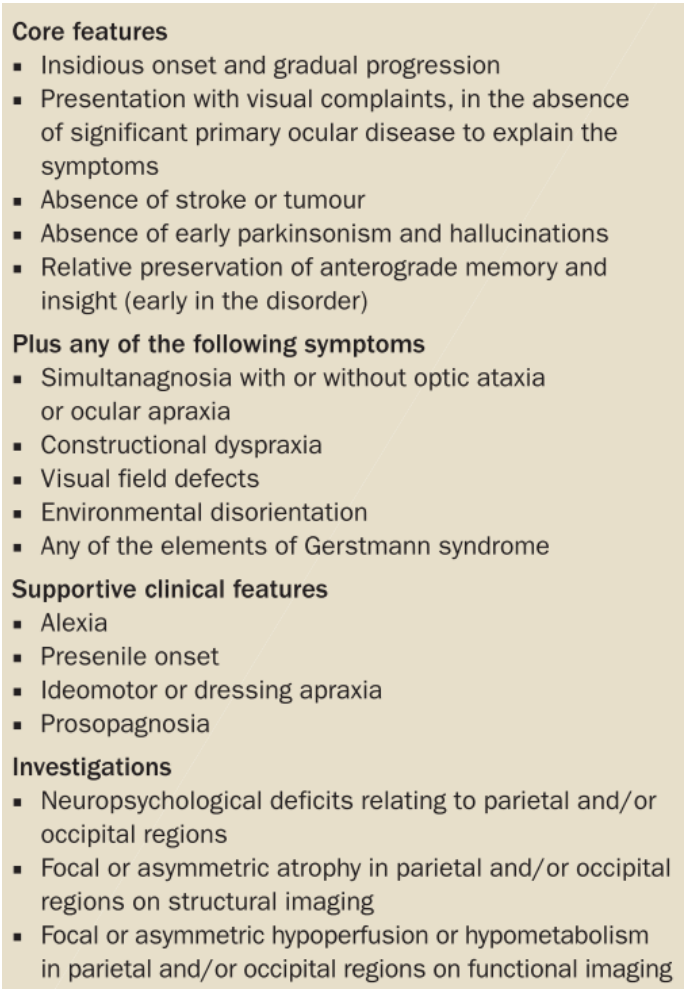

Figure 6.1: Diagnostic criteria for posterior cortical atrophy. Based on Tang-Wai et al. (2004), taken from Warren et al. (2012).

for revisions to these diagnostic criteria have included apraxia (Mendez et al., 2002), prosopagnosia, and visual field defects (Tang-Wai et al., 2004). This addition of visual field defect as a core clinical feature present in PCA is notable, as it contradicts previous diagnostic criteria that stated that primary visual function should be intact for a diagnosis of PCA. Tang-Wai et al's diagnostic criteria is reproduced in Figure 6.1.

6.2.2 Hemianopia in PCA

Hemianopia has been reported as being present in PCA patients in a number of studies, with incidence ranging from approximately 10-20% (Whitwell et al., 2007; McMonagle et al., 2006; Schmidtke et al., 2005) See table 6.1 for an overview of the incidence of hemianopia in the literature. Tang-Wai et al. (2004) found hemianopia to be one of the most prevalent visual deficits in their cohort of PCA patients, with 35% exhibiting a homonymous field deficit, and a further 12.5% having less consistent field deficits. As such, they proposed that visual field deficits should be considered a core clinical feature in diagnosing PCA. However, in spite of the number of studies reporting hemianopia in PCA patients, the prevalence, and indeed the existence of visual field deficits in these patients remains controversial. Crutch et al. (2012) state that hemianopia is often misdiagnosed in PCA patients due to the presence of higher level visual deficits such as hemispatial neglect, and other studies of the visual deficits in PCA patients have failed to report any visual field deficits (Benson et al., 1988; Victoroff et al., 1994). Mendez et al. (2002) actively screened out patients with visual field deficits when constructing a cohort with which to study the clinical characteristics of PCA, citing intact primary visual function as a core diagnostic feature of PCA. Indeed many studies investigating the visual deficits characteristic of PCA do not include visual field testing in their study battery, although field deficits may be incidentally reported. Where visual field loss has been accounted for, visual confrontation is often used (Benson et al., 1988; Andrade et al., 2010), which is not as reliable as perimetry in detecting field deficits (Johnson and Baloh, 1991).

Table 6.1: Prevalence of hemianopia in PCA

	total subjects	visual field deficits	VF testing method	proportion (%)
Benson et al. (1988)	5	0	confrontation	0
Delamont et al. (1989)	2	2		100
Tang-Wai et al. (2004)	40	14 (19)	medical records*	35 (47)
Schmidtke et al. (2005)	9	1	no standardised scheme*	11
McMonagle et al. (2006)	19	3	unknown	16
Whitwell et al. (2007)	38	7	medical records*	18
Andrade et al. (2010)	24	3	confrontation	13

* Data collected retrospectively. For Tang-Wai et al. (2004), figures are shown for homonymous VF loss, and then all VF deficits in parentheses.

Formaglio et al. (2009) attempted to remedy this by employing perimetry to characterize the visual field deficits in 6 patients with PCA. They found that hemianopia can be demonstrated early in the progression of the disease. Half of the patients studied also had hemineglect, however in some of these cases the neglect appeared at a later date, supporting the argument that the hemianopia found is not a misdiagnosed higher order deficit. As is often found in patients with hemianopia following cortical damage, many of the patients had macular sparing. MRI showed damage to the calcarine sulcus in patients with the most complete visual field deficits, giving further support to the argument that these patients have a loss of primary visual function. Pelak et al. (2011) used computerised perimetry (in most cases Humphrey Visual Field testing) to characterize the visual field deficits in 9 patients with PCA. Bilateral field loss was found in two patients, and homonymous field deficits were found in the remaining 7 patients, with the majority demonstrating left visual field deficits. Autopsy information was available for two patients, and showed pathological changes in the striate

cortex, together with intact optic radiation and pre-chiasmal and geniculostriate visual pathways, as is generally found in hemianopia following stroke affecting the visual cortex. However, while patient MRI scans were examined in addition to visual fields, the authors were unable to assess whether the size and location of the visual field deficits were related to specific patterns in brain atrophy.

6.2.3 Neuroimaging in PCA

Suggested diagnostic criteria for PCA have generally agreed that MRI scans of patients show atrophy in the parietal and/or occipital lobes, with frontal areas remaining more intact (Mendez et al., 2002; Tang-Wai et al., 2004). In general, the neurological deterioration underlying this disorder has been less well characterised than the resulting neuropsychological deficits. However, in the last decade an increasing number of studies have used neuroimaging to shed light on the pattern of atrophy that sets PCA apart from other dementias, resulting in the varied visual deficits indicative of the disorder.

Voxel-based morphometry (VBM) has been used in a number of studies to investigate the extent and location of grey matter atrophy in PCA. Atrophy has been shown to affect the occipital, parietal, and posterior temporal lobes (Whitwell et al., 2007; Migliaccio et al., 2012b, 2011). This degeneration is bilateral, although a significant number of studies have noted that atrophy in PCA appears to be greater in the right hemisphere (Whitwell et al., 2007; Migliaccio et al., 2011, 2012a), particularly in patients with more dorsal symptoms (Migliaccio et al., 2012b). This may be a factor underlying the asymmetrical field loss noted in many PCA patients, however it has been argued

that this asymmetry is largely due to selection biases towards patients with extensive visual dysfunction (Crutch et al., 2012). Thus while the left-right asymmetry noted may not be characteristic of the PCA population as a whole, it may be a facet of the pattern of atrophy underlying those with the most profound visual loss, as exhibited in those with hemianopia.

Studies comparing PCA and AD patients has generally only shown subtle differences in levels of atrophy between PCA and AD. Regions of greater atrophy in PCA have included the visual, sensory and motor cortex, and the right posterior parietal lobe, and the left medial, inferior, and middle temporal lobe in AD. However, only the effects in a small region in the right visual association cortex and the left hippocampus survive correction for multiple comparisons (Whitwell et al., 2007). This suggests that direct damage to the visual cortex may underlie loss of primary visual function in these patients. Longitudinal analysis of differences in disease progress showed no between groups differences unless a more sensitive classifier approach was used, which suggested that the left medial temporal lobe, inferior parietal lobe, and frontal lobe regions were the key regions of difference in atrophy between groups (Lehmann et al., 2012). Overall, it is thought that both patient groups show a global pattern of grey matter atrophy, with PCA and AD showing more marked atrophy in the posterior and temporal regions respectively throughout the progression of the disease. A recent meta-analysis of these VBM studies refined the key regions showing greater atrophy in PCA than in Alzheimer's to be the right occipital gyrus extending to the right posterior lobule (Alves et al., 2013). It is notable that again, the brain regions showing

consistently greater degeneration are reported as being in the right hemisphere, showing a lateralisation in atrophy in PCA.

Evidence from diffusion-tensor imaging suggests that the atrophy is not limited to the grey matter, but extends to the white matter in the parietal and occipital lobes (Duning et al., 2009) and indeed may be present throughout the major white matter pathways involved in visuo-spatial processing (Migliaccio et al., 2012b). Loss of fractional anisotropy has also been noted in the splenium, the region of the corpus collosum through which visual information crosses hemispheres (Yoshida et al., 2004). However these studies have been case studies, and given the heterogeneity of the disorder, replication is required in larger patient groups. Furthermore, with the exception of Migliaccio et al. (2012b), all studies examined only fractional anisotropy, and not other diffusion indices such as mean diffusivity. In the Migliaccio study, MD was found to be more sensitive to differences between PCA patients and controls than FA, a finding which is consistent with work by Acosta-Cabronero et al. (2010), who showed that MD is a better indication of degeneration in Alzheimer's patients than FA, in spite of the fact that the majority of studies on neurodegeneration have a tendency to report FA changes. Nonetheless, it appears to be confirmed that the impairments exhibited by PCA patients result from a combination of grey and white matter damage.

Perhaps surprisingly given the range of higher order and primary visual deficits experienced by PCA patients, only a handful of functional MRI studies have been carried out on these patients. Of those that have (Delazer et al., 2006; Barbarulo et al., 2008; Feldmann et al., 2008), all were carried out on single cases, and only one

study (Feldmann et al., 2008) quantified visual activation, finding decreased activation in areas V1 and V2. Further investigation of visual function may help to elucidate whether the visual loss is attributable to damage early in the visual pathway, or to higher cortical areas.

6.2.4 Aims of the present study

While a number of groups have recently used MRI to investigate neural degeneration in PCA, studies have frequently found only subtle differences between PCA and AD patients, and several of the studies with stronger results have only investigated single cases. The exact neurological basis of PCA is still not well enough understood beyond 'general posterior atrophy', neither in terms of the features which dissociate it from the more common presentation of Alzheimer's disease, nor in terms of the patterns of degeneration which underlie the visual field deficits similar to those found in hemianopia following more common causes. Here we investigate the structural and functional changes present in a group of 7 PCA patients, using a range of imaging techniques, in order to better describe the atrophy that occurs in PCA, and explain the asymmetric loss of vision experienced by patients.

6.3 Methods

6.3.1 Subjects

Seven subjects with posterior cortical atrophy were recruited from the National Hospital for Neurology and Neurosurgery. For a diagnosis of PCA, patients needed to demonstrate progressive impairment of posterior cortical function with relative preservation of memory and other cognitive functions. Patient ages ranged from 53 to 77 years of age (mean 67 years), and included four females and three males. Six out of seven patients displayed a visual field deficit, all of which were asymmetric, with three only affecting one hemifield. The longest known history of PCA was 6 years (pca1),

Table 6.2: PCA patient details

Patients	Age	Visual Deficit	Duration	Diagnosis
pca1	66	$R > L$	6 years	Jan 06
pca2	77	LH	5 years	Sep 07
pca3	72	RH	4 years	Sep 08
pca4	61	N	5.5 years	Nov 06
pca5	53	RH	2.5 years	May 10
pca6	68	$R > L$	3 months	Jul 12
pca7	72	$R > L$	4 months	Jul 12

	WAIS Vocab	WAIS Arith	Naming	Spelling	Object Perception	Spatial Perception
pca1	N **N**	N **N**	N N	N N	I **I**	I **I**
pca2	N **N**	N **I**	N **I**	N **I**	I **I**	N **I**
pca3	N **N**	N **N**	I **I**	N **I**	I **I**	I **I**
pca4	N **N**	N **I**	N **I**	N **I**	I **I**	I **I**
pca5					I **I**	I **I**
pca6		I		I	I	I
pca7		I	I	N	I	I

Age age when scanned. **Duration** time since diagnosis. For patients tested twice, **bold** 2nd test indicates reduced performance. **I** impaired, **N** average or better. Pca5-7 did not complete all neuropsychological tests.

and the shortest was three months (pca6), although usually PCA is thought to have been present for some time before diagnosis. To satisfy inclusion criteria for the study, all patients were screened by a clinical neuropsychologist to ensure their memory had not deteriorated beyond mild cognitive impairment. In addition, patients were tested for a range of processing deficits. Full details for these patients are given in Table 6.2.

Six healthy controls were used (age range 52 - 74, mean 61 years, 2 females) from the hemianopia study. In addition, scans from a further eight healthy older controls (age range 73 - 85, mean age 77, 4 females) and twelve patients with Alzheimer's disease (AD), were also used for comparison with PCA patients. As AD typically has a later onset than PCA, the AD group were slightly older than the PCA group, with a mean age of 74 (age range 57 - 82, 5 females) compared to 67 for the PCA patients. These subjects were recruited as part of the Oxford Project to Investigate Memory and Ageing (OPTIMA) and from the Oxford Memory Assessment Clinic at the John Radcliffe Hospital. Subjects scanned for OPTIMA had been scanned using the same scanner and structural protocols as the PCA patients and hemianopia controls.

6.3.2 Neuropsychological assessment

Patients were assessed by a neuropsychologist on a range of tasks in order to identify key areas of loss of function, the results of which are summarised in Table 6.2. Assessed abilities included WAIS vocabulary and arithmetic, memory, naming, spelling, object perception, and spatial perception. Naming was tested using the graded naming test (McKenna and Warrington, 1980). Memory was tested using Warrington recognition

memory tests (Warrington, 1984, 1996). Spelling was tested using the Baxter spelling test (Baxter, 1982). Object and spatial perception were assessed using the visual object and spatial perception battery (Warrington and James, 1991).

6.3.3 Perimetry

Humphrey visual fields had been acquired for PCA patients with a Zeiss Humphrey Field Analyzer, using central 24-2 threshold test and SITA-FAST strategy. Where HVF were unavailable (patients may struggle with the automated Humphrey test as PCA progresses), Goldman Perimetry was used to assess the visual field. Visual fields are shown in Figure 6.2. One patient (pca4) is not shown, as she had no visual field deficit. Three patients showed visual field loss in both hemifields, although in all cases

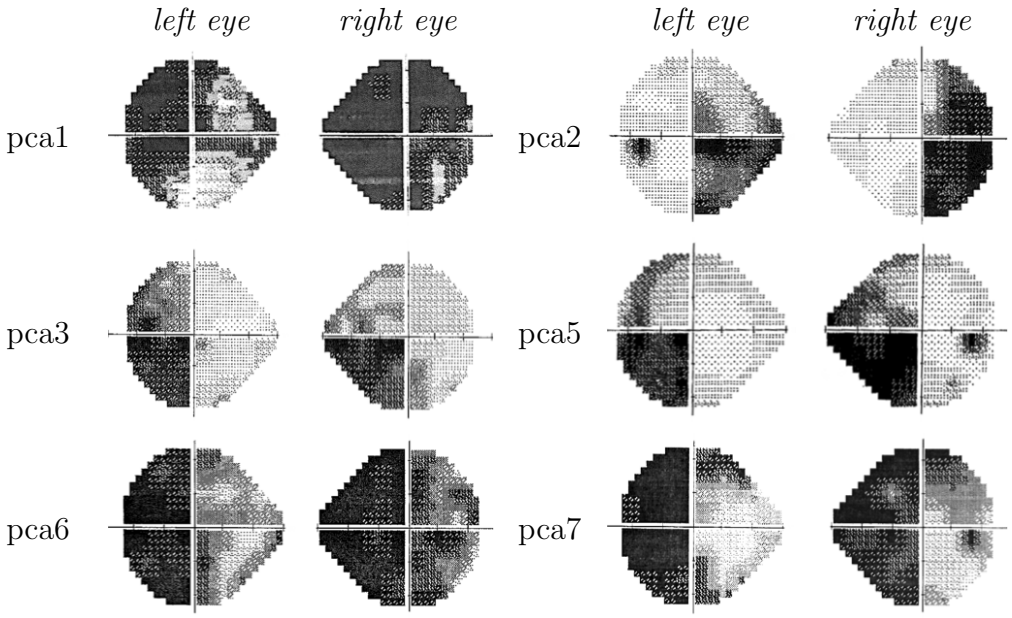

Figure 6.2: Humphrey visual fields for PCA patients. HVF are shown for all patients who have a visual field deficit. Grey scale representations of the visual field loss are used here for display purposes.

the deficit was greater on the left side. Three further patients were found to have homonymous field deficits, two with left visual field loss (pca3 and pca5), and one with right side field loss (pca2). The field loss was less dense than is generally seen in hemianopia acquired following stroke or trauma, and somewhat less congruent between eyes. It should be noted however, that HVF results may be affected by the confounding higher level cognitive deficits experienced by PCA patients, which may interfere with their ability to perform the Humphrey field test. While false positives were low for all patients (ranging from 1% to 7%), and fixation losses were rare, there was a relatively high level of false negatives recorded, in particular in pca1 (66%) and pca6 (59%). It is possible that these occur because the patients are not able to respond quickly enough to report all the visual stimuli that they see. While the other patients had between 0% and 20% false negatives, which would be considered reliable tests, the extensive false negatives in pca1 and pca6 do mean that the field loss may be less extensive in these cases than the HVF results suggest. Where available, Goldman perimetry results showed similar patterns of visual field loss to the Humphrey fields.

6.3.4 Image acquisition

Functional MRI, diffusion-weighted and high-resolution T1 structural scans were acquired for all participants using a 3 T Siemens Trio at the Oxford Centre for Clinical Magnetic Resonance Research. Two sets of whole brain diffusion weighted data were acquired. The diffusion weighting was isotropically distributed along 60 directions, b-value 1000 s/mm^2, 65 slices; 2 mm^3 voxels; TR = 9.3 s, TE = 94 ms. Volumes without

diffusion weighting (b-value 0 s/mm^2) were acquired for both sets of data. T1-weighted structural scans were acquired axially at a resolution of 1 mm^3, 192 slices, TR = 2.04 s, TE = 4.7 ms.

The fMRI stimulus was designed to activate the motion area (area MT bilaterally) in the visual cortex. Motion stimuli consisted of a circular patch of black dots presented centrally on a white background. The dots were either stationary or moving radially at a speed of 30 deg/s, reversing direction every second. 8 cycles of the stimuli were presented, each lasting for 32 seconds, 16 seconds each for moving and stationary blocks (48 transverse slices, TR = 2 s, TE = 49 ms, voxels 3 mm^3). Subjects were instructed to fixate a central cross for the duration of the scan.

6.3.5 Imaging analysis

Segmentation of the brain into tissue types

Brain extracted T1-weighted structural images were segmented into white matter, grey matter, and cerebrospinal fluid (CSF) using FMRIB's automated segmentation tool (FAST, (Zhang et al., 2001)). Binary segmentation was utilised, where FAST produces an output where each voxel is assigned one of the three tissue types. As whole brain volumes can vary significantly between individuals, atrophy was assessed by comparing the proportion of brain volume attributed to grey matter, white matter, and CSF. As well as computing this for the whole brain, these values were also compared for each lobe of the brain, in each hemisphere. Masks for each lobe were taken from the MNI structural atlas (Mazziotta et al., 2001), registered to individual subjects using FLIRT,

and binarised. The number of voxels of each tissue type in each masked region was then calculated for each subject, and converted to a percentage of the total voxels within that region.

Voxel-based morphometry

Grey matter damage was assessed using FSL-VBM software, an optimised VBM protocol carried out using FSL tools. Brain extracted structural images were segmented into different tissue types (grey matter, white matter, and CSF). An equal number of subjects from each group (AD, PCA and control) were randomly selected to form a study specific template, such that each subject group was equally represented. The grey matter segmentation for each of these subjects was non-linearly registered to MNI 152 standard space (Andersson et al., 2007), concatenated, and averaged. They were then flipped along the x-axis and then the two mirror image averages were re-averaged to create a symmetric study specific template. Grey matter segmentations for each subject were then non-linearly registered to the study specific template. This includes compensation for local expansion or contraction due to the non-linear transformations used. Resulting registered grey matter images were then smoothed with an isotropic Gaussian kernel with a sigma of 3 mm. All the processes described here were carried out with FSL scripts in an automated process. A voxelwise general linear model was applied using permutation-based non-parametric testing (5000 permutations) to investigate differences in grey matter volume between PCA patients, AD patients, and controls. Threshold-free cluster enhancement (TFCE) was used to determine regions

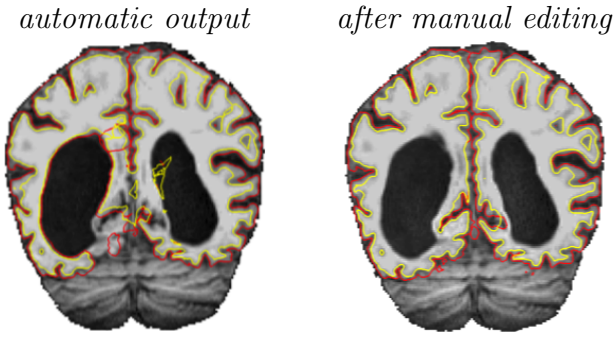

Figure 6.3: Example pial and white matter surfaces before and after manual segmentation of the ventricles. The patient shown is pca1. Note the intrusion into the ventricles on the first image.

with significant differences.

Cortical thickness

Freesurfer was used to analyse cortical thickness. This method extracts the pial and white matter surfaces and computes the distance between them in order to measure the thickness of the cortical ribbon in between. This methodology is described in full in Fischl and Dale (2000). The standard Freesurfer cortical reconstruction processing stream (recon-all) was run on subjects. Initial outputs were inspected and the ventricles manually segmented to correct for reconstruction errors due to enlarged ventricles, before completing reconstruction. Examples in Figure 6.3 showing the pial and white matter surfaces before and after manual segmentation highlight the importance of this step. To enable group analysis, an average brain was constructed from all subjects, and cortical thickness maps were resampled onto this surface using surface based registration. Data was smoothed at a 10 mm width. Group differences were investigated using a GLM (different onset same slope model) incorporating the three

different groups (PCA, AD, control subjects). To investigate which visual areas were most affected by grey matter loss, three particular regions of interest were chosen for further analysis in the visual cortex: V1, V2, and area MT. Labels for each of these areas were used from the automatic brain segmentation in Freesurfer, using the Brodmann atlas. These cytoarchitectonically defined regions are identified on the basis of cortical folding patterns (Fischl et al., 2008). Average cortical thickness measures were extracted for each of these areas for each subject. ANOVAs and T tests were then used to explore group differences, and differences between hemispheres.

White matter integrity

Diffusion data were pre-processed and analysed using FMRIB's diffusion toolbox (FDT). Images were corrected for distortions due to eddy-currents and head movements. The two sets of diffusion data from PCA patients and controls were averaged (a single average was acquired for the AD group). Diffusion tensor models were applied to the data using DTIFIT to obtain maps of fractional anisotropy (FA) and mean diffusivity (MD) levels. Tract-based spatial statistics (TBSS, Smith et al. (2006)) was used to allow voxelwise comparisons across subject groups.

Due to the large degree of atrophy present in patients, a study specific FA template was created to serve as the registration target, an addition to the TBSS pipeline utilised by Douaud et al. (2011) in a similar patient group. The target image was constructed by non-linearly registering individual subject FA maps to the standard FMRIB mean FA image, and then averaging the outputs. FA and MD maps from each subject were

then non-linearly registered to this target.

Thinning was applied to the mean FA image to create a mean FA skeleton, following the centre of the white matter tracts present. This FA skeleton was then thresholded at 0.2 to ensure that voxels included in the voxel-wise cross-subject analysis were white matter and did not have high inter-subject variability. Subject maps were then projected onto this, and voxelwise statistics carried out. Initially, statistics compared all three groups (PCA, AD, and controls). A further analysis was then carried out to assess hemispheric asymmetry in the six PCA patients with VF deficits. Diffusion data for pca2 was flipped in the x axis so that the right hemisphere was the hemisphere contralateral to the greatest VF deficit in all patients. FA and MD maps for all patients were then projected onto a symmetrised FA skeleton, and a 1-sample group-mean test was carried out to identify regions where one hemisphere had different FA or MD levels to the other. In addition to the standard TBSS analysis, The optic radiation was defined as an ROI using the Juelich histological atlas (Bürgel et al., 2006) on the mean FA image. The mean FA and MD were then calculated for voxels in the skeletonised optic radiation ROI in each hemisphere for each subject.

Functional imaging

All PCA patients carried out one fMRI task with the exception of pca2, who was not able to focus on the central fixation point for the duration of the scan as required. Patients were shown a circular patch of moving dots, centrally presented. This fMRI stimulus and protocol has been described previously, in Chapters 2 and 4. Briefly,

subjects fixated a central cross while 8 cycles of the stimuli were presented (16 seconds of dots moving radially at a speed of 30 deg/s, reversing direction every second, followed by 16 seconds of stationary dots).

Data were analysed using FEAT, and GLM analysis was applied to identify voxels which were significantly more active during stimulus blocks than during rest periods. Area MT and V1 were selected as regions of interest, and Featquery (part of FSL) was used to compute mean percentage BOLD changes and average zstat scores for these visual areas in each hemisphere. In addition to these individual analyses, a higher level FEAT analysis was also run on all subjects in order to create group activation maps, and compare activation between groups across the whole brain. PCA patients were compared to the healthy controls scanned in the hemianopia study. As the number of older controls scanned in the hemianopia study was low, all control subjects were included in the analysis (n=12, age range 21 to 74), instead of just using the older controls.

6.4 Results

Structural (T1-weighted) and diffusion images were collected for 7 PCA patients, 12 AD patients, and 14 healthy older controls. Functional MRI was collected for PCA patients and a subset of the controls only, with the exception of pca2. Gross inspection of patient structural scans shows enlargement of the lateral ventricles, together with atrophy in the occipital and parietal lobes. This ventricular enlargement is particularly apparent in those patients with more advanced PCA (pca patients 1-4, Figure 6.4).

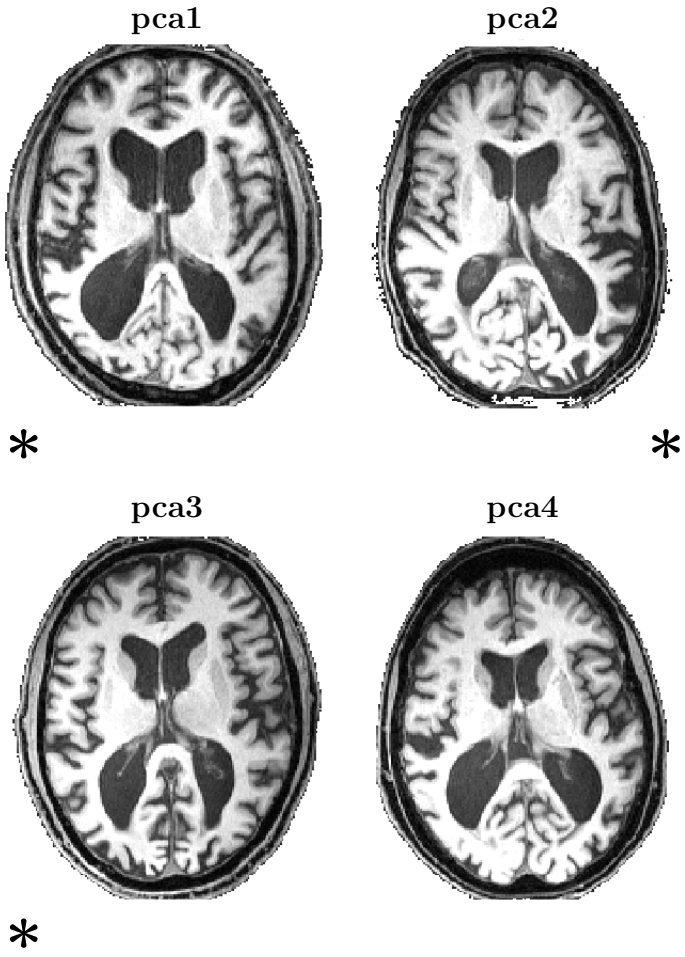

Figure 6.4: T1-weighted structural scans for patients with more advanced PCA. These patients were diagnosed with PCA between 4 and 6 years before being scanned for this study. Asterisks indicate the hemisphere contralateral to the greatest VF deficit. Axial slices are shown with scans oriented radiologically, with the right hemisphere shown on the left. This convention is used for all the brain images which follow.

Some grey matter loss is however evident in all patients, as can be seen in the earlier stage patient scans in Figure 6.5. In some cases, the enlargement of the ventricles and general posterior atrophy appears larger on the side contralateral to the visual field with the most extensive field loss, in particular in the most advanced patients pca1 and pca2, although this is not the case for all patients.

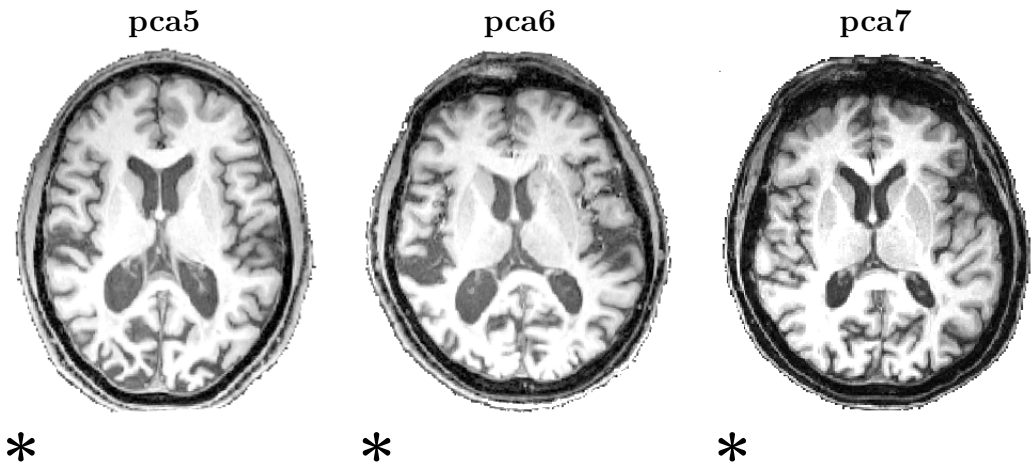

Figure 6.5: T1-weighted structural scans for patients with earlier stage advanced PCA. These patients were diagnosed with PCA between 3 months and 2.5 years before being scanned for this study. Asterisks indicate the hemisphere contralateral to the greatest VF deficit.

6.4.1 Relative atrophy of white and grey matter

In PCA patients, gross examination of T1-weighted structural scans shows an immediately obvious increase in ventricular size compared to that expected in a healthy subject of similar age. This is attributable to an increase in regions filled with CSF as the surrounding brain matter atrophies and reduces in volume. In order to assess whether the brain atrophy observed is predominantly due to grey matter loss, white matter loss, or a combination of both, structural scans were segmented into different tissue types, and the proportional volumes of each compared. Mean values for each subject group are given in table 6.3.

Across the whole brain, one way ANOVAs showed that there were significant differences in volumes of CSF ($F_{(2,30)}$ =9.75, $p < 0.001$) and grey matter (GM) ($F_{(2,30)}$ =5.20, $p < 0.05$) between groups, while white matter (WM) did not differ between groups.

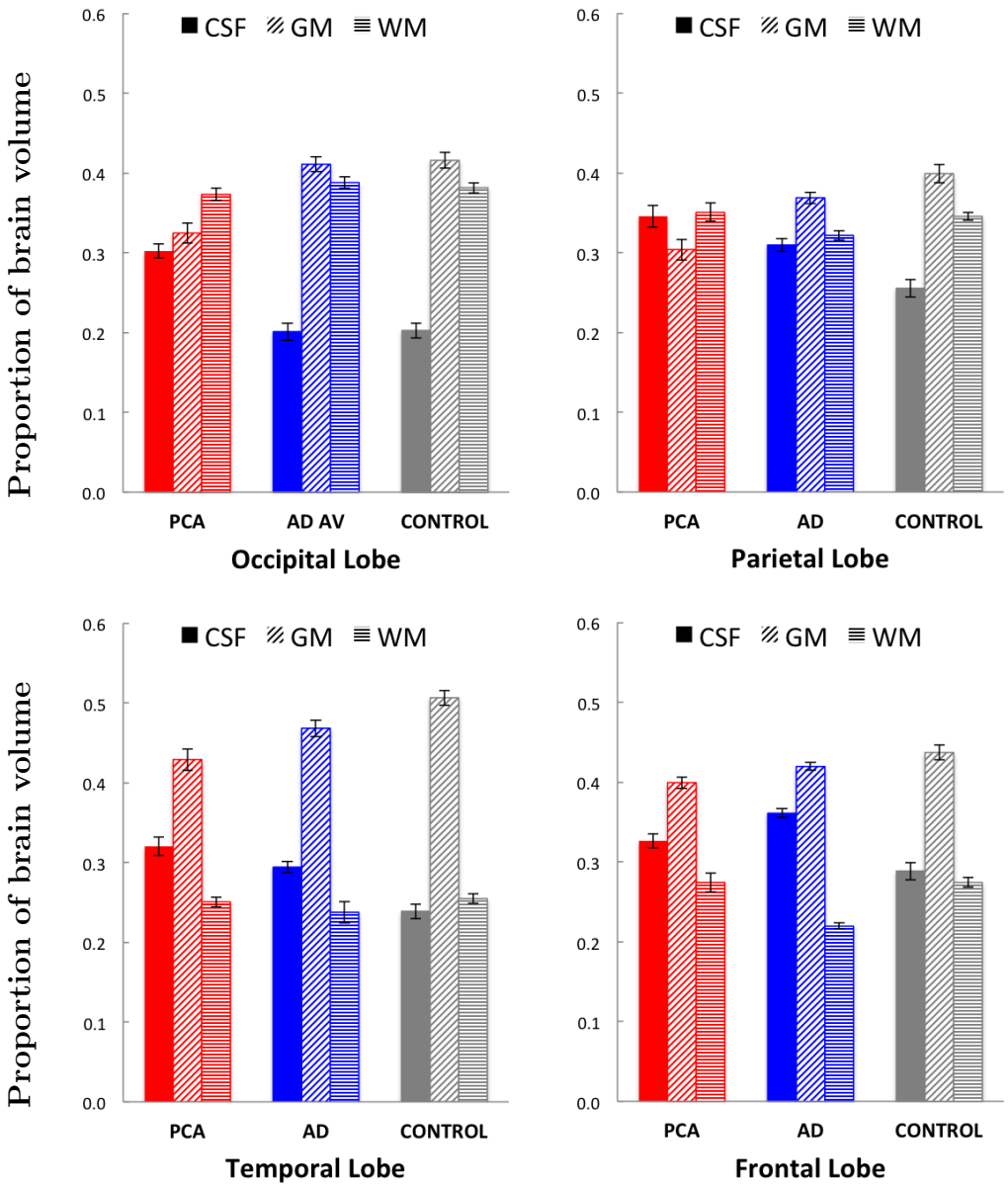

Figure 6.6: Proportions of white matter, grey matter, and CSF in each lobe of the brain. The majority of tissue loss in PCA patients in comparison to controls appears to come from loss of grey matter. Standard errors are shown for each group.

Further analysis of these differences, using post hoc comparisons with Bonferroni correction to adjust for multiple comparisons, showed that absolute numbers of voxels of CSF, GM, and WM were comparable in AD and PCA. However, both patient groups

Table 6.3: Proportion of total brain volume occupied by CSF, grey matter, and white matter

		CSF	GM	WM
Mean	PCA	430327 (21726)*	475002 (12632)*	477862 (22230)
	AD	421316 (14405)*	515964 (17155)	527643 (16738)
	CONTROL	333765 (17495)	552231 (14304)	505817 (11411)
Mean	PCA	0.31 (0.006)*	0.34 (0.003)*	0.34 (0.010)*
	AD	0.29 (0.007)*	0.35 (0.004)*	0.36 (0.007)
	CONTROL	0.24 (0.003)	0.40 (0.003)	0.36 (0.005)

Mean values for tissue volumes (mm^3) and proportions for each subject group
Figures in parentheses indicate standard errors of the mean
* $p < 0.05$ patients compared to controls (Bonferroni post hoc tests). No significant differences between PCA and AD when corrected for multiple comparisons

had significantly higher volumes of CSF than controls (both $p < 0.01$), and PCA patients had significantly lower GM volume than controls ($p < 0.05$).

However, as brain sizes vary substantially between individuals, in order to better investigate changes in the amounts of CSF, GM and WM in patients, proportions of the brain of each subject taken up by each tissue type were also compared. Comparison of the proportions of tissue types showed significant differences between groups in all three tissue types. CSF ($F_{(2,30)}$ =22.27, $p < 0.001$) and GM ($F_{(2,30)}$ =21.40, $p < 0.001$) had the most significant differences between groups, with WM also showing a smaller but still significant difference when assessing proportions instead of absolute volumes ($F_{(2,30)}$ =3.99, $p < 0.05$). Post hoc comparisons showed that PCA and AD patients both had significantly more CSF present than controls (both $p < 0.001$), with PCA patients having more CSF than AD patients (0.31 vs 0.29), although this difference was not statistically significant ($p = 0.12$). This suggests both groups have lost a significant amount of functioning brain tissue. In AD patients, this loss was only significant in the

GM ($p < 0.001$), however PCA patients had significantly reduced proportions of both WM and GM ($p < 0.05$ and $p < 0.001$ respectively). This suggests that the patterns of atrophy in AD and PCA are different. Hereafter, proportions of each of the three tissue types will be considered rather than volumes.

In PCA patients, atrophy has been consistently reported as being more extensive in posterior brain regions, specifically in the occipital and temporal lobes. The different lobes of the brain were therefore analysed separately to identify specific regions of GM and WM loss. Relative proportions of CSF, WM, and GM in the occipital, frontal, parietal, and temporal lobes are shown in Figure 6.6. There were group differences in the amount of CSF in all lobes (all $F_{(2,30)} > 16.27$, $p < 0.001$), and in GM in all lobes ($F_{(2,30)} > 4.93$, $p < 0.05$). White matter proportions only differed across groups in the frontal ($F_{(2,30)} = 24.07$, $p < 0.001$) and parietal ($F_{(2,30)} > 5.46$, $p < 0.01$) lobes. PCA patients differed from both controls and AD patients in a number of ways. In the occipital lobe, while AD patients and controls showed very similar results, PCA patients had markedly increased CSF and reduced GM (both $p < 0.001$), while WM was similar to controls. Indeed PCA patients had significantly greater amounts of CSF and less GM than controls in all four lobes (all $p < 0.05$), with WM not being significantly different from controls. PCA patients had significantly less GM than AD patients in all lobes except the frontal lobe (all $p < 0.05$). The only regions where PCA and AD patients had different proportions of WM were in the frontal ($p < 0.001$) and parietal ($p < 0.05$) lobes, where AD patients had less WM present than PCA patients.

To investigate whether the asymmetrical VF deficits observed in 6 of the PCA

Table 6.4: Proportion of total brain volume in each lobe occupied by CSF, grey matter, and white matter

Lobe	Hemisphere	Tissue Type		
		CSF	GM	WM
Occipital	Contra	0.33 (0.009)	0.30 (0.018)	0.36 (0.009)
	Ipsi	0.28 (0.011)	0.33 (0.012)	0.38 (0.008)
		**	*	
Frontal	Contra	0.33 (0.013)	0.39 (0.007)	0.28 (0.014)
	Ipsi	0.32 (0.009)	0.41 (0.010)	0.27 (0.015)
		*	**	
Temporal	Contra	0.33 (0.019)	0.41 (0.017)	0.27 (0.009)
	Ipsi	0.32 (0.017)	0.45 (0.019)	0.24 (0.008)
			*	**
Parietal	Contra	0.35 (0.018)	0.28 (0.017)	0.37 (0.013)
	Ipsi	0.33 (0.015)	0.33 (0.015)	0.34 (0.015)
			**	**

The mean values for the 6 PCA patients with VF deficits are given
Figures in parentheses indicate standard errors of the mean
Contra indicates the hemisphere opposite the VF deficit
Ipsi indicates the hemisphere on the same side as the VF deficit.
* $p < 0.05$, ** $p < 0.01$. Paired samples t tests

patients were reflected in an asymmetrical atrophy as has sometimes been reported in PCA, the different hemispheres were compared in PCA patients. The hemisphere opposite the visual field with the hemianopia or more severe VF deficit was termed the contralateral hemisphere, while the hemisphere on the same side was termed the ipsilateral hemisphere. This terminology is used throughout.

The contralateral hemisphere had a significantly lower proportion of GM in all lobes in comparison to the ipsilateral hemisphere. In the occipital and frontal lobes, this was balanced by an increase in CSF, suggesting greater overall atrophy in the contralateral lobe. However in the parietal and temporal lobes, the decrease in GM volume was combined with an increase in WM volume, therefore the overall proportion of GM and

WM to CSF was similar in the different hemispheres. Mean values and the results of paired samples t tests comparing groups can be found in Table 6.4.

6.4.2 Grey matter degeneration

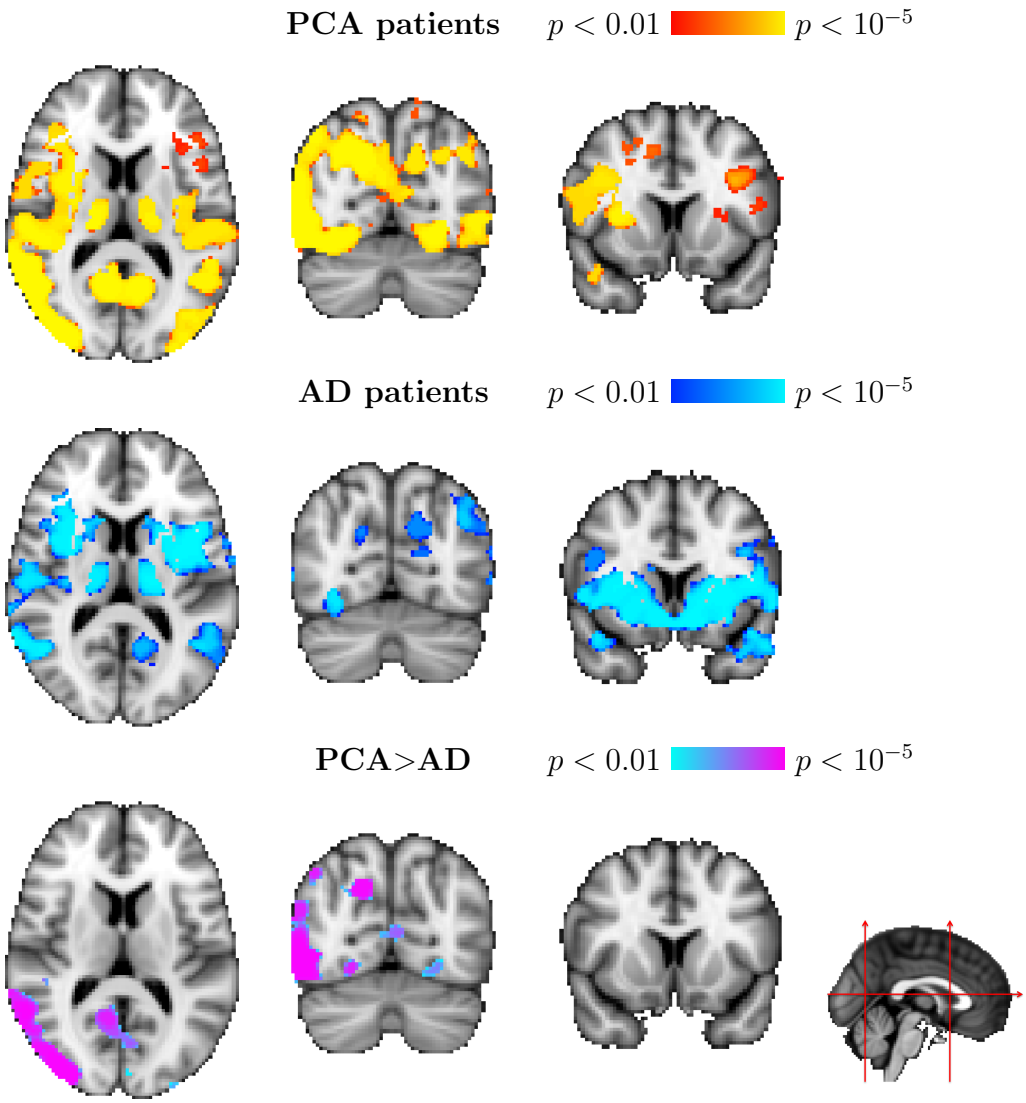

Figure 6.7: VBM analysis of grey matter atrophy. The first two rows show regions with decreased GM volume relative to controls in PCA and AD patients respectively. Regions where PCA patients have greater GM loss than AD patients are shown in the third row. All coloured voxels are significant at $p < 0.01$, cluster corrected. The location of the axial and coronal slices are shown with the red arrows on the sagittal image.

Both PCA and AD patients showed widespread grey matter atrophy compared to controls (corrected, $p < 0.01$, Figure 6.7). The two patient groups show slightly different patterns of atrophy, as can be seen in the frontal and posterior slices shown, which show greater atrophy in AD and PCA respectively. However, direct comparison between the two patient groups only found significant differences in grey matter in the occipital lobes, where PCA patients showed a greater level of atrophy than AD patients. This difference was greater in the right hemisphere than the left hemisphere. There were no areas for which grey matter was significantly more atrophied in AD than PCA.

Grey matter atrophy was further investigated using measurements of cortical thickness, which estimates the width of the cortical ribbon throughout the brain. Freesurfer was used to compute cortical thickness across the brain in each subject individually, and cortical thickness maps were projected onto an average brain in order to evaluate differences between groups. Figure 6.8 shows that there are significant differences between healthy controls and PCA patients, and healthy controls and Alzheimer's patients. These differences are, however, in different brain regions for the different patient groups. In PCA patients, cortical thickness is significantly lower than controls in posterior brain regions. Interestingly, with regard to the occipital cortex, the reduction in cortical thickness appears to be located in extrastriate areas rather than in primary visual cortex. In AD patients, cortical thickness was normal in the occipital lobe, but reduced in some more frontal and temporal regions. Overall, the AD patients appear to show more similar patterns of cortical thickness to control subjects than is the case

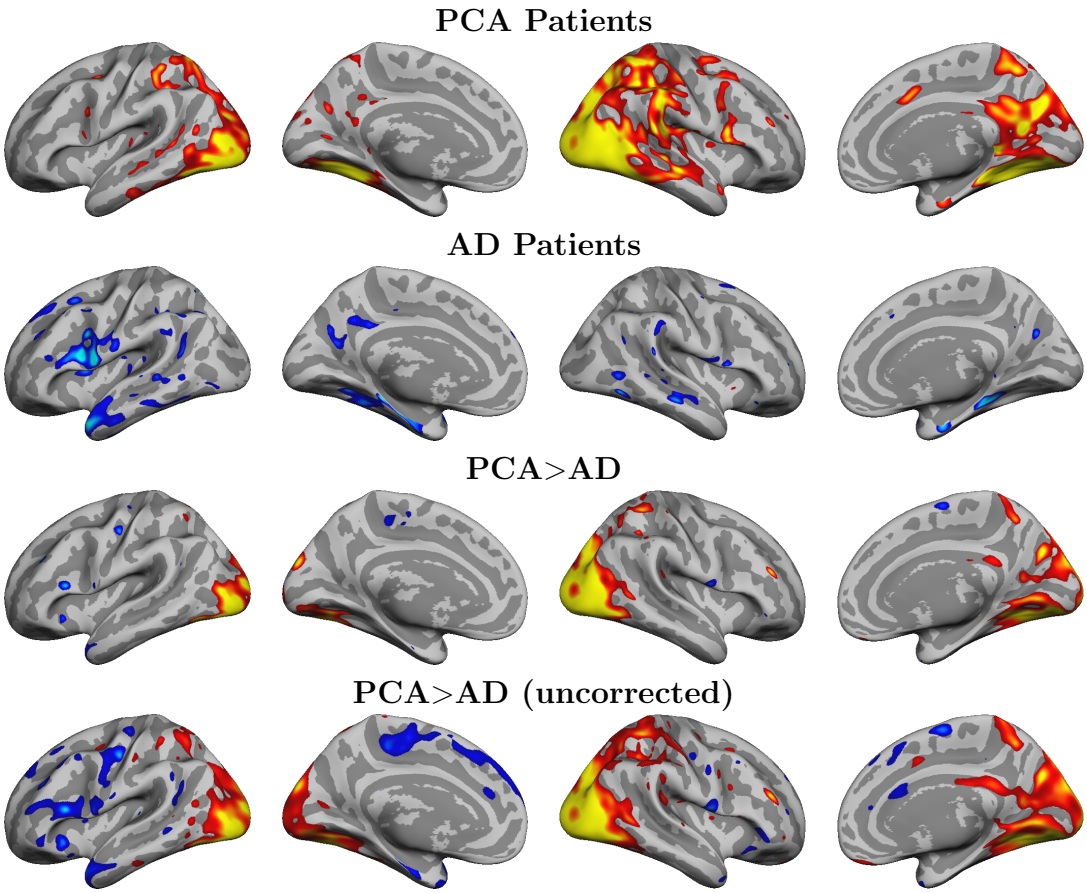

Figure 6.8: Cortical thinning in PCA and AD. There are significant differences in cortical thickness between PCA patients and controls (top row) and AD patients and controls (second row), with the patient groups showing thinning of the cortex in different regions. In the third row, regions where PCA patients have lower cortical thickness than AD patients are shown in red-yellow, and regions where AD patients have lower cortical thickness are shown in blue. Lighter colours are more significant. The first three rows show results corrected with false discovery rate, $p < 0.05$, with a smoothing of 10 mm. Uncorrected results for the comparison of PCA and AD subjects are shown in the bottom row, showing a broader pattern of differences that did not survive statistical correction.

in PCA patients. In direct comparison between the PCA and AD patient groups, PCA patients show extensive cortical thinning in the occipital lobe and some parietal regions also. At $p < 0.05$ corrected for false discovery rate, AD patients show greater loss of cortical thickness in relatively few regions; uncorrected significance maps $p < 0.05$ show a clear anterior posterior separation in regions where AD and PCA show greater loss

Table 6.5: Cortical thickness in the visual areas

Groups	area V1	area V2	area MT
PCA vs Control	NS	**	**
AD vs Control	NS	NS	NS
PCA vs AD	*	**	**
PCA ipsi vs PCA contra	NS	**	**

** $p < 0.001$, * $p < 0.05$, NS non significant $p > 0.05$
ANOVAs used to compare cortical thickness across groups.
Post hoc analyses corrected for multiple comparisons (Bonferroni).
Asymmetries in PCA (row 4) analysed using paired samples t tests.

of cortical thickness respectively.

Three regions of interest in the visual cortex were defined for further investigation: V1, V2, and MT. Initially, results from each hemisphere were combined for each subject, and groups of subjects were compared using one way ANOVAs for each visual area. Group effects were present for all of the visual areas, with the greatest difference between groups being in area MT ($F_{(2,30)}$ =35.76, $p < 0.001$), followed by V2 ($F_{(2,30)}$ =20.41, $p < 0.001$). Primary visual cortex had the smallest differences in cortical thickness between groups, however there was still a significant main effect ($F_{(2,30)}$ =4.67, $p < 0.05$). PCA patients had lower cortical thickness than controls in all of the visual areas investigated except area V1, which also did not show a clear difference in the whole brain maps. Looking at the graph in Figure 6.9, we can see that thicknesses increase from V1 to V2 to MT, however thinning in comparison to controls also increases through the visual hierarchy. AD patients did not show significant cortical thinning in any of the visual areas investigated; indeed they had slightly higher cortical thickness than controls in V1 and V2.

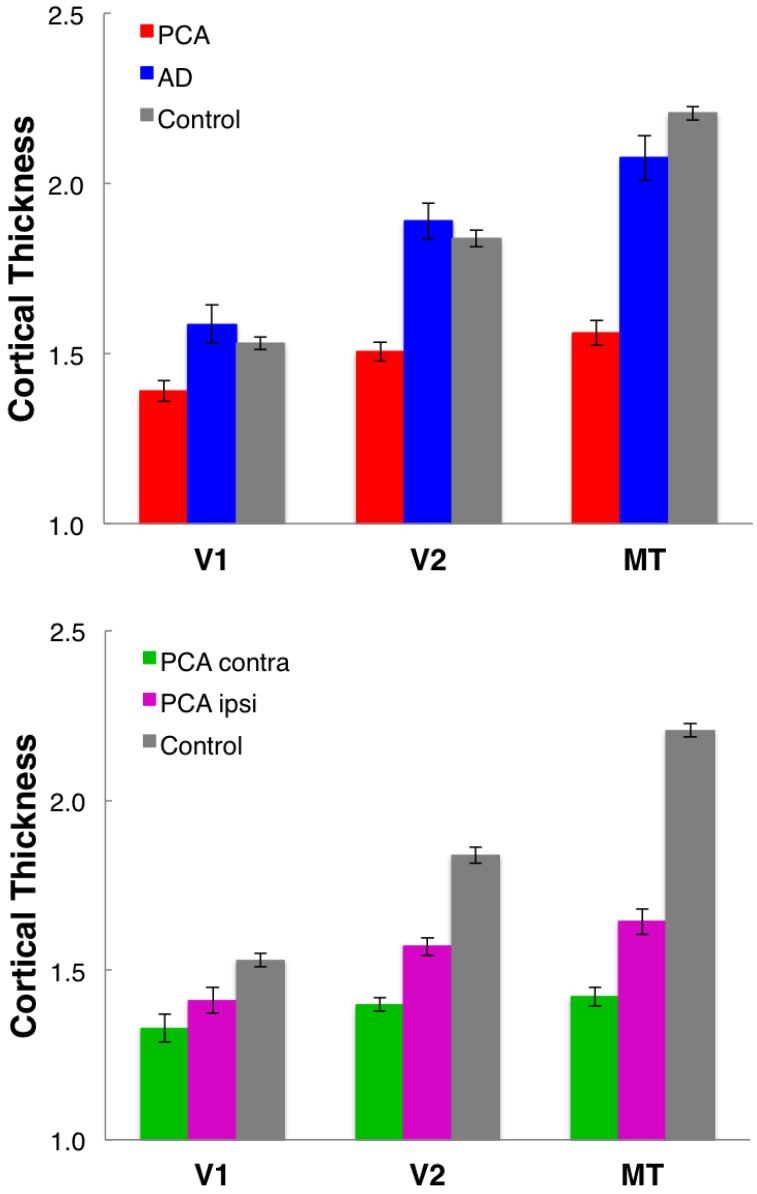

Figure 6.9: Cortical thickness in areas V1, V2, and MT. When cortical thickness measures are combined across hemispheres, PCA patients have cortical thinning in all the visual areas investigated, in contrast to AD patients, who only have reduced cortical thickness in area MT compared to controls. The second chart shows results for PCA patients separately for each hemisphere. The hemispheric asymmetry in cortical thickness gets progressively larger for higher cortical areas, with lower cortical thickness found in the hemisphere contralateral to the VF deficit. Standard errors are shown for all groups.

If the homonymous visual field loss exhibited by PCA patients results from damage to the visual cortex in a similar manner to hemianopia patients, we would expect that cortical thickness be reduced to a greater extent in the hemisphere contralateral to the field deficit than the ipsilateral hemisphere, and for there to be more extensive loss in the primary visual cortex. Surprisingly, there was no significant difference in cortical thickness between ipsi- and contralateral V1 in PCA patients. However, in areas V2 and, even more so, MT, cortical thickness was lower in the contralateral hemisphere.

6.4.3 White matter degeneration

White matter was atrophied in both PCA and AD patients in comparison to controls. The pattern of atrophy was broadly similar in analysis of both fractional anisotropy (Figures 6.10) and mean diffusivity (Figure 6.11), with patients showing reduced FA and increased MD in degenerated white matter regions. In AD patients, this atrophy was more extensive in the frontal and temporal lobes, while in PCA, the greatest white matter atrophy was in the occipital and parietal lobes. Comparatively, PCA showed more widespread white matter loss than was present in AD, however this degeneration was significantly greater in PCA only in posterior brain regions ($p < 0.05$, corrected for multiple comparisons). Notably PCA patients show a greater degree of atrophy in the splenium of the corpus callosum, where the fibres from the visual cortex cross hemispheres. There were no regions where the white matter was more significantly atrophied in AD patients compared to PCA patients.

A further TBSS analysis was run on the PCA patients with visual field deficits

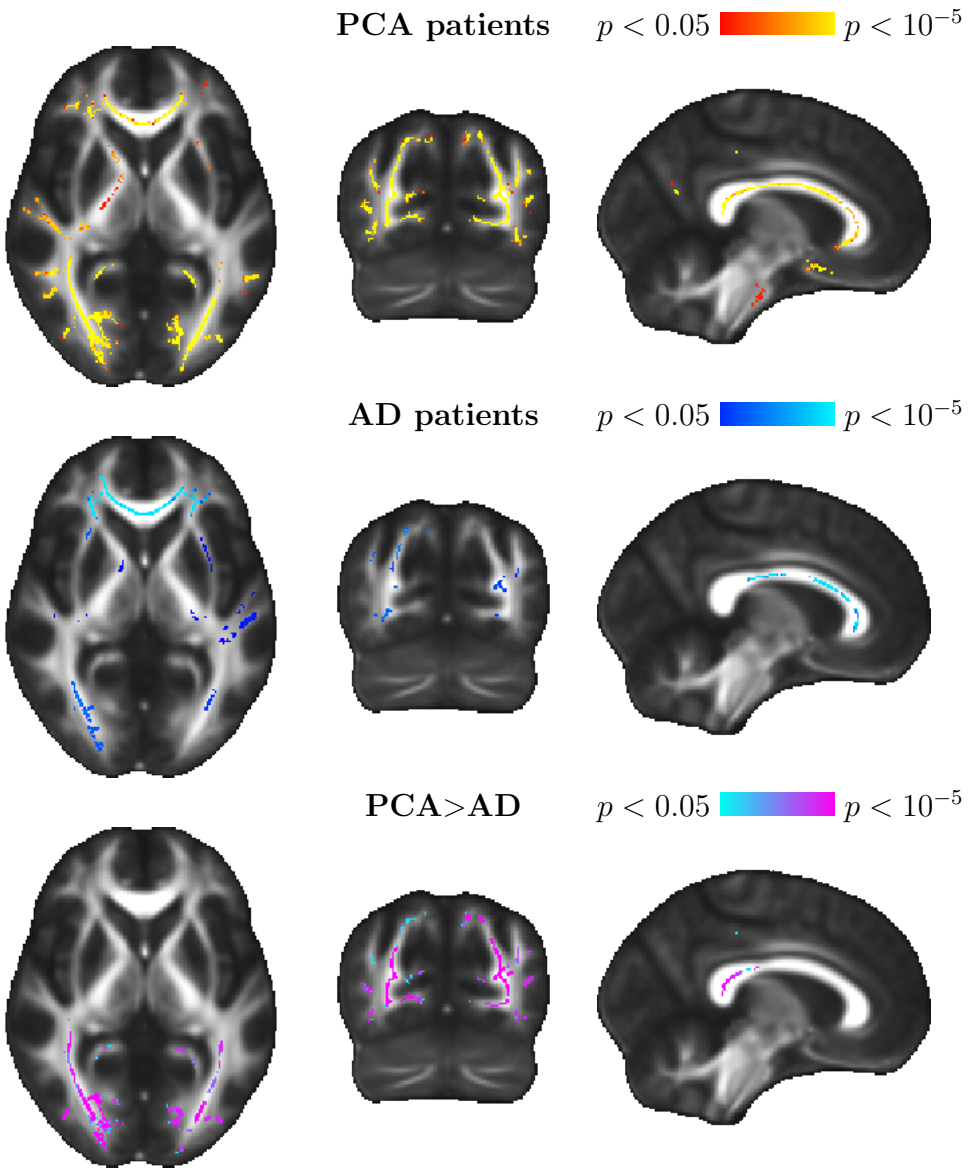

Figure 6.10: Group differences in fractional anisotropy. Both PCA patients (top row) and AD patients (middle row) have extensive regions of white matter with significantly lower FA than controls. The third row shows regions where PCA patients have lower FA than AD patients, predominantly located in the occipital lobe. Significant voxels are cluster corrected, $p < 0.05$.

(all subjects except pca4) in order to see whether there were any regions where white matter integrity was lower in the hemisphere contralateral to the visual field deficit. For ease of analysis, data for pca2, who was the only subject with a right hemianopia,

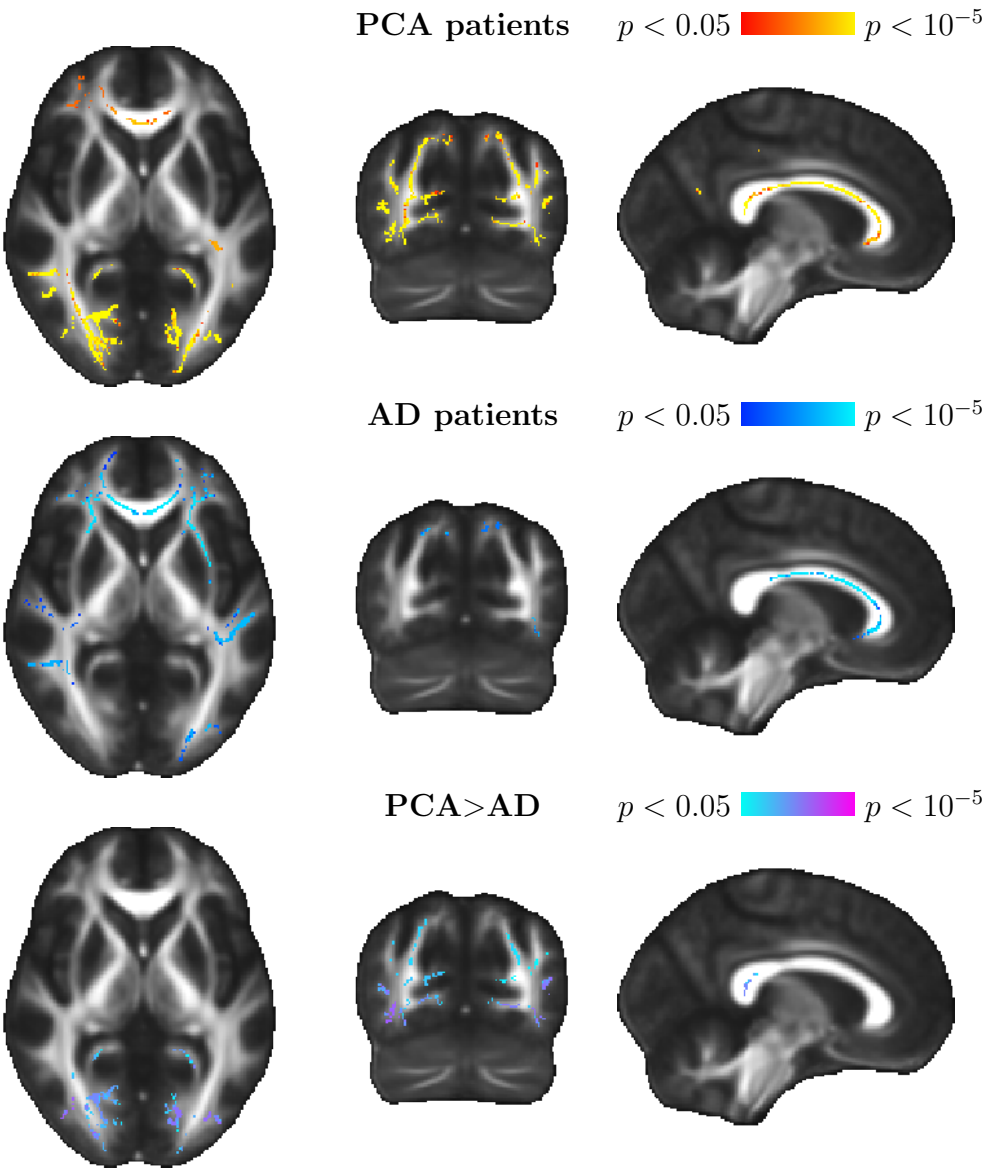

Figure 6.11: Group differences in mean diffusivity. Compared to controls, both PCA (top row) and AD patients (second row) have widespread regions of white matter with higher mean diffusivity. The bottom row shows regions where PCA patients have greater MD than AD patients, signifying greater WM atrophy. Significant voxels are cluster corrected, $p < 0.05$.

was flipped in the x axis, so that the right hemisphere was the contralateral hemisphere in all cases. In the comparison of FA across hemispheres, almost no regions were found that had significantly lower FA in the right hemisphere than the left hemisphere, with

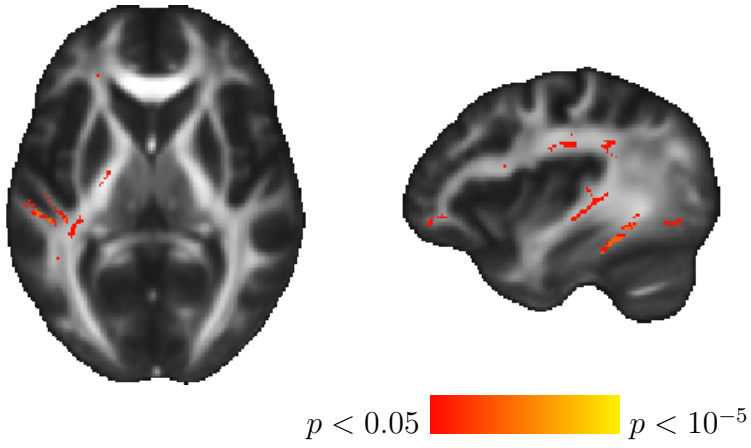

Figure 6.12: Asymmetries in mean diffusivity in PCA patients. Regions where MD is significantly higher in the hemisphere contralateral to the VF deficit than the ipsilateral hemisphere in PCA patients are shown. Significant voxels are cluster corrected, $p < 0.05$.

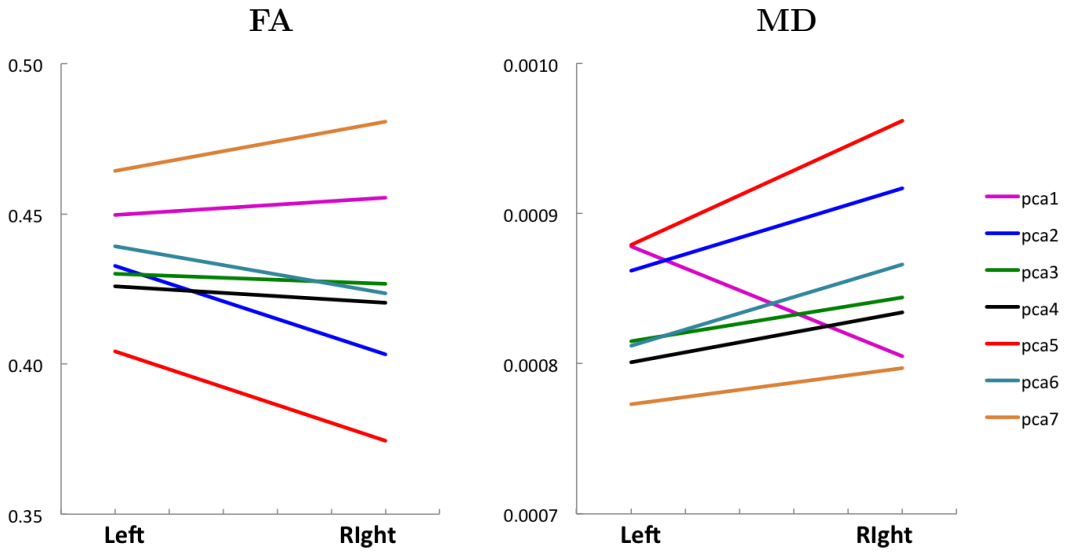

Figure 6.13: FA and MD in the optic radiation Mean FA (left graph) and mean MD (right graph) in the optic radiation in the ipsi (left) and contralateral (right) hemispheres of PCA patients. Lower FA and higher MD on the right suggest greater loss in white matter integrity in the hemisphere contralateral to the visual field deficit.

the exception of one voxel in the brain stem and two in the temporal lobe. For mean diffusivity however, which has been argued to be a more sensitive measure of atrophy in neurodegenerative disorders than FA (Acosta-Cabronero et al., 2010), increased MD

was found in the right hemisphere in a variety of brain areas, as shown in Figure 6.12. In contrast to the expected asymmetry in areas related to visual processing, very little difference was found in MD in the occipital lobe or the majority of the optic radiation. However there was evidence of greater MD in more anterior parts of the optic radiation. The opposite contrasts (left hemisphere having greater loss of white matter integrity than the right) yielded no significant results for either FA or MD.

As there were relatively small subject numbers in the analysis of asymmetries in PCA patients (n = 6), differences in MD and FA in the optic radiation were further investigated in individual subjects. All subjects had a greater average MD in the optic radiation in the contralateral hemisphere, with the exception of pca1 who showed the reverse effect. Results for FA were more variable. Pca5 and pca2, who showed some of the most asymmetric field deficits, followed the expected pattern of lower FA in the contralateral hemisphere, as did pca6 whose VF deficit is somewhat more extensive. Pca4, who had no VF deficit, unsurprisingly showed fairly similar FA in the radiations, as did pca3 and pca1, while pca7 had greater FA in the contralateral radiation. This is particularly surprising in the cases of pca3 and pca7, whose VF deficits are very lateralised.

6.4.4 Cortical response to visual stimuli

fMRI scans were acquired for all PCA patients except pca2. In all of these patients, the field deficit was greater in the left hemifield, and so for the fMRI results, the right hemisphere is termed the contralateral hemisphere, and the left hemisphere is termed

the ipsilateral hemisphere, in terms of their relationship to the affected hemifield. From results in hemianopia patients, we expected activation in the ipsilateral hemisphere to be relatively unaffected as visual processing is preserved, while activation in the contralateral hemisphere is expected to be reduced. In order to investigate differences in responses to visual stimuli in PCA patients compared to controls, a higher level FEAT analysis was run to combine individual data sets, enabling the extraction of group means and identification of regions with differences between groups.

Activation maps showing clusters with significant cortical responses to motion stimuli ($z > 2.3$) are shown in Figure 6.14. As expected, controls show widespread activation in the visual cortex in both hemispheres. In PCA hemispheres, similar regions are activated, however the activation is greatly reduced in comparison to controls, in particular in extrastriate regions in the right hemisphere, where the expected activation in area MT is either absent or greatly reduced. However direct statistical comparison of the two groups (row 3) shows that in fact the regions where BOLD activation is most reduced in PCA patients is centred around the primary visual cortex. In contrast, PCA patients have greater BOLD activation from control subjects in just one region, localised to the inferior parietal lobule.

In addition to examining group effects, percentage BOLD changes and the number of active voxels (where $z > 23$) were extracted for areas V1 and MT in each subject in order to further examine differences in activation. The graphs in Figure 6.15 show mean values for percentage signal change and number of activated voxels in each group. In addition to this, scores for each individual subject are also plotted on the graphs.

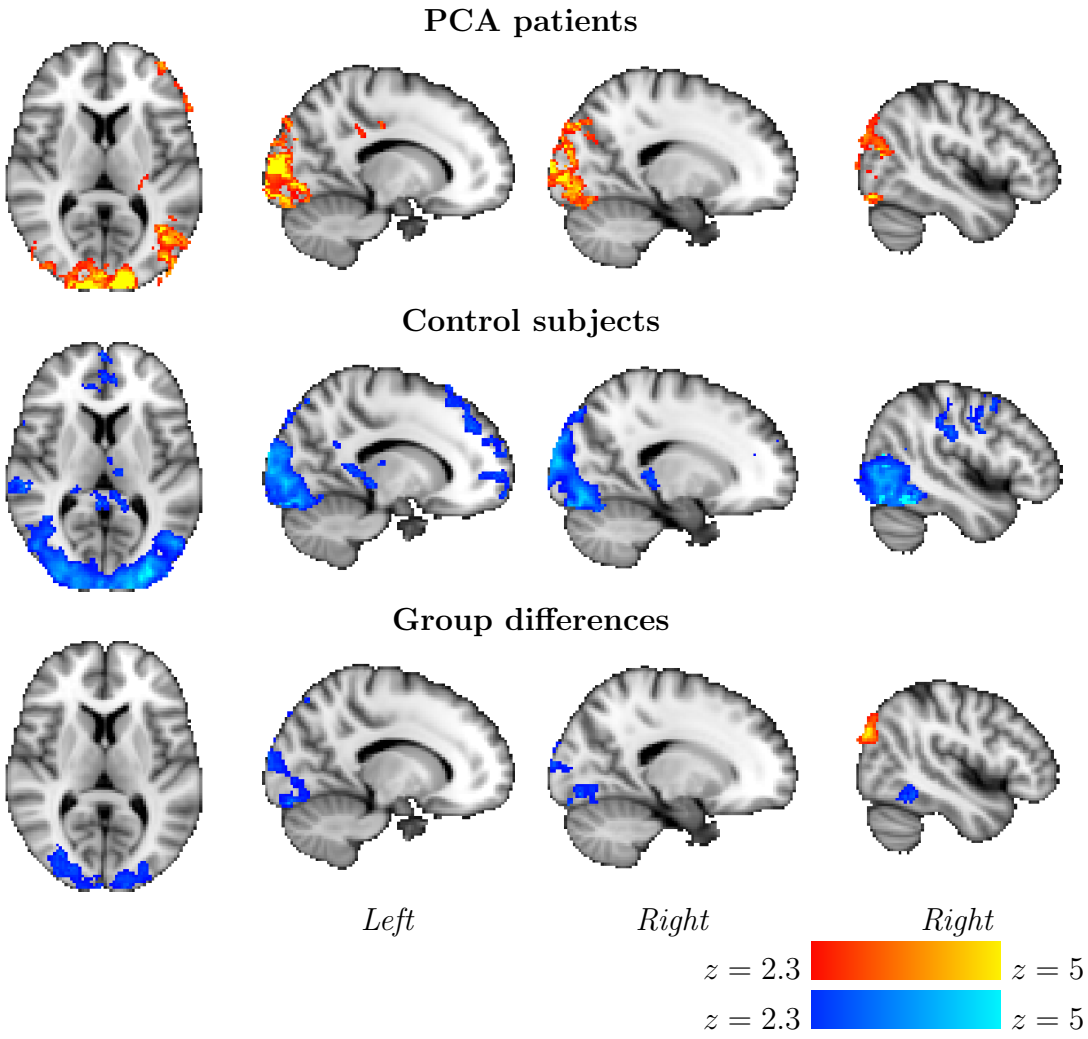

Figure 6.14: Activation in PCA patients and controls to centrally placed motion stimuli. All subjects show bilateral activation to motion stimuli. In PCA (top row), activation is greater in the left hemisphere, particularly in extrastriate cortex. In controls (middle row), activation is more extensive and less asymmetric. In the bottom row, regions where there are significant group differences are shown. Regions where controls have more activation than patients, primarily in early visual cortex, are in blue. PCA patients have greater activation than controls in one region, the right inferior parietal lobule (red-yellow). Significant voxels are cluster corrected, $z > 2.3$.

Comparing BOLD activation in PCA patients in areas MT and V1, it is notable that while all subjects show low activation in area V1, in MT results are more variable, with two patients in particular showing activation that is more comparable to controls

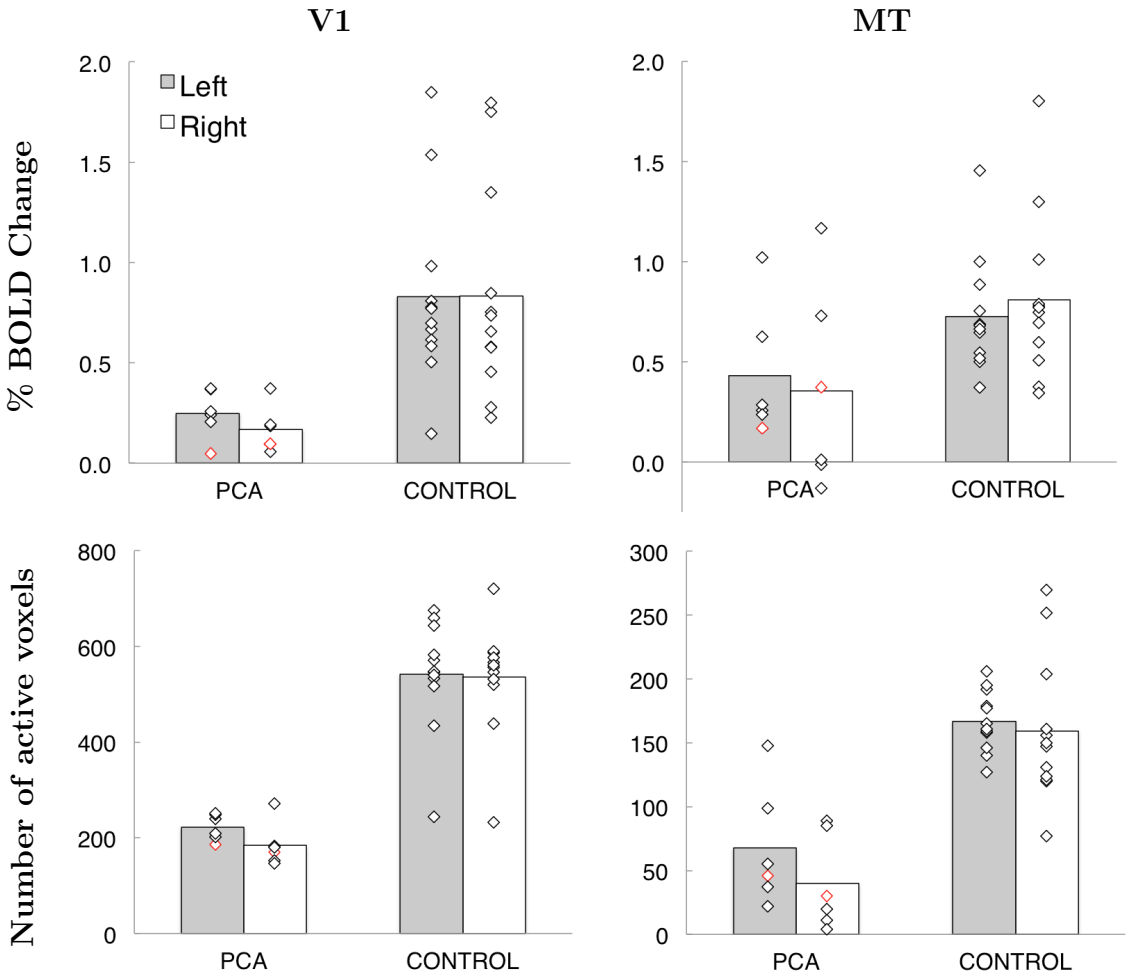

Figure 6.15: Response to visual stimuli in areas V1 and MT. The average percentage BOLD change and number of significantly active voxels (where $z > 2.3$) are shown, together with results for each individual subject. PCA patients have consistently lower activation than controls, and the patients with no visual field deficit (pca4, shown in red) has similar activation to the other patients. Activation in the left (grey) and right (white) hemispheres are similar.

than the other PCA patients. These patients are pca5 and pca7, who both have more recently diagnosed PCA than several of the other patients. Interestingly, pca4, who has no VF deficit (marked in red in Figure 6.15), has similar cortical responses to the motion stimuli as the other patients.

Repeated measures ANOVAs were run with hemisphere and brain region as within

subjects factors, and subject group as a between subject factor. For percentage BOLD change, the only significant difference between contrasts was an overall group difference, with PCA patients having a significantly lower change in BOLD activity in the visual cortex in response to motion stimuli ($F_{(1,16)}$ =9.099, $p < 0.01$).

In terms of the number of active voxels, there was more evidence for differences in activity between the visual areas and different hemispheres. As with the average percentage BOLD change, there was a group difference in the number of active voxels, with control subjects having a larger number of active voxels than PCA patients ($F_{(1,16)}$ =74.290, $p < 0.001$). As would be expected given the relative sizes of V1 and MT, there were significantly more active voxels in area V1 ($F_{(1,16)}$ =116.175, $p < 0.001$), however the disparity between activity in the different brain regions was significantly greater for controls than PCA patients ($F_{(1,16)}$ =21.574, $p < 0.001$), as the extent of activity in PCA is reduced further in V1 than MT. This follows the trend shown in the structural data, with area MT appearing more greatly affected by PCA than V1.

As expected from the lateralised VF deficits of patients, there was a significant effect of hemisphere on the number of activated voxels, with fewer active voxels found in the right hemisphere ($F_{(1,16)}$ =10.141, $p < 0.01$). There was also a significant interaction between hemisphere and group ($F_{(1,16)}$ =4.507, $p < 0.05$), as controls showed very little difference between hemispheres, in contrast to PCA patients where the hemispheric differences were far greater.

6.5 Discussion

6.5.1 Posterior cortical atrophy shows a distinct pattern of grey and white matter degeneration

Extensive degeneration was found in the grey and white matter of PCA patients. Clear differences in tissue volume and integrity existed throughout the brain between the PCA group and healthy older controls, and between PCA and AD patients.

Grey and white matter loss in PCA compared to controls

Patients with posterior cortical atrophy have decreased grey matter volume in the brain, leading to increases in CSF and enlarged ventricles. Comparison of early and late stage PCA demonstrates that this ventricular enlargement is increasingly evident as the disease progresses. Loss of grey matter volume is present in all lobes of the brain, however it is most extensive in the occipital and parietal lobes, with the frontal lobes least affected. Loss of cortical thickness also appears to be concentrated in more posterior regions.

In proportion to brain size, white matter constitutes the same percentage of the brain in PCA patients as it does in healthy older controls. However, analysis of fractional anisotropy and mean diffusivity in the white matter shows that the integrity of the white matter pathways is severely compromised. As with grey matter loss, this degeneration is widespread, however is more extensive in the occipital and parietal lobes, particularly with regards to increases in mean diffusivity.

Grey and white matter loss in PCA compared to AD

In comparison to AD patients, patients with PCA showed more extensive loss of both grey and white matter in the occipital lobes, and had broadly similar patterns of atrophy elsewhere in the brain. There was an effect of hemisphere in several of the analyses, with the difference in atrophy between patients being greater in the right hemisphere, in particular with respect to the VBM, and to a lesser extent, the cortical thickness analyses. The integrity of white matter pathways were similar between patient groups in more frontal brain regions. In comparison to AD patients, however, PCA patients had decreased FA and increased MD in the pathways towards the back of the brain, including the optic radiations and the splenium. In this case, the difference between groups in white matter degeneration was broadly similar across hemispheres.

Measures of grey matter atrophy were most informative in looking for brain regions where AD patients showed greater degeneration than PCA patients. While analysis of FA and MD using TBSS showed no areas of greater loss of white matter integrity in AD patients, in the frontal and temporal lobes, regions with thinner cortices were found in AD patients compared to PCA patients. Additionally, although comparison of groups in the VBM analysis found no regions where AD patients showed greater atrophy than PCA patients, separate maps for the patient groups do show more extensive loss of grey matter volume in the frontal and temporal areas in the AD patients.

Summary

This study demonstrates a pattern of atrophy in PCA that is clearly distinct from both normal ageing and typical Alzheimer's disease. While atrophy of both grey and white matter is present throughout the brain in PCA, it is the posterior regions, specifically the occipital and posterior parietal lobes that set PCA apart from healthy subjects and AD patients. In patients with more advanced PCA, the enlarged lateral ventricles due to the loss of surrounding white matter is clearly apparent on T1-weighted structural imaging, together with substantial grey matter atrophy in posterior regions. With regards to the differences between dementia patient groups, all analyses converge on the conclusion that PCA patients have significantly greater degeneration throughout the occipital and parietal regions that subserve visual and attentional processing than AD patients, to a far greater extent than has been shown in previous comparisons of these two groups. As has been anecdotally noted in a number of studies of PCA, in the majority of patients, atrophy is more pervasive in the right hemisphere. As the right hemisphere is noted as being more sophisticated than the left hemisphere in its ability to process complex visuo-spatial stimuli (Corballis, 2003), this observation, in combination with the location of the atrophy in the posterior brain regions, is consistent with the higher order visual deficits exhibited by PCA patients.

6.5.2 Comparability of AD and PCA patients

Previous studies have generally found only small differences between groups, with a general trend of greater atrophy in the right occipital gyrus, right posterior lobe (Alves et al., 2013) and right visual association cortex (Whitwell et al., 2007) in PCA patients, and greater atrophy in the left hippocampus (Whitwell et al., 2007; Alves et al., 2013) and the left parahippocampal gyrus (Alves et al., 2013) in AD patients. In this study, highly significant differences in the amount of occipital lobe atrophy were found between PCA and AD patients, with PCA patients showing greater degeneration in both the grey and white matter of posterior occipital and parietal regions. While the pattern of deficits exhibited by these patients may predict such an effect, it is surprising that this is the first study to demonstrate such an extensive difference between these patient groups. Furthermore, the small differences between PCA and AD groups found in previous studies have tended to extend in both directions; i.e. different specific brain regions of greater atrophy were found for both AD and PCA, in comparison to the other patient group. In contrast, in the present study, while brain regions showing increased atrophy in AD were small and limited to certain types of analyses, brain areas showing greater atrophy in PCA were extensive, and pervasive across all analyses performed.

It is possible that the magnitude of the differences in degeneration found were influenced by the stage of disease of the two patient groups, as it was not possible to directly compare the severity of disease in the groups. In general, studies of the two patient groups have attempted to ensure comparability of disease progression in the patients groups by comparing mini-mental state exam (MMSE) scores (Lehmann

et al., 2012; Migliaccio et al., 2012a), disease duration (Migliaccio et al., 2012a) or by recruiting age and sex matched patients (Whitwell et al., 2007). The latter method is questionable, as PCA is known to typically have an earlier onset than AD, and so age matched patients are likely to have progressed further in the disease in the case of PCA. There are also issues inherent to measuring disease progression in dementia. It can be very difficult to pinpoint when a neurodegenerative disease begins, and this will be greatly affected by the circumstances of the individual patient, for example in terms of whether they have a good enough support network for the changes in their behaviour to have been noticed at an early stage. In the case of the patients included in this study, it was unfortunately not possible to compare the severity of disease based on an assessment of cognitive ability, as while the AD patients had undergone typical dementia tests such as the MMSE and MoCA due to their inclusion in the OPTIMA cohort, the PCA patients had not taken these tests, but instead had undergone other neuropsychological assessments. However, the recruitment criteria for the present study required that PCA patients showed only 'mild cognitive impairment', with minimal memory impairments. Therefore while known disease duration in these patients varied from 3 months up to 6 years, none of the patients had entered the latter stages of the disorder where memory decline has become more evident.

It should be noted also that while analysis of white matter integrity found no regions where AD patients showed significantly more atrophy than PCA patients, analysis of grey matter loss consistently showed small but significant regions in the frontal and temporal lobes where AD patients showed greater grey matter loss. It is therefore

not the case that the PCA group have simply more degeneration throughout the brain than the AD patients studied. Similarly, the consistency with which PCA patients show greater degeneration than AD patients only within posterior regions in the parietal and occipital lobes does suggest that the differences are not purely driven by an effect of disease progression. Indeed a longitudinal study by Lehmann et al. (2012) suggests that as PCA progresses, neuroimaging markers of the disorder become more similar to typical AD.

It is possible that the greater difference between groups found here was due to the selection of patients with loss of primary visual function. While in this group, these patients constituted over 85% of the cohort, visual fields deficits were not noted as deficits in patients in most imaging studies, except in Whitwell et al. (2007), where 18% of PCA patients demonstrated a visual field deficit. It is possible that as visual field deficits in PCA do not appear to result from direct damage to the primary visual cortex, they instead require widespread damage to either the optic radiations or extrastriate cortex in order to manifest. PCA patients with loss of primary visual function may therefore have more substantial damage to these areas than other patients with different clinical symptoms. Furthermore, as these patients have been selected for this exact deficit, they are likely to have more homogeneous damage than a sample taken more broadly from the PCA population, increasing the likelihood of finding specific regions with extensive atrophy within the group.

6.5.3 Visual field deficits in PCA may not reflect direct damage to the primary visual cortex

As described previously, PCA patients show significant degeneration in the occipital lobe, with a tendency towards greater atrophy in the right hemisphere in comparison to healthy older controls and AD patients. Further analyses investigated whether significant differences existed between hemispheres of the PCA patients, directly comparing the hemispheres ipsi- and contralateral to the hemifield with the most severe visual field deficit. Cortical thickness was more significantly reduced in extrastriate visual areas (V2 and MT) in the contralateral hemisphere, however in primary visual cortex, there was minimal cortical thinning, and thickness did not differ between hemispheres. Group analysis found little evidence for hemispheric asymmetries in white matter degeneration in the visual pathways, with the exception of some regions of the anterior optic radiation. However, analysis of optic radiation integrity in individual subjects did show a trend for greater mean diffusivity (suggesting loss of fibre integrity) in the contralateral optic radiation in the majority of subjects; this pattern was not present in analysis of FA.

Investigation of BOLD activation in the visual cortex in response to visual stimuli showed reduced activation compared to controls, in both areas MT and V1. Hemispheric asymmetries in BOLD activation were minimal, however there was a trend towards lower activation in the contralateral hemisphere in both areas MT and V1. Where data points were extracted for subjects individually, results for pca4 (who had no visual field deficit) were not outside of the range of the other PCA patients. This

last result is difficult to interpret. This patient had advanced PCA in comparison to some of the other patients, and so might be expected to show a reasonable degree of atrophy throughout the brain, as appears to be the case in all of the subjects with more long-standing PCA. However, the lack of evidence of some preservation in the visual pathways in this patient means that interpretations of results in terms of explaining VF deficits should be made with caution. To further investigate this, it may be necessary to compare a larger number of patients without VF deficits to those with VF deficits, in order to ascertain where differences in atrophy exists between these groups.

Taking the results on atrophy in the visual system together, the most notable observation is that unlike in cases of hemianopia diagnosed following a stroke, where the most common cause of the VF deficit is direct damage to primary visual cortex, in the case of PCA, V1 is relatively preserved in comparison to other areas. Indeed specific analysis of area V1 found no evidence of cortical thinning in this region in comparison to controls, in contrast to extrastriate visual regions where cortical loss was extensive. It is more likely therefore, that the homonymous visual field deficits noted result from damage to the optic radiations, extrastriate cortex, or a combination of both. Incomplete extrastriate damage may account for the differences in the types of VF deficits found in PCA, which are in many cases not as clearly defined hemianopia or quadranatanopia as is the case in more typically occurring cases of hemianopia, which have more clearly defined boundaries along the horizontal and vertical meridians.

6.5.4 Conclusions

Posterior cortical atrophy patients show a pattern of atrophy that is clearly distinct from Alzheimer's disease in posterior brain regions, and which affects both the white and grey matter throughout the brain. While atrophy is more extensive in the hemisphere contralateral to any existing visual field deficit, the pattern of degeneration underlying the visual field loss is complex and more difficult to identify than is generally the case in sudden onset hemianopia in adults. From the results in the present study, it seems likely that the deficit stems from a combination of white matter degeneration and extrastriate cortical damage, and not direct atrophy of the primary visual cortex.

Chapter 7

General Discussion

7.1 Overview of thesis

A range of neuroimaging techniques have been used to examine the functional and structural changes that occur in patients with damage to the post-chiasmal visual pathway, leaving them with a homonymous visual field deficit. A great deal of heterogeneity exists among this patient group, both in terms of the pathology giving rise to the hemianopia, and with regard to the functional consequences of the brain damage for the patient.

Investigation of transneuronal degeneration in the optic tract found that degeneration was present in all patients with established lesions, regardless of lesion location, cause, and size, although the extent of degeneration was influenced by these factors. The degeneration occurs rapidly, with evidence of degeneration in some patients within just a few years of sustaining a lesion to the visual pathway. This suggests that if re-

habilitation is to be attempted in patients with hemianopia, this must begin quickly, before the pathways have significantly degenerated.

In spite of this degeneration, there is some evidence of spared function in the ipsilesional hemisphere, together with a possibility of cortical reorganisation following the insult. There is evidence of a strengthening of the projection from the pulvinar to the motion area MT in the lesioned hemisphere, which may underlie some of the residual motion processing found in a subset of patients.

Evidence for the location of a lesion affecting the level of cortical reorganisation was limited. While plasticity might be expected to be most limited in patients with early visual pathway lesions, this was not the case. Indeed there was substantial variation in patients with lesions to similar locations. There was, however, an indication that the size of a lesion affects both degeneration and function, as patients with larger lesions had higher levels of transneuronal degeneration and more greatly reduced neural activity in ipsilesional MT. It was expected that patients with congenital hemianopia would show a greater capacity for reorganisation than patients who acquired hemianopia in adulthood. This was not the case, however, as results from both the DTI and fMRI investigations were similar across these patient groups. There was some evidence of congenital patients showing greater levels of optic tract atrophy following V1 lesions than acquired patients, an effect that has been reported in the TRD animal literature.

Recruitment of patients with posterior cortical atrophy provided an interesting opportunity to investigate the neural correlates of a hemianopia arising from an unusual underlying pathology. PCA patients were found to have extensive atrophy of both the

grey and white matter throughout the brain. It was in the occipital regions, including extrastriate cortex and the optic radiations, that PCA patients had greater levels of degeneration than patients with non-visual neurodegeneration due to Alzheimer's disease. In contrast to the majority of patients with hemianopia, it seems likely that in PCA the deficit stems from a combination of white matter degeneration and extrastriate cortical damage, and not direct atrophy of the primary visual cortex. Further work is needed, however, to uncover the relationship between the extent and lateralisation of neurodegeneration, and the pattern of visual field loss exhibited. In the present study, six PCA patients with at least a hemianopia were included, plus one PCA patient with no visual field loss. As this project is ongoing, further patients will be recruited and scanned, including more patients with no visual field loss, in order to be better able to ascertain the differences in atrophy that cause the asymmetric visual field deficits found in PCA patients.

It is possible that the differences found between PCA patients and AD patients are due to differences in the progression of disease between the two groups, as this was difficult to quantify. The PCA group may therefore show greater degeneration than AD due to further progression of disease. However, while this cannot be ruled out, it is unlikely that this is the case. None of the PCA patients had more than mild cognitive impairment, meaning that PCA was not in the advanced stages in any patient. Indeed some of the patients were very early stage, having been diagnosed within the 4 months prior to being scanned. Furthermore, the regions where PCA patients showed more extensive degeneration were restricted to posterior regions, rather than being present

throughout the brain. As discussed in Chapter 6, it is difficult to pinpoint a procedure whereby comparability of the groups can be determined. Time since diagnosis is erratic in dementia, as often the disease can progress undiagnosed for years. Ensuring the groups are age-matched is also problematic, as PCA typically has an earlier onset than AD. Finally, assessments of cognitive impairment are also difficult to evaluate, as tests do not all give equal weight to memory and visuospatial impairments. Nonetheless, in line with previous comparisons of these groups, in future work collection of MMSE scores for the PCA patients in addition to the AD patients would assist in ascertaining whether disease severity is comparable between the two groups.

7.2 Factors to consider when studying hemianopia patients

One of the goals of this thesis was to characterise the differences in how the brain alters in patients with hemianopia stemming from different pathologies, therefore it was necessary to recruit a heterogeneous cohort of patients. This also enabled study of a larger group, as the inclusion criteria were not restricted to stroke patients with occipital damage, as is the case in many studies. There are a number of caveats though that should be considered within these different groups of patients, and concerning the hemianopia population in general.

Within the group classed as having congenital hemianopia, it is usually not possible to discern exactly when the lesion causing the hemianopia was sustained, or the precise

cause of the lesion. It could be argued that as the group probably includes patients with peri-natal injury in addition to those with developmental abnormalities, that the group should not, strictly speaking, be termed 'congenital'. However, as there was no history of trauma or any post-natal illness in any of the subjects studied (with the possible exception of the patient with epilepsy), it may be assumed that all lesions were present from birth, which makes the use of the term 'congenital' to describe the group consistent with the ophthalmic literature, including previous work using the same patient group (Jindahra et al., 2009). The nature of the way in which hemianopia comes to light in congenital patients also means that those patients with the greatest degree of cortical reorganisation following a visual pathway lesion are unlikely to be diagnosed, due to greater levels of compensation. This may be one of the reasons why the differences between the congenital and acquired groups in this study were not as large as expected.

Although comparison of hemianopia arising from different underlying causes, for example epilepsy vs stroke, was not a key consideration in this thesis, this is likely to still have some impact on how the brain responds to damage, and might also have some effect on the specific methodologies used. This was unlikely to be a significant factor in analyses such as the optic tract analysis, which used laterality measures, effectively using each subject's unlesioned hemisphere as their own control, although this may have impacted on other analyses. Functional MRI in particular is likely to be affected differently in patients with different underlying pathologies, as the baseline BOLD signal is affected by physiological differences. Iannetti and Wise (2007) outlines

ways in which different disorders can affect MRI, with abnormal spiking activity in epilepsy, and abnormal vasculature in stroke patients given as examples of disorders which may impact negatively on the usefulness of fMRI results.

It was necessary in this study to include patients with hemianopia stemming from varied underlying causes, in part due to difficulties in recruiting sufficient patient numbers if inclusion criteria were too restrictive. This is an issue that may improve over time, as a larger patient database is built up, enabling comparison of larger numbers of patients with more similar lesions, so that specific differences, such as lesion size and location, can be compared within an otherwise homogeneous group.

7.3 Future directions

Plasticity in the visual pathways

In the present DTI study, it was found that the projection to area MT was increased in the lesioned hemisphere in patients, together with a decrease in the V1 projection. It is difficult to determine whether this alteration in connectivity is a result of plasticity in the visual pathways, or is due to methodological issues. In order to ascertain whether the alteration in connectivity results from the loss of a target region in the lesioned area, an addition to the methodology could be utilised whereby lesions are simulated in control subjects. A 'lesion' mask may be added to the diffusion and structural data for control subjects, imitating the lesions found in hemianopia patients. The DTI could then be run with this data, to see whether the increase in connectivity between the

pulvinar and area MT is found in this case, as in the hemianopia patients. If this does occur, we might conclude that the result found is due to the methodology used, and the difficulties in disentangling the overlapping MT and V1 projections, as the loss of the V1 target in control subjects ought not to alter the strength of the pathway to MT.

In addition to investigating the pathway between the pulvinar and area MT, DTI could also be used to explore other pathways which have a potential for involvement in residual visual function. The pathway from the koniocellular layers of the LGN to MT has been suggested as the 'blindsight' pathway (Sincich et al., 2004; Schmid et al., 2010), and tractography could be used to assess the strength of this pathway in hemianopia. As some patients showed an advantage in processing blue stimuli over other colours, it is possible that the strength of the pathway from the LGN to area MT may be a better predictor of function in area MT than the pulvinar pathway, in some patients. In addition to this ipsilateral LGN-MT pathway, it would also be of interest to explore the existence of other pathways to area MT in hemianopia. Pathways have been found in GY that project from LGN to MT in the opposite hemisphere, together with an increased cortico-cortical connection between areas MT bilaterally (Bridge et al., 2008). It would therefore be of interest to see whether these pathways exist in other hemianopia patients, and to see whether such plasticity is limited to those patients who acquired the hemianopia early in life.

Further investigation of residual visual function

Further elucidation of this question may benefit from more extensive testing of motion discrimination capacities in these patients, together with assessment of other visual functions such as acuity and form processing. Eliciting true blindsight is a complicated task, with patients varying in the parameters under which they can respond to stimuli in the blind field. Here, more patients were able to discriminate luminance defined motion than colour defined motion, which was itself possible only for certain colours. The dissociation between performance on these two tasks may shed light on the likely pathways underlying residual vision in these patients, as the luminance discrimination performance may utilise information from magnocellular cells, in contrast to blue stimuli which require koniocellular input, and red/yellow stimuli, which require parvocellular input. However, it may be that instead of being determined by the availability of different visual pathways, performance was instead a function of task difficulty. Luminance defined motion has been described in a number of studies (Azzopardi and Cowey, 2001; Weiskrantz, 1986), whereas colour defined motion is arguably a more difficult task, requiring the ability not only to process chromatic differences, which is considered more difficult than luminance changes, but also the direction of movement occurring. Indeed Alexander and Cowey (2013) found that luminance contrast was necessary in order to respond to moving colour stimuli in the blind field, although the present results suggest this may not always be the case, as in the present study, luminance contrast was masked for the colour defined motion stimuli.

While more extensive testing has been carried out on some of the patients who

participated in this study, showing no evidence of blindsight (Ajina, unpublished data), it is likely that with more thorough testing, some of the patients who did not here show any evidence of residual visual processing may in fact have some capacity to process stimuli in the blind field. In order to ensure that results are the product of residual visual processing, and not saccades into the blind field, it would be useful to record eye movements during these tests. A thorough evaluation of the extent of residual processing abilities in each patient would be valuable in interpreting results from DTI, as it would then be possible to assess whether pathways found using tractography are likely to have a functional use.

Long term assessment of TRD and plasticity

In this thesis, patients with damage acquired more than 2.5 years prior to being scanned (3 years for those with cortical damage) have been considered here to have established lesions, and it has been assumed that trans-synaptic degeneration has stabilised in these cases. Data in monkeys supports this assumption, as it has been shown that the majority of TRD occurs in the first three years after an occipital lesion is sustained (Cowey et al., 2011). However, it is possible that degeneration in humans occurs over a longer period than this. Of the patients included, only five had their lesion for more than 5 years, and those patients who were scanned multiple times had had a hemianopia between 2 and 4 years at the point of the final scan. Only additional longitudinal scanning of patients between 2.5 and 5 years can determine whether no further degeneration occurs beyond 2.5 - 3 years. If further scans show no increase in

optic tract laterality beyond this period, it can then be argued that TRD is effectively complete in these patients. DTI analyses may also benefit from longer term follow up of these patients, as this would enable comparison of the strength of different subcortical pathways over time, such that plasticity can be identified where it occurs.

Comparison with patients who recover from hemianopia

A final point of interest relates to patients who recover their visual function following a lesion to the visual pathway. It is generally not possible to predict which patients will spontaneously recover in the first few months after acquisition of a hemianopic field deficit, as two patients with apparently similar lesions can have different outcomes. In the initial months when the hemianopia persists, and longer term after it has resolved, these patients could be another point of comparison with the established hemianopia cohort, alongside the healthy controls, in order to better understand the range of ways in which the visual system can respond to damage.

7.4 Final conclusions

Homonymous hemianopia is a disorder which can arise from a wide variety of causes, including stroke, trauma, and neurodegenerative disease. The one core factor that is true for all of these patients is that there must be some disruption of the post-chiasmal visual pathway present. Perhaps the most prevalent neural change among these patients is that given sufficient time, trans-synaptic degeneration occurs in all of these patients, meaning that the previously intact visual pathway in the lesioned hemisphere

atrophies over time. There is however evidence that in spite of this degeneration, some degree of function is retained by the visual cortex, possibly through the use of subcortical visual pathways. The impact of different lesion locations on the way the brain changes after visual pathway damage is as yet unclear, as is the extent to which congenital and adult acquired hemianopias differ. Extending the imaging methods used here to a larger patient population may help to answer these questions in the future.

Appendix A

Additional patient details

In each patient, lesion location was identified in the first instance using T1-weighted MRI images, with additional reference to T2-weighted images and patient notes where available. Where the lesion location was unclear or ambiguous, clinicians were consulted to ensure that lesion identification was as accurate and well informed as possible.

A.1 Patients scanned in the UK

T1a and **T2a** both have damage to the optic tract following a traumatic incident. T1a suffered damage to the right tract at the age of 36, causing a left hemianopia and was scanned three times, at one, two and three years after his accident. The left optic tract was damaged in T2a, leaving a right hemianopia. This subject was scanned three and a half years after their having had their accident at the age of 53.

L1a has damage to the left lateral geniculate nucleus following an ischemic stroke at age 40. As a result, she has a right superior quadrantanopia. The subject was scanned

at two separate intervals after her stroke, the first time at 3 months, with follow ups at two and three years post stroke.

L2c has damage to the left lateral geniculate nucleus, due to an arteriovenous malformation, presumed to be congenital. As a result, the patient has a right superior quadrantanopia.

R1a has basal ganglia damage, including the right optic radiation, following an haemorrhagic stroke at age 45. The subject has a left hemianopia, and was scanned 3 years after the stroke occurred.

R2a has a focal lesion to the optic radiation just posterior to the lateral geniculate nucleus, with some evidence of additional grey matter loss in the striate cortex, although this is minimal. The lesion occurred following a stroke at the age of 49. The patient has a left hemianopia, and was scanned 5 years after suffering the stroke.

R4c has atrophy of the medial occipital lobe, with loss of white matter in the left optic radiation leading to expansion of the left lateral ventricle. The atrophy extends to the grey matter of striate cortex, however some regions of V1 are preserved, and the damage is presumed to be congenital

R5c has a large lesion affecting both the white matter of the optic radiations, and a large portion of extrastriate cortex, sparing V1 and most of area MT. The lesion may be peri-natal, following a difficult birth.

S1a had an extensive left occipital lobe resection to remove a tumor, sparing area MT. The surgery, performed at the age of 55, 18 years prior to being scanned for this study, resulted in a right-sided hemianopia

S2a had a stroke affecting the left hemisphere at the age of 41, resulting in a right hemianopia. The damage encompasses medial and ventral occipital cortex, and extends into the temporal lobe, with sparing of dorsolateral regions. Brain images were acquired 5 years after the damage occurred.

S3a acquired a right hemianopia at the age of 8, following a traumatic incident. Left striate cortex and parts of prestriate cortex were damaged, with sparing at the occipital pole. The subject was scanned for this study at the age of 53, 45 years after the damage occurred.

S4a acquired damage to the right ventromedial occipital lobe following an ischemic stroke, resulting in a left hemianopia. The stroke occurred at the age of 67, and the subject was initially scanned 3 months later, with a follow up at 2 years.

S6a has incomplete damage to right striate cortex, extending to the posterior optic radiation. The damage followed an ischemic stroke at the age of 56, resulting in a left inferior quadrantanopia. The patient was initially scanned at 18 months post-stroke, and then again at three years.

A number of patients have small congenital lesions to striate cortex. In **S7c**, **S9c** and **S12c** the lesion is in the left hemisphere, and in **S8c** and **S10c**, the lesion is to right V1. In most of these patients, lesions do not extend far beyond primary visual cortex, and in S9c, S10c, and S12c, the lesions do not encompass the entirety of striate cortex. In S7c however, there is some damage to the anterior optic radiation in addition to focal atrophy of anterior V1 and the majority of posterior V1. In S12c, rather than having a lesioned area, there is extensive occipital atrophy in the pericalcarine region,

specifically the lingual gyrus parallel to the tentorium.

A.2 Patients scanned in Brazil

The patients recruited and scanned in Brazil all suffered from epilepsy, and have all had surgical resections to prevent seizures with a resultant hemianopia, with the exception of S11c, who had yet to have surgery to resolve her epilepsy at the time of scanning.

T3a had the left medial temporal lobe removed at the age of 54. The resection included the optic tract, and the anterior portion of the optic radiation. The patient was scanned 1.5 years after surgery.

T4a had pre-existing right hippocampal atrophy prior to surgery, where the resection included the right optic tract and the optic radiation, extending to the lateral geniculate nucleus. The surgery resulted in a left hemiparesis, which resolved after a year, and a persistent left hemianopia. The subject had the surgery at the age of 38, and was scanned twice afterwards, at 18 months and 3.5 years post-operatively.

R3a acquired a left superior quadrantanopia at the age of 48 following temporal lobe surgery, which was successful in leaving the patient seizure free. The surgery removed the right anterior temporal lobe, including Meyer's loop of the optic radiation. The patient was scanned 2.5 years after surgery.

S5a had left lateral posterior cortex removed, including part of the optic radiation and dorsal striate cortex. The surgery was performed when the subject was 27 years of age, and resulted in a right inferior quadrantanopia, although earlier perimetry shows some peripheral field loss prior to surgery. The brain images used in this study were

acquired 8 and 22 months post-operatively.

S11c has damage to the right occipital lobe, including striate cortex and dorsal extrastriate cortex, and extending into regions of the parietal lobe. The defect is presumed to be congenital, as is the resultant left field deficit, an incomplete hemianopia. The subject was scanned for this study at age 27. As S11c has yet to undergo surgery to resolve her epilepsy, she still has frequent seizures, one of which occurred during an fMRI scan.

O1a, O2a and **O3a** had their entire occipital lobe removed, at the ages of 22, 38, and 33 respectively. O1a and O3a had right-sided damage causing a left hemianopia, with the resection extending into the posterior temporal region, while O2a had left occipital cortex removed, leaving a right hemianopia. In this patient, the resection also includes the majority of the parietal lobe. These patients are all reportedly unaware of their field deficit, and exhibited some signs of neglect.

Appendix B

Perimetry Results

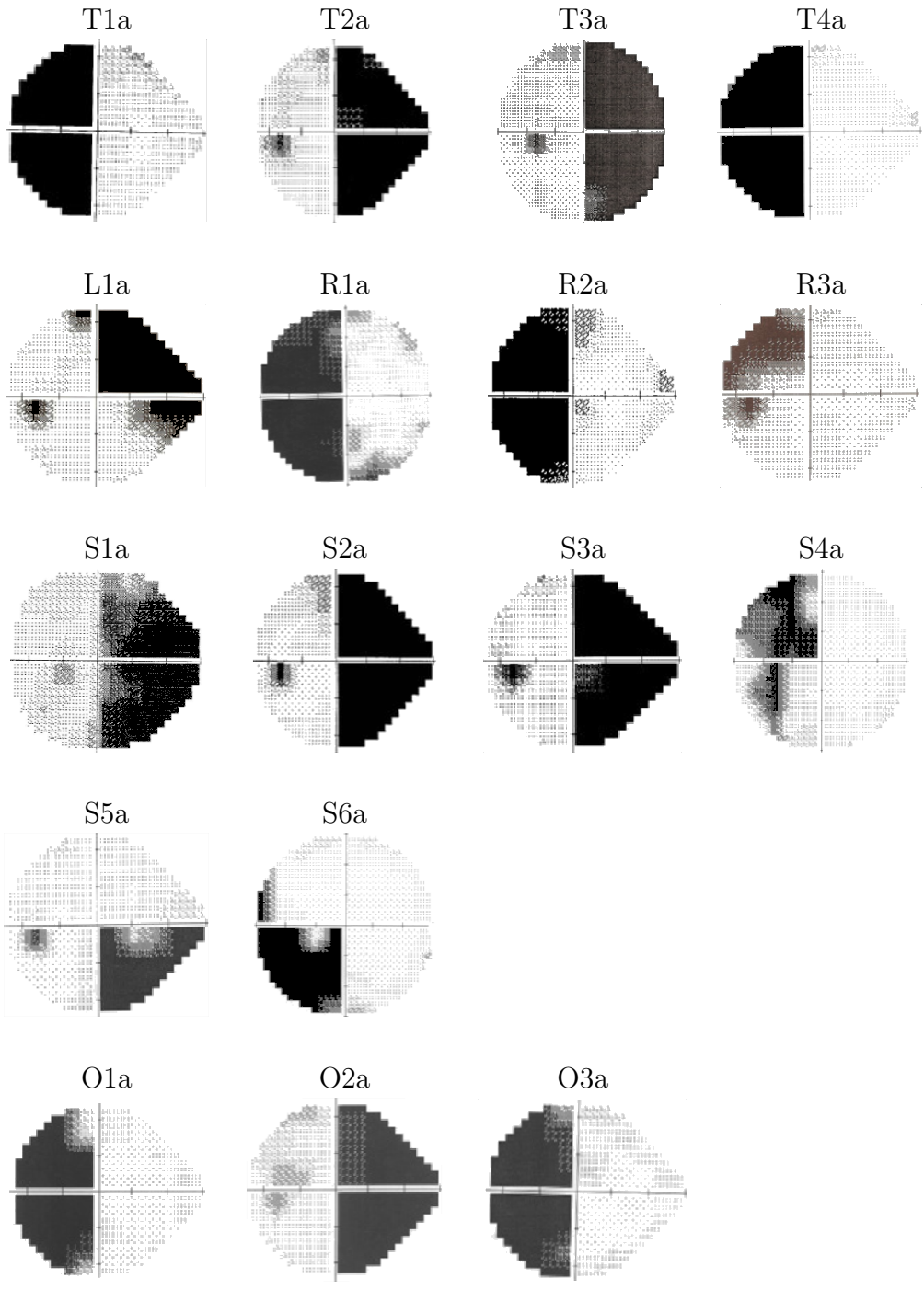

Figure B.1: Humphrey visual fields for patients with adult acquired lesions.

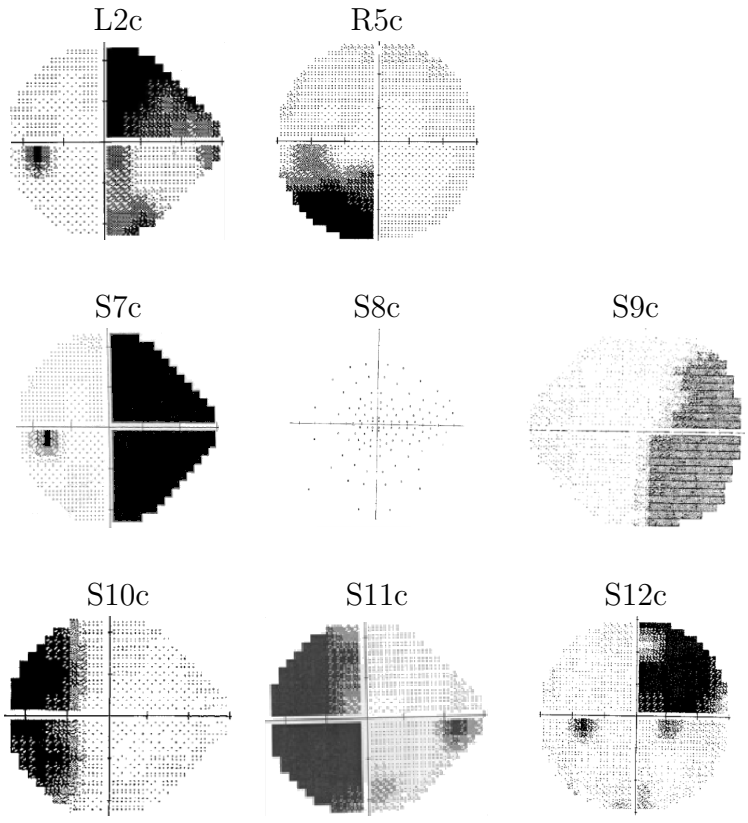

Figure B.2: Humphrey visual fields for congenital patients. Perimetry for R4c was not available. S8c had perimetry using a different method.

Table B.1: Mean Deviation in each hemifield, measured using Humphrey perimetry.

	Damaged hemisphere	Mean Deviation affected hemifield	Mean Deviation good hemifield
T1a	Right	−31.7	−3.8
T2a	Left	−30.8	−2.8
T3a	Left	−30.0	+0.2
T4a	Right	−32.6	−2.7
L1a	Left	−22.1	−2.9
R1a	Right	−30.2	−5.2
R2a	Right	−31.3	−5.7
R3a	Right	−16.6	−1.8
S1a	Left	−23.2	−2.3
S2a	Left	−29.3	−5.7
S3a	Left	−31.5	−5.1
S4a	Right	−15.6	+0.5
S5a	Left	−17.2	−1.5
S6a	Right	−16.0	−0.4
O1a	Right	−32.2	−1.7
O2a	Left	−30.8	−4.2
O3a	Right	−30.9	−2.2
L2c	Left	−20.8	−0.5
R4c	Left	NA	NA
R5c	Right	−12.6	−1.5
S7c	Left	−34.0	−2.4
S8c	Right	NA	NA
S9c	Left	−24.3	−3.2
S10c	Right	−25.1	−1.0
S11c	Right	−28.8	−5.3
S12c	Left	−16.9	−3.0

Bibliography

Acosta-Cabronero, J., Williams, G. B., Pengas, G., and Nestor, P. J. (2010). Absolute diffusivities define the landscape of white matter degeneration in Alzheimer's disease. *Brain : a journal of neurology*, 133(Pt 2):529–39.

Ajina, S. and Kennard, C. (2012). Rehabilitation of damage to the visual brain. *Revue neurologique*, 168(10):754–61.

Alexander, I. and Cowey, A. (2010). Edges, colour and awareness in blindsight. *Consciousness and Cognition*, 19(2):520–533.

Alexander, I. and Cowey, A. (2013). Isoluminant coloured stimuli are undetectable in blindsight even when they move. *Experimental brain research. Experimentelle Hirnforschung. Expérimentation cérébrale*, 225(1):147–52.

Alves, J., Soares, J. M., Sampaio, A., and Gonçalves, O. F. (2013). Posterior cortical atrophy and Alzheimer's disease: a meta-analytic review of neuropsychological and brain morphometry studies. *Brain imaging and behavior*.

Amunts, K., Malikovic, a., Mohlberg, H., Schormann, T., and Zilles, K. (2000). Brodmann's areas 17 and 18 brought into stereotaxic space-where and how variable? *NeuroImage*, 11(1):66–84.

Andersson, J. L. R., Jenkinson, M., and Smith, S. (2007). Non-linear registration aka Spatial normalisation FMRIB Technial Report TR07JA2. (June).

Andrade, K., Samri, D., Sarazin, M., de Souza, L. C., Cohen, L., Thiebaut de Schotten, M., Dubois, B., and Bartolomeo, P. (2010). Visual neglect in posterior cortical atrophy. *BMC neurology*, 10:68.

Andrews, T. J., Halpern, S. D., and Purves, D. (1997). Correlated size variations in human visual cortex, lateral geniculate nucleus, and optic tract. *The Journal of neuroscience : the official journal of the Society for Neuroscience*, 17(8):2859–68.

Azzopardi, P. and Cowey, a. (2001). Motion discrimination in cortically blind patients. *Brain: A journal of neurology*, 124(Pt 1):30–46.

Barbarulo, A. M., Pappatà, S., Puoti, G., Prinster, A., Grossi, D., Cotrufo, R., Salvatore, M., and Trojano, L. (2008). Rehabilitation of gesture imitation: a case study with fMRI. *Neurocase*, 14(4):293–306.

Barbur, J. L. and Connolly, D. M. (2011). Effects of hypoxia on color vision with emphasis on the mesopic range. *Expert Review of Ophthalmology*, 6(4):409–420.

Bartels, a. and Zeki, S. (2000). The architecture of the colour centre in the human visual brain: new results and a review. *The European journal of neuroscience*, 12(1):172–93.

Baseler, H. a., Morland, a. B., and Wandell, B. a. (1999). Topographic organization of human visual areas in the absence of input from primary cortex. *The Journal of neuroscience : the official journal of the Society for Neuroscience*, 19(7):2619–27.

Baxter, D. (1982). The development of a graded spelling test for adults. In *Fifth International Neuropsychology Society Conference, Deauville, France. International Neuropsychology Society Bulletin*, page 34.

Beaulieu, C. (2002). The basis of anisotropic water diffusion in the nervous system - a technical review. *NMR in biomedicine*, 15(7-8):435–55.

Behrens, T. E. J., Berg, H. J., Jbabdi, S., Rushworth, M. F. S., and Woolrich, M. W. (2007). Probabilistic diffusion tractography with multiple fibre orientations: What can we gain? *NeuroImage*, 34(1):144–55.

Behrens, T. E. J., Johansen-Berg, H., Woolrich, M. W., Smith, S. M., Wheeler-Kingshott, C. a. M., Boulby, P. a., Barker, G. J., Sillery, E. L., Sheehan, K., Ciccarelli, O., Thompson, a. J., Brady, J. M., and Matthews, P. M. (2003a). Non-invasive mapping of connections between human thalamus and cortex using diffusion imaging. *Nature neuroscience*, 6(7):750–7.

Behrens, T. E. J., Woolrich, M. W., Jenkinson, M., Johansen-Berg, H., Nunes, R. G., Clare, S., Matthews, P. M., Brady, J. M., and Smith, S. M. (2003b). Characterization and propagation of uncertainty in diffusion-weighted MR imaging. *Magnetic resonance in medicine : official journal of the Society of Magnetic Resonance in Medicine / Society of Magnetic Resonance in Medicine*, 50(5):1077–88.

Benson, D. F., Davis, R. J., and Snyder, B. D. (1988). Posterior Cortical Atrophy. *Archives of Neurology*, 45(7):789–793.

Blume, W. T., Whiting, S. E., and Girvin, J. P. (1991). Epilepsy surgery in the posterior cortex. *Annals of neurology*, 29(6):638–45.

Bourne, J. a. (2010). Unravelling the development of the visual cortex: implications for plasticity and repair. *Journal of anatomy*, 217(4):449–68.

Bowers, A. R., Keeney, K., and Peli, E. (2008). Community-based trial of a peripheral prism visual field expansion device for hemianopia. *Archives of ophthalmology*, 126(5):657–64.

Bridge, H. (2011). Mapping the visual brain: how and why. *Eye (London, England)*, 25(3):291–6.

Bridge, H., Hicks, S. L., Xie, J., Okell, T. W., Mannan, S., Alexander, I., Cowey, A., and Kennard, C. (2010). Visual activation of extra-striate cortex in the absence of V1 activation. *Neuropsychologia*, 48(14):4148–4154.

Bridge, H., Jindahra, P., Barbur, J., and Plant, G. T. (2011). Imaging reveals optic tract degeneration in hemianopia. *Investigative Ophthalmology & Visual Science*, 52(1):382–388.

Bridge, H. and Plant, G. T. (2012). Conclusive Evidence for Human Transneuronal Retrograde Degeneration in the Visual System. *Journal of Clinical & Experimental Ophthalmology*, S3:003.

Bridge, H., Thomas, O., Jbabdi, S., and Cowey, A. (2008). Changes in connectivity after visual cortical brain damage underlie altered visual function. *Brain: A journal of neurology*, 131(Pt 6):1433–1444.

Brodtmann, A., Puce, A., Darby, D., and Donnan, G. (2009). Serial functional imaging poststroke reveals visual cortex reorganization. *Neurorehabilitation and neural repair*, 23(2):150–9.

Bruce, B. B., Zhang, X., Kedar, S., Newman, N. J., and Biousse, V. (2006). Traumatic homonymous hemianopia. *Journal of neurology, neurosurgery, and psychiatry*, 77(8):986–8.

Bürgel, U., Amunts, K., Hoemke, L., Mohlberg, H., Gilsbach, J. M., and Zilles, K. (2006). White matter fiber tracts of the human brain: three-dimensional mapping at microscopic resolution, topography and intersubject variability. *NeuroImage*, 29(4):1092–105.

Campion, J., Latto, R., and Smith, Y. M. (1983). Is blindsight an effect of scattered light, spared cortex, and near-threshold vision? *Behavioral and Brain Sciences*, 6(3):423.

Corballis, P. M. (2003). Visuospatial processing and the right-hemisphere interpreter. *Brain and Cognition*, 53(2):171–176.

Cowey, A. (2010). The blindsight saga. *Experimental brain research. Experimentelle Hirnforschung. Expérimentation cérébrale*, 200(1):3–24.

Cowey, A., Alexander, I., and Stoerig, P. (2011). Transneuronal retrograde degeneration of retinal ganglion cells and optic tract in hemianopic monkeys and humans. *Brain : a journal of neurology*, 134(Pt 7):2149–57.

Cowey, A. and Stoerig, P. (1991). The neurobiology of blindsight. *Trends in neurosciences*, 14(4):140–5.

Cowey, a., Stoerig, P., and Perry, V. H. (1989). Transneuronal retrograde degeneration of retinal ganglion cells after damage to striate cortex in macaque monkeys: selective loss of P beta cells. *Neuroscience*, 29(1):65–80.

Cowey, a., Stoerig, P., and Williams, C. (1999). Variance in transneuronal retrograde ganglion cell degeneration in monkeys after removal of striate cortex: effects of size of the cortical lesion. *Vision research*, 39(21):3642–52.

Crutch, S. J., Lehmann, M., Schott, J. M., Rabinovici, G. D., Rossor, M. N., and Fox, N. C. (2012). Posterior cortical atrophy. *Lancet neurology*, 11(2):170–8.

Danckert, J. and Rossetti, Y. (2005). Blindsight in action: what can the different subtypes of blindsight tell us about the control of visually guided actions? *Neuroscience and biobehavioral reviews*, 29(7):1035–46.

Darian-Smith, C., Darian-Smith, I., and Cheema, S. S. (1990). Thalamic projections to sensorimotor cortex in the newborn macaque. *The Journal of comparative neurology*, 299(1):47–63.

Dasenbrock, H. H., Smith, S. a., Ozturk, A., Farrell, S. K., Calabresi, P. a., and Reich, D. S. (2011). Diffusion tensor imaging of the optic tracts in multiple sclerosis: association with retinal thinning and visual disability. *Journal of neuroimaging : official journal of the American Society of Neuroimaging*, 21(2):e41–9.

de Gelder, B., Vroomen, J., Pourtois, G., and Weiskrantz, L. (1999). Non-conscious recognition of affect in the absence of striate cortex. *Neuroreport*, 10(18):3759–63.

Delamont, R. S., Harrison, J., Field, M., and Boyle, R. S. (1989). Posterior cortical atrophy. *Clinical and experimental neurology*, 26:225–7.

Delazer, M., Benke, T., Trieb, T., Schocke, M., and Ischebeck, A. (2006). Isolated numerical skills in posterior cortical atrophy–an fMRI study. *Neuropsychologia*, 44(10):1909–13.

Dilks, D. D., Serences, J. T., Rosenau, B. J., Yantis, S., and McCloskey, M. (2007). Human adult cortical reorganization and consequent visual distortion. *The Journal of neuroscience : the official journal of the Society for Neuroscience*, 27(36):9585–94.

Douaud, G., Jbabdi, S., Behrens, T. E. J., Menke, R. a., Gass, A., Monsch, A. U., Rao, A., Whitcher, B., Kindlmann, G., Matthews, P. M., and Smith, S. (2011). DTI measures in crossing-fibre areas: increased diffusion anisotropy reveals early white matter alteration in MCI and mild Alzheimer's disease. *NeuroImage*, 55(3):880–90.

Duning, T., Warnecke, T., Mohammadi, S., Lohmann, H., Schiffbauer, H., Kugel, H., Knecht, S., Ringelstein, E. B., and Deppe, M. (2009). Pattern and progression of white-matter changes in a case of posterior cortical atrophy using diffusion tensor imaging. *Journal of neurology, neurosurgery, and psychiatry*, 80(4):432–6.

Fazekas, F., Kleinert, R., Roob, G., Kleinert, G., Kapeller, P., Schmidt, R., and Hartung, H. P. (1999). Histopathologic analysis of foci of signal loss on gradient-echo T2*-weighted MR images in patients with spontaneous intracerebral hemorrhage: evidence of microangiopathy-related microbleeds. *AJNR. American journal of neuroradiology*, 20(4):637–42.

Feldmann, A., Trauninger, A., Toth, L., Kotek, G., Kosztolanyi, P., Illes, E., Pfund, Z., Komoly, S., Nagy, F., and Illes, Z. (2008). Atrophy and decreased activation of frontoparietal attention areas contribute to higher visual dysfunction in posterior cortical atrophy. *Psychiatry research*, 164(2):178–84.

Fischl, B. and Dale, a. M. (2000). Measuring the thickness of the human cerebral cortex

from magnetic resonance images. *Proceedings of the National Academy of Sciences of the United States of America*, 97(20):11050–5.

Fischl, B., Rajendran, N., Busa, E., Augustinack, J., Hinds, O., Yeo, B. T. T., Mohlberg, H., Amunts, K., and Zilles, K. (2008). Cortical folding patterns and predicting cytoarchitecture. *Cerebral cortex (New York, N.Y. : 1991)*, 18(8):1973–80.

Formaglio, M., Krolak-Salmon, P., Tilikete, C., Bernard, M., Croisile, B., and Vighetto, A. (2009). [Homonymous hemianopia and posterior cortical atrophy]. *Revue neurologique*, 165(3):256–62.

Geyer, S., Schormann, T., Mohlberg, H., and Zilles, K. (2000). Areas 3a, 3b, and 1 of human primary somatosensory cortex. Part 2. Spatial normalization to standard anatomical space. *NeuroImage*, 11(6 Pt 1):684–96.

Gilhotra, J. S., Mitchell, P., Healey, P. R., Cumming, R. G., and Currie, J. (2002). Homonymous visual field defects and stroke in an older population. *Stroke; a journal of cerebral circulation*, 33(10):2417–20.

Goebel, R., Muckli, L., Zanella, F. E., Singer, W., and Stoerig, P. (2001). Sustained extrastriate cortical activation without visual awareness revealed by fMRI studies of hemianopic patients. *Vision research*, 41(10-11):1459–74.

Goodale, M. A. and Milner, A. D. (1992). Separate visual pathways for perception and action. *Trends in neurosciences*, 15(1):20–5.

Grieve, K. L., Acuña, C., and Cudeiro, J. (2000). The primate pulvinar nuclei: vision and action. *Trends in neurosciences*, 23(1):35–9.

Harting, J. K., Glendenning, K. K., Diamond, I. T., and Hall, W. C. (1973). Evolution of the primate visual system: anterograde degeneration studies of the tecto-pulvinar system. *American journal of physical anthropology*, 38(2):383–92.

Hofer, S., Karaus, A., and Frahm, J. (2010). Reconstruction and dissection of the entire human visual pathway using diffusion tensor MRI. *Frontiers in neuroanatomy*, 4(April):15.

Horton, J. C. (2005a). Disappointing results from Nova Vision's visual restoration therapy. *The British journal of ophthalmology*, 89(1):1–2.

Horton, J. C. (2005b). Vision restoration therapy: confounded by eye movements. *The British journal of ophthalmology*, 89(7):792–4.

Hoyt, C. S. (2003). Visual function in the brain-damaged child. *Eye (London, England)*, 17(3):369–84.

Hubel, D. (1995). *Eye, brain, and vision.* New York, NY, US: Scientific American Library/Scientific American Books.

Huber, A. (1992). Homonymous hemianopia. *Neuro-ophthalmology*, 12(6):351–366.

Huffman, K. J. and Krubitzer, L. (2001). Thalamo-cortical connections of areas 3a and M1 in marmoset monkeys. *The Journal of comparative neurology*, 435(3):291–310.

Iannetti, G. D. and Wise, R. G. (2007). BOLD functional MRI in disease and pharmacological studies: room for improvement? *Magnetic resonance imaging*, 25(6):978–88.

Jenkinson, M. and Smith, S. (2001). A global optimisation method for robust affine registration of brain images. *Medical image analysis*, 5(2):143–56.

Jindahra, P., Petrie, A., and Plant, G. T. (2009). Retrograde trans-synaptic retinal ganglion cell loss identified by optical coherence tomography. *Brain : a journal of neurology*, 132(Pt 3):628–34.

Jindahra, P., Petrie, A., and Plant, G. T. (2012a). The time course of retrograde trans-synaptic degeneration following occipital lobe damage in humans. *Brain : a journal of neurology*, 135(Pt 2):534–41.

Jindahra, P., Petrie, A., and Plant, G. T. (2012b). Thinning of the Retinal Nerve Fibre Layer in Homonymous Quadrantanopia: Further Evidence for Retrograde Trans-Synaptic Degeneration in the Human Visual System. *Neuro-Ophthalmology*, 36(3):79–84.

Johansen-Berg, H., Behrens, T. E. J., Sillery, E., Ciccarelli, O., Thompson, A. J., Smith, S. M., and Matthews, P. M. (2005). Functional-anatomical validation and individual variation of diffusion tractography-based segmentation of the human thalamus. *Cerebral cortex (New York, N.Y. : 1991)*, 15(1):31–9.

Johnson, L. N. and Baloh, F. G. (1991). The accuracy of confrontation visual field test in comparison with automated perimetry. *Journal of the National Medical Association*, 83(10):895–8.

Kaas, J. H. (1983). What, if anything, is SI? Organization of first somatosensory area of cortex. *Physiological reviews*, 63(1):206–31.

Kaas, J. H. and Hackett, T. a. (2000). Subdivisions of auditory cortex and processing streams in primates. *Proceedings of the National Academy of Sciences of the United States of America*, 97(22):11793–9.

Kasten, E., Wüst, S., Behrens-Baumann, W., and Sabel, B. a. (1998). Computer-based training for the treatment of partial blindness. *Nature medicine*, 4(9):1083–7.

Krubitzer, L. a. and Kaas, J. H. (1992). The somatosensory thalamus of monkeys: cortical connections and a redefinition of nuclei in marmosets. *The Journal of comparative neurology*, 319(1):123–40.

Leh, S. E., Chakravarty, M. M., and Ptito, A. (2007). The connectivity of the human pulvinar: a diffusion tensor imaging tractography study. *International journal of biomedical imaging*, 2008:789539.

Leh, S. E., Johansen-Berg, H., and Ptito, A. (2006a). Unconscious vision: new insights into the neuronal correlate of blindsight using diffusion tractography. *Brain : a journal of neurology*, 129(Pt 7):1822–32.

Leh, S. E., Mullen, K. T., and Ptito, A. (2006b). Absence of S-cone input in human blindsight following hemispherectomy. *The European journal of neuroscience*, 24(10):2954–60.

Leh, S. E., Ptito, A., Schönwiesner, M., Chakravarty, M. M., and Mullen, K. T. (2010). Blindsight mediated by an S-cone-independent collicular pathway: an fMRI study in hemispherectomized subjects. *Journal of cognitive neuroscience*, 22(4):670–82.

Lehmann, M., Barnes, J., Ridgway, G. R., Ryan, N. S., Warrington, E. K., Crutch, S. J., and Fox, N. C. (2012). Global gray matter changes in posterior cortical atrophy: a serial imaging study. *Alzheimer's & dementia : the journal of the Alzheimer's Association*, 8(6):502–12.

Luu, S., Lee, A. W., Daly, A., and Chen, C. S. (2010). Visual field defects after stroke–a practical guide for GPs. *Australian family physician*, 39(7):499–503.

Malikovic, A., Amunts, K., Schleicher, A., Mohlberg, H., Eickhoff, S. B., Wilms, M., Palomero-Gallagher, N., Armstrong, E., and Zilles, K. (2007). Cytoarchitectonic analysis of the human extrastriate cortex in the region of V5/MT+: a probabilistic, stereotaxic map of area hOc5. *Cerebral cortex (New York, N.Y. : 1991)*, 17(3):562–74.

Mazziotta, J., Toga, a., Evans, a., Fox, P., Lancaster, J., Zilles, K., Woods, R., Paus, T., Simpson, G., Pike, B., Holmes, C., Collins, L., Thompson, P., MacDonald, D., Iacoboni, M., Schormann, T., Amunts, K., Palomero-Gallagher, N., Geyer, S., Parsons, L., Narr, K., Kabani, N., Le Goualher, G., Boomsma, D., Cannon, T., Kawashima, R., and Mazoyer, B. (2001). A probabilistic atlas and reference system for the human brain: International Consortium for Brain Mapping (ICBM). *Philosophical transactions of the Royal Society of London. Series B, Biological sciences*, 356(1412):1293–322.

McKenna, P. and Warrington, E. K. (1980). Testing for nominal dysphasia. *Journal of neurology, neurosurgery, and psychiatry*, 43(9):781–8.

McMonagle, P., Deering, F., Berliner, Y., and Kertesz, A. (2006). The cognitive profile of posterior cortical atrophy. *Neurology*, 66(3):331–8.

Mendez, M. F., Ghajarania, M., and Perryman, K. M. (2002). Posterior cortical atrophy: clinical characteristics and differences compared to Alzheimer's disease. *Dementia and geriatric cognitive disorders*, 14(1):33–40.

Migliaccio, R., Agosta, F., Possin, K. L., Rabinovici, G. D., Miller, B. L., and Gorno-Tempini, M. L. (2012a). White matter atrophy in Alzheimer's disease variants. *Alzheimer's & dementia : the journal of the Alzheimer's Association*, 8(5 Suppl):S78–87.e1–2.

Migliaccio, R., Agosta, F., Scola, E., Magnani, G., Cappa, S. F., Pagani, E., Canu, E., Comi,

G., Falini, A., Gorno-Tempini, M. L., Bartolomeo, P., and Filippi, M. (2012b). Ventral and dorsal visual streams in posterior cortical atrophy: a DT MRI study. *Neurobiology of aging*, 33(11):2572–84.

Migliaccio, R., Agosta, F., Toba, M. N., Samri, D., Corlier, F., de Souza, L. C., Chupin, M., Sharman, M., Gorno-Tempini, M. L., Dubois, B., Filippi, M., and Bartolomeo, P. (2011). Brain networks in posterior cortical atrophy: a single case tractography study and literature review. *Cortex; a journal devoted to the study of the nervous system and behavior*, 48(10):1298–309.

Milesi, J., Rocca, M. a., Bianchi-Marzoli, S., Petrolini, M., Pagani, E., Falini, A., Comi, G., and Filippi, M. (2012). Patterns of white matter diffusivity abnormalities in Leber's hereditary optic neuropathy: a tract-based spatial statistics study. *Journal of neurology*, 259(9):1801–7.

Morel, a., Magnin, M., and Jeanmonod, D. (1997). Multiarchitectonic and stereotactic atlas of the human thalamus. *The Journal of comparative neurology*, 387(4):588–630.

Morland, A. B., Lê, S., Carroll, E., Hoffmann, M. B., and Pambakian, A. (2004). The role of spared calcarine cortex and lateral occipital cortex in the responses of human hemianopes to visual motion. *Journal of cognitive neuroscience*, 16(2):204–18.

Morosan, P., Rademacher, J., Schleicher, a., Amunts, K., Schormann, T., and Zilles, K. (2001). Human primary auditory cortex: cytoarchitectonic subdivisions and mapping into a spatial reference system. *NeuroImage*, 13(4):684–701.

Mueller, I., Mast, H., and Sabel, B. a. (2007). Recovery of visual field defects: a large

clinical observational study using vision restoration therapy. *Restorative neurology and neuroscience*, 25(5-6):563–72.

Nelles, G., de Greiff, A., Pscherer, A., Forsting, M., Gerhard, H., Esser, J., and Diener, H. C. (2007). Cortical activation in hemianopia after stroke. *Neuroscience letters*, 426(1):34–8.

Nelles, G., Esser, J., Eckstein, a., Tiede, a., Gerhard, H., and Diener, H. C. (2001). Compensatory visual field training for patients with hemianopia after stroke. *Neuroscience letters*, 306(3):189–92.

Newsome, W. T. and Paré, E. B. (1988). A selective impairment of motion perception following lesions of the middle temporal visual area (MT). *The Journal of neuroscience : the official journal of the Society for Neuroscience*, 8(6):2201–11.

Pambakian, a. L. and Kennard, C. (1997). Can visual function be restored in patients with homonymous hemianopia? *The British journal of ophthalmology*, 81(4):324–8.

Pegna, A. J., Khateb, A., Lazeyras, F., and Seghier, M. L. (2005). Discriminating emotional faces without primary visual cortices involves the right amygdala. *Nature neuroscience*, 8(1):24–5.

Pelak, V. S., Smyth, S. F., Boyer, P. J., and Filley, C. M. (2011). Computerized visual field defects in posterior cortical atrophy. *Neurology*, 77(24):2119–22.

Peli, E. (2000). Field expansion for homonymous hemianopia by optically induced peripheral exotropia. *Optometry and vision science : official publication of the American Academy of Optometry*, 77(9):453–64.

Plow, E. B., Obretenova, S. N., Fregni, F., Pascual-Leone, A., and Merabet, L. B. (2012). Comparison of visual field training for hemianopia with active versus sham transcranial direct cortical stimulation. *Neurorehabilitation and neural repair*, 26(6):616–26.

Plow, E. B., Obretenova, S. N., Halko, M. a., Kenkel, S., Jackson, M. L., Pascual-Leone, A., and Merabet, L. B. (2011). Combining visual rehabilitative training and noninvasive brain stimulation to enhance visual function in patients with hemianopia: a comparative case study. *PM & R : the journal of injury, function, and rehabilitation*, 3(9):825–35.

Pons, T. P. and Kaas, J. H. (1985). Connections of area 2 of somatosensory cortex with the anterior pulvinar and subdivisions of the ventroposterior complex in macaque monkeys. *The Journal of comparative neurology*, 240(1):16–36.

Radoeva, P. D., Prasad, S., Brainard, D. H., and Aguirre, G. K. (2008). Neural activity within area V1 reflects unconscious visual performance in a case of blindsight. *Journal of cognitive neuroscience*, 20(11):1927–39.

Ragge, N. K., Barkovich, A. J., Hoyt, W. F., and Lambert, S. R. (1991). Isolated congenital hemianopia caused by prenatal injury to the optic radiation. *Archives of neurology*, 48(10):1088–91.

Reinhard, J., Schreiber, a., Schiefer, U., Kasten, E., Sabel, B. a., Kenkel, S., Vonthein, R., and Trauzettel-Klosinski, S. (2005). Does visual restitution training change absolute homonymous visual field defects? A fundus controlled study. *The British journal of ophthalmology*, 89(1):30–5.

Riddoch, G. (1917). Dissociation of visual perceptions due to occipital injuries, with especial reference to appreciation of movement. *Brain*, 40:15–57.

Ruis, C., van den Berg, E., van Zandvoort, M. J. E., Boshuisen, K., and Frijns, C. J. M. (2012). Ophthalmic impairment or higher-order visual deficit? Posterior cortical atrophy: a case report. *Applied neuropsychology. Adult*, 19(2):153–7.

Sabel, B. A. (2006). Vision restoration therapy and raising red flags too early. *The British journal of ophthalmology*, 90(5):659–60.

Sahraie, A., Macleod, M.-J., Trevethan, C. T., Robson, S. E., Olson, J. a., Callaghan, P., and Yip, B. (2010). Improved detection following Neuro-Eye Therapy in patients with post-geniculate brain damage. *Experimental brain research. Experimentelle Hirnforschung. Expérimentation cérébrale*, 206(1):25–34.

Sahraie, A., Trevethan, C. T., MacLeod, M. J., Murray, A. D., Olson, J. a., and Weiskrantz, L. (2006). Increased sensitivity after repeated stimulation of residual spatial channels in blindsight. *Proceedings of the National Academy of Sciences of the United States of America*, 103(40):14971–14976.

Sanders, M. D., Warrington, E. K., Marshall, J., and Wieskrantz, L. (1974). "Blindsight": Vision in a field defect. *Lancet*, 1(7860):707–8.

Schmid, M. C., Mrowka, S. W., Turchi, J., Saunders, R. C., Wilke, M., Peters, A. J., Ye, F. Q., and Leopold, D. a. (2010). Blindsight depends on the lateral geniculate nucleus. *Nature*, 466(7304):373–377.

Schmidtke, K., Hüll, M., and Talazko, J. (2005). Posterior cortical atrophy: variant of Alzheimer's disease? A case series with PET findings. *Journal of neurology*, 252(1):27–35.

Schmielau, F. and Wong, E. K. (2007). Recovery of visual fields in brain-lesioned patients by reaction perimetry treatment. *Journal of neuroengineering and rehabilitation*, 4:31.

Schofield, T. M. and Leff, A. P. (2009). Rehabilitation of hemianopia. *Current opinion in neurology*, 22(1):36–40.

Schuett, S., Heywood, C. a., Kentridge, R. W., and Zihl, J. (2008). Rehabilitation of hemianopic dyslexia: are words necessary for re-learning oculomotor control? *Brain : a journal of neurology*, 131(Pt 12):3156–68.

Shipp, S. (2003). The functional logic of cortico-pulvinar connections. *Philosophical transactions of the Royal Society of London. Series B, Biological sciences*, 358(1438):1605–24.

Silvanto, J., Walsh, V., and Cowey, A. (2009). Abnormal functional connectivity between ipsilesional V5/MT+ and contralesional striate cortex (V1) in blindsight. *Experimental Brain Research*, 193(4):645–650.

Sincich, L. C., Park, K. F., Wohlgemuth, M. J., and Horton, J. C. (2004). Bypassing V1: a direct geniculate input to area MT. *Nature neuroscience*, 7(10):1123–8.

Smith, S. M. (2002). Fast robust automated brain extraction. *Human brain mapping*, 17(3):143–55.

Smith, S. M., Jenkinson, M., Johansen-Berg, H., Rueckert, D., Nichols, T. E., Mackay, C. E., Watkins, K. E., Ciccarelli, O., Cader, M. Z., Matthews, P. M., and Behrens, T. E. J. (2006). Tract-based spatial statistics: voxelwise analysis of multi-subject diffusion data. *NeuroImage*, 31(4):1487–505.

Smith, S. M., Jenkinson, M., Woolrich, M. W., Beckmann, C. F., Behrens, T. E. J., Johansen-Berg, H., Bannister, P. R., De Luca, M., Drobnjak, I., Flitney, D. E., Niazy, R. K., Saunders, J., Vickers, J., Zhang, Y., De Stefano, N., Brady, J. M., and Matthews, P. M.

(2004). Advances in functional and structural MR image analysis and implementation as FSL. *NeuroImage*, 23 Suppl 1:S208–19.

Snowden, J. S., Stopford, C. L., Julien, C. L., Thompson, J. C., Davidson, Y., Gibbons, L., Pritchard, A., Lendon, C. L., Richardson, A. M., Varma, A., Neary, D., and Mann, D. (2007). Cognitive phenotypes in Alzheimer's disease and genetic risk. *Cortex; a journal devoted to the study of the nervous system and behavior*, 43(7):835–45.

Standage, G. P. and Benevento, L. a. (1983). The organization of connections between the pulvinar and visual area MT in the macaque monkey. *Brain research*, 262(2):288–94.

Stepniewska, I., Ql, H. X., and Kaas, J. H. (2000). Projections of the superior colliculus to subdivisions of the inferior pulvinar in New World and Old World monkeys. *Visual neuroscience*, 17(4):529–49.

Stoerig, P. and Cowey, a. (1992). Wavelength discrimination in blindsight. *Brain : a journal of neurology*, 115 (Pt 2:425–44.

Tang-Wai, D. F., Graff-Radford, N. R., Boeve, B. F., Dickson, D. W., Parisi, J. E., Crook, R., Caselli, R. J., Knopman, D. S., and Petersen, R. C. (2004). Clinical, genetic, and neuropathologic characteristics of posterior cortical atrophy. *Neurology*, 63(7):1168–1174.

Tinelli, F., Cicchini, G. M., Arrighi, R., Tosetti, M., Cioni, G., and Morrone, M. C. (2012). Blindsight in children with congenital and acquired cerebral lesions. *Cortex; a journal devoted to the study of the nervous system and behavior*, 49(6):1636–1647.

Van Buren, J. M. (1963). Trans-synaptic retrograde degeration in the visual system of primates. *Journal of neurology, neurosurgery, and psychiatry*, 26:402–9.

Victoroff, J., Ross, G. W., Benson, D. F., Verity, M. A., and Vinters, H. V. (1994). Posterior cortical atrophy. Neuropathologic correlations. *Archives of neurology*, 51(3):269–74.

Warner, C. E., Goldshmit, Y., and Bourne, J. a. (2010). Retinal afferents synapse with relay cells targeting the middle temporal area in the pulvinar and lateral geniculate nuclei. *Frontiers in neuroanatomy*, 4(February):8.

Warner, C. E., Kwan, W. C., and Bourne, J. a. (2012). The early maturation of visual cortical area MT is dependent on input from the retinorecipient medial portion of the inferior pulvinar. *The Journal of neuroscience : the official journal of the Society for Neuroscience*, 32(48):17073–85.

Warren, J. D., Fletcher, P. D., and Golden, H. L. (2012). The paradox of syndromic diversity in Alzheimer disease. *Nature reviews. Neurology*, 8(8):451–64.

Warrington, E. K. (1984). *Recognition Memory Test: Rmt.(Words). Test Booklet 1.* NFER-Nelson Publishing Company.

Warrington, E. K. (1996). *The Camden Memory Tests: Manual*, volume 1. Psychology Press.

Warrington, E. K. and James, M. (1991). *The visual object and space perception battery.* Thames Valley Test Company Bury St Edmunds.

Weiskrantz, L. (1986). *Blindsight: A case study and implications*, volume 12. Clarendon Press Oxford.

Weiskrantz, L. (1998). Consciousness and commentaries. *International Journal of Psychology*, 33(3):227–233.

Weiskrantz, L., Warrington, E. K., Sanders, M. D., and Marshall, J. (1974). Visual capacity in the hemianopic field following a restricted occipital ablation. *Brain : a journal of neurology*, 97(4):709–28.

Weller, R. E. and Kaas, J. H. (1989). Parameters affecting the loss of ganglion cells of the retina following ablations of striate cortex in primates. *Visual neuroscience*, 3(4):327–49.

Werth, R. (2006). Visual functions without the occipital lobe or after cerebral hemispherectomy in infancy. *The European journal of neuroscience*, 24(10):2932–44.

Whitwell, J. L., Jack, C. R., Kantarci, K., Weigand, S. D., Boeve, B. F., Knopman, D. S., Drubach, D. a., Tang-Wai, D. F., Petersen, R. C., and Josephs, K. a. (2007). Imaging correlates of posterior cortical atrophy. *Neurobiology of aging*, 28(7):1051–61.

Wilms, M., Eickhoff, S. B., Specht, K., Amunts, K., Shah, N. J., Malikovic, A., and Fink, G. R. (2005). Human V5/MT+: comparison of functional and cytoarchitectonic data. *Anatomy and embryology*, 210(5-6):485–95.

Yacoub, E., Shmuel, A., Logothetis, N., and Uurbil, K. (2007). Robust detection of ocular dominance columns in humans using Hahn Spin Echo BOLD functional MRI at 7 Tesla. *NeuroImage*, 37(4):1161–77.

Yoshida, T., Shiga, K., Yoshikawa, K., Yamada, K., and Nakagawa, M. (2004). White matter loss in the splenium of the corpus callosum in a case of posterior cortical atrophy: a diffusion tensor imaging study. *European neurology*, 52(2):77–81.

Zeki, S. and Ffytche, D. H. (1998). The Riddoch syndrome: insights into the neurobiology of conscious vision. *Brain : a journal of neurology*, 121 (Pt 1):25–45.

Zhang, X., Kedar, S., Lynn, M. J., Newman, N. J., and Biousse, V. (2006a). Homonymous hemianopia in stroke. *Journal of neuro-ophthalmology : the official journal of the North American Neuro-Ophthalmology Society*, 26(3):180–3.

Zhang, X., Kedar, S., Lynn, M. J., Newman, N. J., and Biousse, V. (2006b). Homonymous hemianopias: clinical-anatomic correlations in 904 cases. *Neurology*, 66(6):906–10.

Zhang, X., Kedar, S., Lynn, M. J., Newman, N. J., and Biousse, V. (2006c). Natural history of homonymous hemianopia. *Neurology*, 66(6):901–905.

Zhang, Y., Brady, M., and Smith, S. (2001). Segmentation of brain MR images through a hidden Markov random field model and the expectation-maximization algorithm. *IEEE transactions on medical imaging*, 20(1):45–57.

Zihl, J. (1980). "Blindsight": improvement of visually guided eye movements by systematic practice in patients with cerebral blindness. *Neuropsychologia*, 18(1):71–7.

Zihl, J. (1995). Visual scanning behavior in patients with homonymous hemianopia. *Neuropsychologia*, 33(3):287–303.